January 2009

Development of Shell-Crosslinked Knedel-like Nanoparticles as Intracellular Delivery Vehicles and Gene Regulation Agents

Ke Zhang
Washington University in St. Louis

WASHINGTON UNIVERSITY IN ST. LOUIS

Department of Chemistry

Dissertation Examination Committee:
Prof. Karen L. Wooley, Chairperson
Prof. John-Stephen A. Taylor
Prof. Jacob Schaefer
Prof. William E. Buhro
Prof. Steven L. Brody
Prof. Shelly E. Sakiyama-Elbert

Development of Shell-Crosslinked Knedel-like Nanoparticles as Intracellular Delivery Vehicles and Gene Regulation Agents

by

Ke Zhang

A dissertation presented to the
Graduate School of Arts and Sciences
of Washington University in
partial fulfillment of the
requirements for the degree
of Doctor of Philosophy

December 2009

Saint Louis, Missouri

ABSTRACT OF THE DISSERTATION

Development of Shell-Crosslinked Knedel-like Nanoparticles

as Intracellular Delivery Vehicles

and Gene Regulation Agents

by

Ke Zhang

Doctor of Philosophy in Chemistry

Washington University in St. Louis, 2009

Professor Karen L. Wooley, Chairperson

This dissertation focuses on the development of polymer-based nanomaterials, termed shell-crosslinked knedel-like (SCK) nanoparticles, as vehicles to carry specific guest molecules or guest structures into the cell. Detailed synthetic procedures for and characterization of well-defined block copolymers, as well as the nanostructures resulted from their self-assembly are reported. The nanoparticles exhibited different but controlled sizes and shapes, depending on the conditions for their preparation. To incorporate functionality into these materials, both pre- and post-particle functionalization methods, as well as their combination, were used. The nanostructures involved in this dissertation include protein transduction domain (PTD)-functionalized SCK, folate-functionalized SCK and cationic SCK (cSCK). Biological evaluation of

each type of nanoparticles is described. For the PTD- and the folate-SCKs, a particle shape/size dependence on their ability to undergo cell uptake was found, although their trends were opposite. The cSCKs were designed to bear primary amines, which rendered the nanoparticles a positively charged character in solution that was utilized to condense and protect DNA. The cSCKs were shown to be highly effective in transporting DNA into the cell to allow the DNA to function. Peptide nucleic acids (PNAs) were also effectively transported into the cell by covalent conjugation to or electrostatically complexation with the cSCKs. Finally, the cSCKs were shown to be able to form hierarchical nanoscale structures with anionc, cylindrical SCKs, and transport the cylinders into the cell.

Acknowledgements

I would like to thank my advisor and mentor, Professor Karen L. Wooley, for her support and invaluable guidance over the last four years. It has been a privilege and honor of mine to be her student. I have learned far more important values than knowledge from her, which is by no means short. Her passion to science and her warm personality makes life in her laboratory filled with excitement. Her concern for me and my career is forever remembered. I feel enormously fortunate and proud that Karen is my advisor. I have learnt in my childhood an old Chinese axiom, that a day as a mentor constitutes a lifetime of parenthood. Karen had me really believe in it.

I thank Professor John-Stephen A. Taylor and Professor Jacob Schaefer for having served as my research committee members and offering advice through the past four years. I appreciate their helpful suggestions and discussions. I also appreciate the opportunity for collaboration with Prof. Taylor, whose support and concern for me is sincerely acknowledged. I thank Professor William E. Buhro, Professor Steven L. Brody and Professor Shelly E. Sakiyama-Elbert for providing help and critical suggestions while serving on my defense committee. I want to extend my gratitude to Professor Craig J. Hawker for helping me in many, many ways. His scientific insights and superb skills in conveying them are very enlightening and worthy of every effort to emulate.

Because of the interdisciplinary nature of my PhD research, I collaborated closely with many other researchers. I owe special thanks to Dr. Huafeng Fang and Dr. Gang Shen, without whom I could not have made nearly as much progress. Other individuals who have contributed to my PhD career include Professor. Michael J. Welch, Dr.

Raffaella Rossin, Dr. Aviv Hagooly, Dr. Zhiyun Chen, Dr. Guorong Sun, Dr. Yali Li, Dr. Wenjun Du, Mr. Michael G. Veith, Ms. Sophia V. Hohlbauch, Mr. Zhou Li, Mr. Jun Ma, Mr. Zhenghui Wang, Dr. Yongjian Liu, Dr. Tetsuya Mori and Ms. Aida Ibricevic. Their hard work and scientific contribution are deeply appreciated. I would also like to express my gratitude to all Wooley group members, who have created a friendly and helpful laboratory environment which I have truly enjoyed. Some of them were not only wonderful colleagues but also my best friends.

Finally, I would like to sincerely thank my parents, for always supporting me and raising me up knowing the values of hard working. They supported my decision to study in the United States, always believed in me and encouraged me whenever, wherever I needed.

Financial support from the National Heart Lung and Blood Institute of the National Institutes of Health as a Program of Excellence in Nanotechnology (NHLBI-PEN HL080729) is acknowledged.

To my parents

TABLE OF CONTENTS

LIST OF FIGURES

Chapter 4

Chapter 5

LIST OF SCHEMES

Chapter 1

Introduction

On December 29, 1959, at an American Physical Society meeting at the California Institute of Technology, physicist Dr. Richard Feynman gave birth to the concepts found in *nanotechnology* in his ground-breaking lecture *There's Plenty of Room at the Bottom* (*1*), and triggered the campaign to study and control matter over atomic and/or molecular scale. Feynman described a process by which the ability to manipulate individual atoms and molecules might be developed, using one set of precise tools to build and operate another proportionally smaller set, and so on down to the needed scale. Later in the 1980s, this basic idea was explored in much more depth by Dr. K. Eric Drexler, who promoted the technological significance of nano-scale phenomena and devices through lectures and the books *Engines of Creation: The Coming Era of Nanotechnology* (1986) and *Nanosystems: Molecular Machinery, Manufacturing, and Computation* (1991), and so the term acquired its current sense. Nanotechnology gained momentum in the early 1980s with two major developments: the birth of cluster science and the invention of the scanning tunneling microscope (STM). Ever since, nanotechnology enjoyed rapid growth in academic and industrial laboratories, across disciplines, through the efforts and devotion from several generations of scientific researchers and has become a robust and well-accepted scientific field. Meanwhile, profound impacts of nanoscience and technology have been growing explosively worldwide in manufacturing and scientific research, such as miniaturization of electronic

and memory devices, design and synthesis of more robust and efficient catalysts, development of more accurate and effective diagnostic procedures, and exploration of "smart" drugs that recognize and attack only the diseased regions.

Two main approaches are used in nanotechnology. In the "bottom-up" approach, materials and devices are built from molecular components which assemble themselves chemically by principles of molecular recognition (*2-10*). In the "top-down" approach, nanostructures are constructed from larger entities without atomic level control, using physical and lithographical techniques (*11-18*). Both approaches provide specific capacities that can be complemented by the other (*19-23*). Nature achieved the very summit of nanostructure creation through the "bottom-up" approach. The self assembly of polypeptides into proteins with intricate supramolecular structures and specific functionalities represents one of the most elegant manners in the construction of complex nanostructures. This phenomenon not only proves that nanoscale synthesis and control is possible, but also inspires scientists to exploit Nature-mimicking nanoscale materials having unique optical, electrical, catalytic, and biological properties (*24-26*). By synthetically preparing molecules that interact with each other through weak non-covalent interactions, which included van der Waals, electrostatic, hydrophobic interactions, hydrogen and coordination bonds (*27-31*), various kinds of nanostructures can be assembled *via* a balanced reversible process (*32-34*). These nano-assemblies exhibit diverse non-spherical morphologies, such as belt (*35*), cylinder (*36*), fiber (*37-40*), helix (*41-43*), lamella (*44*), and vesicle (*45-47*), depending upon the intrinsic compositions and physical properties of the molecular constituent and its environment during the assembly process.

Among the many kinds of synthetic molecules that can undergo self-assembly, amphiphilic block copolymers have attracted significant attention recently from both academic and industrial investigators (*48-50*). Many interesting/beneficial properties are offered by amphiphilic block copolymer systems: facile tuning of dimensions, compositions, and components; ability to introduce of functionalities; large phase segregation tendency (*51-52*) and slow assembly kinetics (*53*).

Advances in living polymerization techniques, especially the development of controlled radical polymerizations (CRP) (*54*), have dramatically improved the availability of well-defined block copolymers, thereby enriching the types of nanoassemblies that can be prepared, studied and used. Using atom transfer radical polymerizations (ATRP) (*55-58*), a type of CRP independently discovered by Mitsuo Sawamoto and Krzysztof Matyjaszewki in 1995, various kinds of polymers having narrow molecular weight distributions, controlled architectures and chemical compositions can be produced. These polymers may be further processed or modified to incorporate desired functionalities (*59*). A wide range of conventional and unconventional morphologies have been prepared from these block copolymers, such as cylinders (*60-69*), vesicles (*70-80*), segmented rods (*81*), bowls (*82*), discs (*83*), helices (*84*) and toroids (*85*). The versatility in morphology, composition and particle size of these polymer-based nanoparticles offer a rich selection of building blocks for the construction of higher-level, more complex and/or hierarchical nanostructured materials for use in biomedical applications.

The impact of nanotechnology in healthcare resulted in a specific field – *Nanomedicine* (*86-93*), the medical applications of nanotechnology to improve the

performance of existing therapeutic and diagnostic modalities and to establish novel modalities for diagnostics, treatment, and therapy of diseases. Block copolymer-based micelles (*94-106*) have already been widely studied in nanomedicine and found promising applications in both therapeutic delivery and diagnostics. However, such self-assembled entities are equilibrium products formed in solution. Once diluted below critical micelle concentrations (usually at the order of 10^{-7} M), collapsing of their ordered structures and re-organization into unimers (amphiphilic block copolymer precursor) becomes thermodynamically favored. As a result, properties intrinsic to the nanoscale size are lost. Covalent (*107-112*) and non-covalent (*113*) crosslinkings have been introduced to these micellar assemblies to enhance their structural stability, resulting in several new classes of materials termed shell crosslinked knedel-like (SCK) nanoparticles, which remain stable under very dilution conditions. These SCKs have also been further decorated with different functionalities for *in vitro* and *in vivo* applications (*114-117*).

This dissertation is focused on the design, synthesis, and characterization of SCK nanostructures (spheres and cylinders) bearing different moieties that allowed for the targeted/non-targeted cell entry, DNA packaging and cell transfection, as well as the formation of complex, hierarchical nanostructures. Previous studies on poly(acrylic acid)-shelled SCKs that were functionalized with the protein transduction domain of human immunodeficiency virus type 1 Tat protein (HIV Tat PTD) suggest that these materials may potentially serve as diagnostic and therapeutic agents with cell entry capabilities (*118*). However, it was not well understood whether there is a particle size/shape preference to the mammalian cell. In order to probe the nanoparticle

shape/size effect on cellular uptake, a spherical and two cylindrical nanoparticles, whose lengths were distinctively varied, were constructed by the selective crosslinking of amphiphilic block copolymer micelles. In **Chapter 2**, it is demonstrated that, when the nanoparticles were functionalized with the protein transduction domain of human immunodeficiency virus type 1 Tat protein (HIV Tat PTD), the smaller, spherical nanoparticles had a higher rate of cell entry into Chinese Hamster Ovary (CHO) cells than did the larger, cylindrical nanoparticles. It was also found that nanoparticles were released after internalization, and that the rate of cell exit was dependent on both the nanoparticle shape and the amount of surface-bound PTD.

The PTD-assisted cell entry mechanism is known to be receptor-independent (*119*). As a result, larger structures with a higher surface area may not benefit from a multivalent effect, where one nanoparticle is attached to the cell at multiple receptor sites. On the contrary, receptor-dependent cell internalizations are affected to a great extent by the multivalent effect. It was, therefore, of interest to determine whether the trend observed in Chapter 2 is different for particles bearing not PTD, but ligands that can bind to cell surface receptors. **Chapter 3** reports the synthesis of spherical and cylindrical SCKs of exact physical sizes and shapes as those used in Chapter 2, but functionalized with folate using a poly(ethylene glycol) (PEG) that has folate and an amine group as the opposing chain termini. By use of confocal microscopy, it is demonstrated that the delivery of folate-conjugated SCKs are selective to human KB cells, a cell line that overexpresses the folate receptor (FR). A higher extent of polymer uptake by the cells occurred with the cylindrical SCK morphology, relative to the spherical SCKs, when both samples had the same fluorescein-5-thiosemicarbazide and polymer concentrations. In

both cases, by using excess free folic acid as a block or SCKs lacking the folate-PEG conjugate, cell uptake was significantly reduced. These results suggest that particle shape may play an important role in receptor-mediated cell uptake, and may be exploited in the targeted delivery of nanoscopic drugs.

These PTD- and folate-functionalized SCKs described in Chapters 2 and 3 may be further loaded with small molecule therapeutics in the shell and/or core of the nanoparticles, and be used for intracellular delivery in a systemic or specific fashion, respectively. However, the negatively-charged, poly(acrylic acid)-based shell of the SCK negates the notion of DNA packaging, which in recently years are being considered as a highly promising therapeutic that potentially could treat diseases currently considered incurable. Nature's material for DNA packaging and storage are the histones, which form disc-like nanoparticles of roughly 10 nm in diameter, around each of which 146 base pairs of DNA can wrap. Taking advantage of the concept of biomimicry, the SCKs were chemically altered to bear primary amines which could then be protonated to carry a positive charge for DNA packaging and transport, while being roughly the same size as a histone core particle. **Chapter 4** describes the detailed synthetic route for these cationic SCKs (cSCKs), and demonstrates that they are in fact efficient agents for cell transfection, comparing favorably with commercially available agents. The structure-activity relationship of the cSCK and cell transfection efficiency/cytotoxicity was further explored in **Chapter 5**, where it is shown that, through introduction of tertiary amine to the primary amine-containing shell of the cSCK, better release of DNA inside a cell can be achieved while maintaining sufficient buffering capacity, thereby significantly increasing cell transfection efficiency without increase in cytotoxicity.

Because DNA is native to humans and other organisms, its use as a therapeutic poses a safety risk. Moreover, DNA is readily degraded. As an alternative, peptide nucleic acids (PNAs) have been developed as a functional replacement of oligo DNAs. Carrying a peptidyl backbone, PNAs have a number of features that make them an ideal platform for use as DNA replacements, such as higher binding affinity and stability towards enzymatic degradation. Unfortunately, their inability to pass through membranes has limited their *in vivo* application as diagnostic and therapeutic agents. In **Chapter 6**, two strategies involving the use of the cSCKs as PNA delivery vehicles are described. PNAs are associated with the cSCKs either through electrostatic complexation with a PNA•ODN hybrid, or through a bioreductively-cleavable disulfide linkage. These delivery systems are better than the standard lipofectamine/ODN-mediated method and much better than the Arg_9-mediated method for PNA delivery in HeLa cells, showing lower toxicity and higher bioactivity. The cSCKs were also found to facilitate both endocytosis and endosomal release of the PNAs, while themselves remaining trapped in the endosomes

In the last part of this dissertation, **Chapter 7**, a "bottom-up" approach was utilized to construct hierarchical, complex nanoparticles using cSCKs and cylindrical SCKs as building blocks. These composite materials are well-defined, hierarchically-organized nanoscale objects of a cylindrical form and core-shell morphology, having an outer coating of cationic shell-crosslinked cSCK. In addition to standard characterization techniques, a fluorescent resonance energy transfer (FRET) experiment was designed and used to study the coating of anionic cylinders by cationic spheres. Expedited HeLa cell uptake was observed for the composite nanostructures compared with the non-coated

cylinders, indicating that this simple assembly strategy is a facile method to allow the secondary structure to inherit properties from its individual building blocks.

Nanotechnology holds significant promise in advancing the field of medicine. With increased understanding of the molecular mechanisms of the human body, nanoscale, targeted drugs are being developed, and many have become available for clinical application. Some of these drugs function by *intracellularly* manipulating the cells' protein function/expression, signal transduction or genetic make-up, by means of delivering small molecule binders, intercalators, proteins, DNAs or synthetic macromolecules such as PNAs into the cell. It is assumed that the nanoparticles themselves must be able to undergo cell entry in order for them to perform as guest-delivery systems. The following chapter will begin the discussion of nanoscale delivery vehicles by introducing PTD-functionalized SCKs.

References

(1) Feynman, R. P. (1960) There's plenty of room at the bottom. *Eng. Sci. 23*, 22-36.

(2) Chaterji, S., Kwon, I. K., and Park, K. (2007) Smart polymeric gels: Redefining the limits of biomedical devices. *Prog. Polym. Sci. 32*, 1083-1122.

(3) Lu, W., and Lieber Charles, M. (2007) Nanoelectronics from the bottom up. *Nature Mater. 6*, 841-50.

(4) Perepichka, D. F., and Rosei, F. (2007) Metal nanoparticles: from "artificial atoms" to "artificial molecules". *Angew. Chem., Int. Ed. 46*, 6006-6008.

(5) Sada, K., Takeuchi, M., Fujita, N., Numata, M., and Shinkai, S. (2007) Post-polymerization of preorganized assemblies for creating shape-controlled functional materials. *Chem. Soc. Rev. 36*, 415-435.

(6) Xu, H., Srivastava, S., and Rotello, V. M. (2007) Nanocomposites based on hydrogen bonds. *Adv. Polym. Sci. 207*, 179-198.

(7) Bonderer, L. J., Studart, A. R., and Gauckler, L. J. (2008) Bioinspired design and assembly of platelet reinforced polymer films. *Science 319*, 1069-1073.

(8) Tait, S. L. (2008) Function follows form: Exploring two-dimensional supramolecular assembly at surfaces. *ACS Nano 2*, 617-621.

(9) Zabet-Khosousi, A., and Dhirani, A.-A. (2008) Charge Transport in nanoparticle assemblies. *Chem. Rev. 108*, 4072-4124.

(10) Gale, P. A. (2007) *Royal Society Series on Advances in Science*.

(11) Menard, E., Meitl, M. A., Sun, Y., Park, J.-U., Shir, D. J.-L., Nam, Y.-S., Jeon, S., and Rogers, J. A. (2007) Micro- and nanopatterning techniques for organic electronic and optoelectronic systems. *Chem. Rev. 107*, 1117-1160.

(12) Randall, C. L., Leong, T. G., Bassik, N., and Gracias, D. H. (2007) 3D lithographically fabricated nanoliter containers for drug delivery. *Adv. Drug Deliv. Rev. 59*, 1547-1561.

(13) Salaita, K., Wang, Y., and Mirkin, C. A. (2007) Applications of dip-pen nanolithography. *Nature Nanotechnol. 2*, 145-155.

(14) Gratton, S. E. A., Williams, S. S., Napier, M. E., Pohlhaus, P. D., Zhou, Z., Wiles, K. B., Maynor, B. W., Shen, C., Olafsen, T., Samulski, E. T., and DeSimone, J.

M. (2008) The pursuit of a scalable nanofabrication platform for use in material and life science applications. *Acc. Chem. Res.41*, 1685-1695.

(15) Nie, Z., and Kumacheva, E. (2008) Patterning surfaces with functional polymers. *Nature Mater. 7*, 277-290.

(16) Xu, Q., Rioux Robert, M., Dickey Michael, D., and Whitesides George, M. (2008) Nanoskiving: a new method to produce arrays of nanostructures. *Acc. Chem. Res. 41*, 1566-77.

(17) Cavallini, M., Albonetti, C., and Biscarini, F. (2009) Nanopatterning soluble multifunctional materials by unconventional wet lithography. *Adv. Mater. 21*, 1043-1053.

(18) Yang, K.-Y., Kim, J.-W., Byeon, K.-J., Lee, H.-C., and Lee, H. (2009) Fabrication of 70 nm-sized zero residual polymer patterns by thermal nanoimprint lithography. *J. Nanosci. Nanotech. 9*, 5887-5890.

(19) Cheng, J. Y., Ross, C. A., Smith, H. I., and Thomas, E. L. (2006) Templated self-assembly of block copolymers: top-down helps bottom-up. *Adv. Mater. 18*, 2505-2521.

(20) Black, C. T. (2007) Polymer self-assembly as a novel extension to optical lithography. *ACS Nano 1*, 147-150.

(21) Darling, S. B. (2007) Directing the self-assembly of block copolymers. *Prog. Polym. Sci. 32*, 1152-1204.

(22) Huck, W. T. S. (2007) Self-assembly meets nanofabrication: recent developments in microcontact printing and dip-pen nanolithography. *Angew. Chem., Int. Ed. 46*, 2754-2757.

(23) Segalman, R. A. (2008) Directing self-assembly toward perfection. *Science 321*, 919-920.

(24) Pelesko, J. A. (2007) *Self Assembly: The Science of Things That Put Themselves Together*, Chapman & Hall/CRC, Boca Raton.

(25) Lee, Y. S. (2007) *Self-assembly and Nanotechnology: A force balance approach*, John Wiley & Sons, Inc., Hoboken.

(26) Jang, W.-D., Kamruzzaman Selim, K. M., Lee, C.-H., and Kang, I.-K. (2009) Bioinspired application of dendrimers: from bio-mimicry to biomedical applications. *Prog. Polym. Sci. 34*, 1-23.

(27) Raymo, F. M., Bartberger, M. D., Houk, K. N., and Stoddart, J. F. (2001) The magnitude of [C-H center dot center dot center dot O] hydrogen bonding in molecular and supramolecular assemblies. *J. Am. Chem. Soc. 123*, 9264-9267.

(28) Tsonchev, S., Schatz, G. C., and Ratner, M. A. (2003) Hydrophobically-driven self-assembly: A geometric packing analysis. *Nano Lett. 3*, 623-626.

(29) Stendahl, J. C., Rao, M. S., Guler, M. O., and Stupp, S. I. (2006) Intermolecular forces in the self-assembly of peptide amphiphile nanofibers. *Adv. Funct. Mater. 16*, 499-508.

(30) Schatz, G. C. (2007) Using theory and computation to model nanoscale properties. *Proc. Natl. Acad. Sci. USA 104*, 6885-6892.

(31) Chen, C. L., Zhang, P. J., and Rosi, N. L. (2008) A new peptide-based method for the design and synthesis of nanoparticle superstructures: Construction of highly ordered gold nanoparticle double helices. *J. Am. Chem. Soc. 130*, 13555-13557.

(32) Lehn, J.-M. (2002) Toward self-organization and complex matter. *Science 295*, 2400-2403.

(33) Whitesides, G. M., and Grzybowski, B. (2002) Self-assembly at all scales. *Science 295*, 2418-2421.

(34) Hamley, I. W. (2003) Nanotechnology with soft materials. *Angew. Chem., Int. Ed. 42*, 1692-1712.

(35) Cui, H., Muraoka, T., Cheetham, A. G., and Stupp, S. I. (2009) Self-assembly of giant peptide nanobelts. *Nano Lett. 9*, 945-951.

(36) Prehm, M., Liu, F., Baumeister, U., Zeng, X. B., Ungar, G., and Tschierske, C. (2007) The Giant-Hexagon cylinder network - A liquid-crystalline organization formed by a T-shaped quaternary amphiphile. *Angew. Chem., Int. Ed. 46*, 7972-7975.

(37) Hartgerink, J. D., Beniash, E., and Stupp, S. I. (2001) Self-assembly and mineralization of peptide-amphiphile nanofibers. *Science 294*, 1684-1688.

(38) Velonia, K., Rowan, A. E., and Nolte, R. J. M. (2002) Lipase polystyrene giant amphiphiles. *J. Am. Chem. Soc. 124*, 4224-4225.

(39) Guler, M. O., and Stupp, S. I. (2007) A self-assembled nanofiber catalyst for ester hydrolysis. *J. Am. Chem. Soc. 129*, 12082-12083.

(40) Shao, H., and Parquette, J. R. (2009) Controllable peptide-dendron self-assembly: Interconversion of nanotubes and fibrillar nanostructures. *Angew. Chem., Int. Ed. 48*, 2525-2528.

(41) Berl, V., Huc, I., Khoury, R. G., Krische, M. J., and Lehn, J. M. (2000) Interconversion of single and double helices formed from synthetic molecular strands. *Nature 407*, 720-723.

(42) Percec, V., Dulcey, A. E., Balagurusamy, V. S. K., Miura, Y., Smidrkal, J., Peterca, M., Nummelin, S., Edlund, U., Hudson, S. D., Heiney, P. A., Hu, D. A., Magonov, S. N., and Vinogradov, S. A. (2004) Self-assembly of amphiphilic dendritic dipeptides into helical pores. *Nature 430*, 764-768.

(43) Iwaura, R., Hoeben, F. J. M., Masuda, M., Schenning, A., Meijer, E. W., and Shimizu, T. (2006) Molecular-level helical stack of a nucleotide-appended oligo(p-phenylenevinylene) directed by supramolecular self-assembly with a complementary oligonucleotide as a template. *J. Am. Chem. Soc. 128*, 13298-13304.

(44) Lamm, M. S., Rajagopal, K., Schneider, J. P., and Pochan, D. J. (2005) Laminated morphology of nontwisting beta-sheet fibrils constructed via peptide self-assembly. *J. Am. Chem. Soc. 127*, 16692-16700.

(45) Holowka, E. P., Pochan, D. J., and Deming, T. J. (2005) Charged polypeptide vesicles with controllable diameter. *J. Am. Chem. Soc. 127*, 12423-12428.

(46) Yan, X. H., He, Q., Wang, K. W., Duan, L., Cui, Y., and Li, J. B. (2007) Transition of cationic dipeptide nanotubes into vesicles and oligonucleotide delivery. *Angew. Chem., Int. Ed. 46*, 2431-2434.

(47) Schatz, C., Louguet, S., Le Meins, J. F., and Lecommandoux, S. (2009) Polysaccharide-block-polypeptide copolymer vesicles: towards synthetic viral capsids. *Angew. Chem., Int. Ed. 48*, 2572-2575.

(48) Calleja, F. J. B., Roslaniec, Z. (2000) *Block Copolymers*, Marcel Dekker, New York.

(49) Hadjichristidis, N., Pispas., Floudas, G. (2003) *Block copolymers: Synthetic strategies, physical properties and applications*, Wiley-Interscience, New York.

(50) Lazzari, M., Liu, G., Lecommandoux, S. (2006) *Block Copolymers in Nanoscience*, Wiley-VCH, Weinheim.

(51) de Gennes, P. G. (1979) *Scaling concerpts in polymer physics*, Cornell University Press, Ithaca.

(52) Hamley, I. W. (2005) *Block Copolymers in solution: Fundamentals and applications*, John Wiley & Sons, West Sussex.

(53) Hashimoto, T. (2005) "Mechanics" of molecular assembly: Real-time and in-situ analysis of nano-to-mesoscopic scale hierarchical structures and nonequilibrium phenomena. *Bull. Chem. Soc. Jpn. 78*, 1-39.

(54) Braunecker, W. A., and Matyjaszewski, K. (2007) Controlled/living radical polymerization: Features, developments, and perspectives. *Prog. Polym. Sci. 32*, 93-146.

(55) Tsarevsky, N. V., and Matyjaszewski, K. (2007) "Green" atom transfer radical polymerization: From process design to preparation of well-defined environmentally friendly polymeric materials. *Chem. Rev. 107*, 2270-2299.

(56) Matyjaszewski, K., and Xia, J. H. (2001) Atom transfer radical polymerization. *Chem. Rev. 101*, 2921-2990.

(57) Wang, J.-S., and Matyjaszewski, K. (1995) Controlled/"living" radical polymerization: atom transfer radical polymerization in the presence of transition-metal complexes. *J. Am. Chem. Soc. 117*, 5614-5615.

(58) Kato, M., Mamigato, M., Sawamoto, M., and Higashimura, T. (1995) Polymerization of methyl methacrylate with the carbon tetrachloride / dichlorotris-(triphenylphosphine)ruthenium(II) / methylaluminum bis(2,6-di-tert-butylphenoxide) initiating system: possibility of living radical polymerization *Macromolecules 28*, 1721.

(59) Klok, H.-A., Gibson, M. I., and Gauthier, M. A. (2009) Post-polymerization modification. *Angew. Chem., Int. Ed. 48*, 48-58.

(60) Won, Y.-Y., Davis, H. T., and Bates, F. S. (1999) Giant wormlike rubber micelles. *Science 283*, 960-963.

(61) Geng, Y., and Discher, D. E. (2005) Hydrolytic degradation of poly(ethylene oxide)-*block*-polycaprolactone worm micelles. *J. Am. Chem. Soc. 127*, 12780-12781.

(62) Cui, H., Chen, Z., Zhong, S., Wooley, K. L., and Pochan, D. J. (2007) Block copolymer assembly via kinetic control. *Science 317*, 647-650.

(63) Wang, X., Guerin, G., Wang, H., Wang, Y., Manners, I., and Winnik, M. A. (2007) Cylindrical block copolymer micelles and co-micelles of controlled length and architecture. *Science 317*, 644-647.

(64) Njikang, G., Han, D., Wang, J., and Liu, G. (2008) ABC Triblock copolymer micelle-like aggregates in selective solvents for A and C. *Macromolecules 41*, 9727-9735.

(65) Saito, N., Liu, C., Lodge, T. P., and Hillmyer, M. A. (2008) Multicompartment micelles from polyester-containing ABC miktoarm star terpolymers. *Macromolecules 41*, 8815-8822.

(66) Zhu, J., and Hayward, R. C. (2008) Wormlike micelles with microphase-separated cores from blends of amphiphilic AB and hydrophobic BC diblock copolymers. *Macromolecules 41*, 7794-7797.

(67) Geng, Y., Dalhaimer, P., Cai, S., Tsai, R., Tewari, M., Miniko, T., and Discher, D. E. (2007) Shape effects of filaments *versus* spherical particles in flow and drug delivery. *Nature Nanotechnol. 2*, 249-255.

(68) Cui, H., Chen, Z., Wooley, K. L., and Pochan, D. J. (2006) Controlling micellar structure of amphiphilic charged triblock copolymers in dilute solution *via* coassembly with organic counterions of different spacer lengths. *Macromolecules 39*, 6599-6607.

(69) Hamley, I. (2005) Nanoshells and nanotubes from block copolymers. *Soft Matter 1*, 36-43.

(70) Zhang, L., and Eisenberg, A. (1996) Multiple morphologies and characteristics of "crew-cut" micelle-like aggregates of polystyrene-*b*-poly(acrylic acid) diblock copolymers in aqueous solutions. *J. Am. Chem. Soc. 118*, 3168-3181.

(71) Ding, J., and Liu, G. (1998) Water-soluble hollow nanospheres as potential drug carriers. *J. Phys. Chem. B 102*, 6107-6113.

(72) Discher, B. M., Won, Y.-Y., Ege, D. S., Lee, J. C. M., Bates, F. S., Discher, D. E., and Hammer, D. A. (1999) Polymersomes: Tough vesicles made from diblock copolymers. *Science 284*, 1143-1146.

(73) Napoli, A., Valentini, M., Tirelli, N., Muller, M., and Hubbell, J. A. (2004) Oxidation-responsive polymeric vesicles. *Nature Mater. 3*, 183-189.

(74) Power-Billard, K. N., Spontak, R. J., and Manners, I. (2004) Redox-active organometallic vesicles: aqueous self-assembly of a diblock copolymer with a hydrophilic polyferrocenylsilane polyelectrolyte block. *Angew. Chem., Int. Ed. 43*, 1260-1264.

(75) Koide, A., Kishimura, A., Osada, K., Jang, W. D., Yamasaki, Y., and Kataoka, K. (2006) Semipermeable Polymer Vesicle (PICsome) Self-assembled in aqueous medium from a pair of oppositely charged block copolymers: physiologically stable micro-/nanocontainers of water-soluble macromolecules. *J. Am. Chem. Soc. 128*, 5988-5989.

(76) Li, Y., Lokitz, B. S., and McCormick, C. L. (2006) Thermally responsive vesicles and their structural "locking" through polyelectrolyte complex formation. *Angew. Chem., Int. Ed. 45*, 5792-5795.

(77) Qin, S., Geng, Y., Discher, D. E., and Yang, S. (2006) Temperature-controlled assembly and release from polymer vesicles of poly(ethylene oxide)-block-poly(N-isopropylacrylamide). *Adv. Mater. 18*, 2905-2909.

(78) Zheng, R., and Liu, G. (2007) Water-dispersible oil-filled ABC triblock copolymer vesicles and nanocapsules. *Macromolecules 40*, 5116-5121.

(79) Pasparakis, G., and Alexander, C. (2008) Sweet talking double hydrophilic block copolymer vesicles. *Angew. Chem., Int. Ed. 47*, 4847-4850.

(80) Walther, A., Goldmann, A. S., Yelamanchili, R. S., Drechsler, M., Schmalz, H., Eisenberg, A., and Muller, A. H. E. (2008) Multiple morphologies, phase

transitions, and cross-linking of crew-cut aggregates of polybutadiene-block-poly(2-vinylpyridine) diblock copolymers. *Macromolecules 41*, 3254-3260.

(81) Chen, T., Wang, L., Jiang, G., Wang, J., Wang, X. j., Zhou, J., Wang, W., and Gao, H. (2005) Large-size bamboo-shape nanotube from self-assembly of poly(ferrocenyldimethylsilane-*b*-dimethylsiloxane) block copolymer. *Polym. 46*, 7585-7589.

(82) Liu, X., Kim, J.-S., Wu, J., and Eisenberg, A. (2005) Bowl-Shaped Aggregates from the Self-assembly of an Amphiphilic Random Copolymer of Poly(styrene-*co*-methacrylic acid). *Macromolecules 38*, 6749-6751.

(83) Li, Z., Chen, Z., Cui, H., Hales, K., Qi, K., Wooley, K. L., and Pochan, D. J. (2005) Disk morphology and disk-to-cylinder tunability of poly(acrylic acid)-*b*-poly(methyl acrylate)-*b*-polystyrene triblock copolymer solution-state assemblies. *Langmuir 21*, 7533-7539.

(84) Zhong, S., Cui, H., Chen, Z., Wooley, K. L., and Pochan, D. J. (2008) Helix self-assembly through the coiling of cylindrical micelles. *Soft Matter 4*, 90-93.

(85) Pochan, D. J., Chen, Z. Y., Cui, H. G., Hales, K., Qi, K., and Wooley, K. L. (2004) Toroidal triblock copolymer assemblies. *Science 306*, 94-97.

(86) Moghimi, S. M., Hunter, A. C., and Murray, J. C. (2005) Nanomedicine: current status and future prospects. *FASEB J. 19*, 311-330.

(87) Farokhzad, O. C., and Langer, R. (2006) Nanomedicine: Developing smarter therapeutic and diagnostic modalities. *Adv. Drug Deliv. Rev. 58*, 1456-1459.

(88) Liu, Y. Y., Miyoshi, H., and Nakamura, M. (2007) Nanomedicine for drug delivery and imaging: A promising avenue for cancer therapy and diagnosis using targeted functional nanoparticles. *Int. J. Cancer 120*, 2527-2537.

(89) Jain, K. K. (2008) Nanomedicine: Application of nanobiotechnology in medical practice. *Med. Princ. Pract. 17*, 89-101.

(90) Venugopal, J., Prabhakaran, M. P., Low, S., Choon, A. T., Zhang, Y. Z., Deepika, G., and Ramakrishna, S. (2008) Nanotechnology for nanomedicine and delivery of drugs. *Curr. Pharm. Des. 14*, 2184-2200.

(91) Farokhzad, O. C., and Langer, R. (2009) Impact of nanotechnology on drug delivery. *ACS Nano 3*, 16-20.

(92) Riehemann, K., Schneider, S. W., Luger, T. A., Godin, B., Ferrari, M., and Fuchs, H. (2009) Nanomedicine-challenge and perspectives. *Angew. Chem., Int. Ed. 48*, 872-897.

(93) Sandhiya, S., Dkhar, S. A., and Surendiran, A. (2009) Emerging trends of nanomedicine - an overview. *Fundam. Clin. Pharmacol. 23*, 263-269.

(94) Rosler, A., Vandermeulen, G. W. M., and Klok, H. A. (2001) Advanced drug delivery devices via self-assembly of amphiphilic block copolymers. *Adv. Drug Deliv. Rev. 53*, 95-108.

(95) Lavasanifar, A., Samuel, J., and Kwon, G. S. (2002) Poly(ethylene oxide)-block-poly(L-amino acid) micelles for drug delivery. *Adv. Drug Deliv. Rev. 54*, 169-190.

(96) Harada, A., and Kataoka, K. (2006) Supramolecular assemblies of block copolymers in aqueous media as nanocontainers relevant to biological applications. *Prog. Polym. Sci. 31*, 949-982.

(97) Letchford, K., and Burt, H. (2007) A review of the formation and classification of amphiphilic block copolymer nanoparticulate structures: micelles, nanospheres, nanocapsules and polymersomes. *Eur. J. Pharm. Biopharm. 65*, 259-269.

(98) Torchilin, V. P. (2007) Micellar nanocarriers: Pharmaceutical perspectives. *Pharm. Res. 24*, 1-16.

(99) Blanazs, A., Armes, S. P., and Ryan, A. J. (2009) Self-assembled block copolymer aggregates: From micelles to vesicles and their biological applications. *Macromol. Rapid Commun. 30*, 267-277.

(100) Soussan, E., Cassel, S., Blanzat, M., and Rico-Lattes, I. (2009) Drug delivery by soft matter: Matrix and vesicular carriers. *Angew. Chem., Int. Ed. 48*, 274-288.

(101) Discher, D. E., and Ahmed, F. (2006) Polymersomes. *Annu. Rev. Biomed. Eng. 8*, 323-341.

(102) Discher, D. E., Ortiz, V., Srinivas, G., Klein, M. L., Kim, Y., Christian, D., Cai, S., Photos, P., and Ahmed, F. (2007) Emerging applications of polymersomes in delivery: From molecular dynamics to shrinkage of tumors. *Prog. Polym. Sci. 32*, 838-857.

(103) Kanayama, N., Fukushima, S., Nishiyama, N., Itaka, K., Jang, W.-D., Miyata, K., Yamasaki, Y., Chung, U.-i., and Kataoka, K. (2006) A PEG-based biocompatible block catiomer with high buffering capacity for the construction of polyplex

micelles showing efficient gene transfer toward primary cells. *ChemMedChem 1*, 439-444.

(104) Akagi, D., Oba, M., Koyama, H., Nishiyama, N., Fukushima, S., Miyata, T., Nagawa, H., and Kataoka, K. (2007) Biocompatible micellar nanovectors achieve efficient gene transfer to vascular lesions without cytotoxicity and thrombus formation. *Gene Ther. 14*, 1029-1038.

(105) Read, E. S., and Armes, S. P. (2007) Recent advances in shell cross-linked micelles. *Chem. Commun. 29*, 3021-3035.

(106) Lee, Y., Ishii, T., Cabral, H., Kim, H. J., Seo, J.-H., Nishiyama, N., Oshima, H., Osada, K., and Kataoka, K. (2009) Charge-conversion polyionic complex micelles - efficient nanocarriers for protein delivery into cytoplasm. *Angew. Chem., Int. Ed. 48*, 5309-5312.

(107) Thurmond, K. B., II, Kowalewski, T., and Wooley, K. L. (1996) Water-soluble knedel-like structures: The preparation of shell-cross-linked small particles. *J. Am. Chem. Soc. 118*, 7239-7240.

(108) Huang, H., Kowalewski, T., Remsen, E. E., Gertzmann, R., and Wooley, K. L. (1997) Hydrogel-coated glassy nanospheres: A novel method for the synthesis of shell crosslinked knedels. *J. Am. Chem. Soc. 119*, 11653-11659.

(109) Bütün, V., Billingham, N. C., and Armes, S. P. (1998) Synthesis of shell cross-linked micelles with tunable hydrophilic/hydrophobic cores. *J. Am. Chem. Soc. 120*, 12135-12136.

(110) Ding, J., and Liu, G. (1998) Polystyrene-block-poly(2-cinnamoylethyl methacrylate) nanospheres with cross-linked shells. *Macromolecules 31*, 6554-6558.

(111) Sanji, T., Nakatsuka, Y., Ohnishi, S., and Sakurai, H. (2000) Preparation of nanometer-sized hollow particles by photochemical degradation of polysilane shell cross-linked micelles and reversible encapsulation of guest molecules. *Macromolecules 33*, 8524-8526.

(112) Zhang, Z., Liu, G., and Bell, S. (2000) Synthesis of poly(solketal methacrylate)-*block*-poly(2-(dimethylamino)ethyl methacrylate) and preparation of nanospheres with cross-linked shells. *Macromolecules 33*, 7877-7883.

(113) Chen, D., and Jiang, M. (2005) Strategies for constructing polymeric micelles and hollow spheres in solution via specific intermolecular interactions. *Acc. Chem. Res. 38*, 494-502.

(114) Li, Y., Sun, G., Xu, J., and Wooley, K. L. (2007) Shell crosslinked nanoparticles: A progress report of their design for drug delivery, in *Nanotechnology in Therapeutics: Current technology and applications* (Peppas, N. A., Hilt, Z. J., and Thomas, B. J., Eds.) pp 381-407, Horizon Bioscience, Norfolk.

(115) Rossin, R., Pan, D., Qi, K., Turner, J. L., Sun, X., Wooley, K. L., and Welch, M. J. (2005) ^{64}Cu-labeled folate-conjugated shell cross-linked nanoparticles for tumor imaging and radiotherapy: Synthesis, radiolabeling, and biologic evaluation. *J. Nucl. Med. 46*, 1210-1218.

(116) Pan, D., Turner, J. L., and Wooley, K. L. (2004) Shell cross-linked nanoparticles designed to target angiogenic blood vessels *via* $\alpha_v\beta_3$ receptor-ligand interactions. *Macromolecules 37*, 7109-7115.

(117) Turner, J. L., Pan, D., Plummer, R., Chen, Z., Whittaker, A. K., and Wooley, K. L. (2005) Synthesis of gadolinium-labeled shell-crosslinked nanoparticles for magnetic resonance imaging applications. *Adv. Funct. Mater. 15*, 1248-1254.

(118) Becker, M. L., Remsen, E. E., Pan, D., and Wooley, K. L. (2004) Peptide-derivatized shell-cross-linked nanoparticles. 1. Synthesis and characterization. *Bioconjugate Chem. 15*, 699-709.

(119) Duchardt, F., Fotin-Mleczek, M., Schwarz, H., Fischer, R., and Brock, R. (2007) A comprehensive model for the cellular uptake of cationic cell-penetrating peptides. *Traffic 8*, 848-866.

Chapter 2

Shape effects of nanoparticles conjugated with cell-penetrating peptides (HIV Tat PTD) on CHO cell uptake

[Portions of this work have been published previously as Ke Zhang, Huafeng Fang, Zhiyun Chen, John-Stephen A. Taylor and Karen L. Wooley *Bioconjugate Chem.* **2007**, 19(9), 1880-1887.]

Abstract

In order to probe the nanoparticle shape/size effect on cellular uptake, a spherical and two cylindrical nanoparticles, whose lengths were distinctively varied, were constructed by the selective crosslinking of amphiphilic block copolymer micelles. Herein, we demonstrate that, when the nanoparticles were functionalized with the protein transduction domain of human immunodeficiency virus type 1 Tat protein (HIV Tat PTD), the smaller, spherical nanoparticles had a higher rate of cell entry into Chinese Hamster Ovary (CHO) cells than did the larger, cylindrical nanoparticles. It was also found that nanoparticles were released after internalization, and that the rate of cell exit was dependent on both the nanoparticle shape and the amount of surface-bound PTD.

Introduction

The plasma membrane of a cell serves as one of the major barriers against inward transportation of extraneous materials, such as a gene and/or a nanoscale synthetic delivery system. Modern synthetic designs have incorporated various cell-penetrating peptides (CPPs), borrowed initially from virus particles, to facilitate their uptake by cells through a receptor-independent pathway (*1*), whose mechanism is not yet completely understood. The ability of a nanostructure to translocate across the cell plasma membrane is of fundamental and practical interest, and will determine the possible outcomes of the nanomaterial in a biological context. Nanostructures of various sizes, shapes and chemical compositions have gained access to the cell's interior with or without the assistance of CPPs, including metal nanoparticles (*2*), dendrimers (*3*), liposomes (*4*), single-walled carbon nanotubes (*5*), and virus-mimics (*6*), etc. However, the amount of assistance provided by the CPPs for the nanoparticles to be internalized by a cell may be limited (*7*); eventually the influence of the size and geometric features of the cargo will become increasingly important. Recently, Chan *et al* (*2, 8*) probed the effects of size and shape, for penetratin-coated gold nanoparticles within the 10-100 nm range, on the endo- and exocytosis by mammalian cells. A non-linear relationship between size and uptake was found, and 50 nm spherical particles were identified as having the highest cell uptake. On the micrometer scale, Mitragotri *et al* investigated the shape effect by synthesizing a variety of geometrically-anisotropic polystyrene particles, whose phagocytosis rates were found to be strongly dependent on the shape of the microparticle (*9*). However, a study to compare across the 10-1000 nm region using particles of similar chemical nature is still unavailable. The mechanism of CPP-assisted

cell internalization of the cylindrical structure (several μm in length), which was recently discovered to enhance *in vivo* circulation times much beyond that which can be achieved by other morphologies (*10*), remains largely unknown. It is, therefore, of interest to bridge the gap between nanoscale and microscale structures, in terms of comparing and understanding their CPP-assisted cell uptake and release.

Advances in the design and synthesis of well-controlled block copolymers have given rise to the rapid growth of a new class of complex nanostructures having various compositions, morphologies, sizes, and physical and biological properties (*11-13*), which can serve as the primary materials for examination of the effects of nano- to microstructure size and shape on cell internalization. For example, shell-crosslinked assemblies of amphiphilic block copolymers have in recent years attracted researchers to explore their biological and medicinal uses (*14-17*). These shell-crosslinked nanoparticles have enhanced stability compared to micelles and are capable of carrying biologically-active molecules, which drastically change the biological behavior of the nanoparticles (*15, 18*). In this work, we take advantage of the vast array of morphologies available to polymer micelle-based nanoparticles (*19-23*) and their ability to allow for chemical modifications (*24-25*) in order to study the shape and size effects of a nanoscopic particle in a cellular system.

Herein, we report a method to create spherical and cylindrical nanostructures, of different lengths, from self assembly of block copolymers. After functionalizing the nanostructures with the protein transduction domain of human immunodeficiency virus type 1 Tat protein (HIV Tat PTD, one commonly used CPP, having the sequence: GYGRKKRRQRRR), we demonstrate that the smaller spherical particles (on the 10 nm

scale) are internalized by CHO cells faster than are the larger cylindrical particles (20 or 30 nm diameters and larger than 200 nm in one dimension). It is also shown that, upon cellular uptake, the spherical particles are released from the cell, and the rate of release is also dependent on the amount of PTD loading.

Experimental Procedures

Polymer synthesis. All polymers used in this study were synthesized by atom transfer radical polymerization, according to literature procedures (*26*).

Peptide synthesis. The ivDde-protected HIV Tat PTD peptide (sequence: GGYGRK(ivDde)K(ivDde)RRQRRR) was synthesized manually by standard Fmoc solid-phase chemistry. The two ivDde protecting groups for lysine were intentionally left on the peptide prior to and following cleavage from the solid support, using 95% trifluoroacetic acid : 2.5% triisopropylsilane : 2.5% water solution (volume fractions) for 90 minutes. The beads were treated with cleavage solution 3 times total, and the solutions were combined and concentrated *in vacuo*. The concentrate was precipitated into cold ether, and the precipitates were centrifuged at 3500 rpm for 10 min. The supernatant was decanted, the pellet was resuspended in cold ether, and the centrifugation process was repeated. The pellet was purified by reversed phase HPLC. MS (MALDI-ToF): 2087.532 $[M + H]^+$ (calcd: 2087.529).

Spherical micelle formation. Spherical polymer micelles of narrow size distribution were obtained by dissolving the block copolymer PAA_{128}-*b*-PS_{40} (32.5 mg) in DMF (35 mL) followed by gradual addition (4 mL/h) of an equal volume of nonsolvent (H_2O) for the hydrophobic polystyrene to induce micellization. The micelles were stirred

for 4 h before being transferred to presoaked and rinsed dialysis bags (MWCO 6-8 kDa) and dialyzed against nanopure water (18.0 MΩ·cm) for 3 days to remove the organic solvent. The final volume was 115 mL of aqueous micelle solution for a final concentration of 0.28 mg/mL. TEM: 11 ± 2 nm (diameter).

Short cylindrical micelle formation. PAA_{96}-*b*-PS_{48} block copolymer (10 mg) was dissolved in THF (50 mL) and was dried in a round-bottom flask *in vacuo*, leaving a thin membrane of the polymer in the flask. To the flask, nanopure water (58.8 mL) was added and then sonicated while rotating in an aqueous sonicator (VMR Aquasonic 75T) for 40 min. The resulting solution contained short cylindrical micelles, which gave a light-blue color to the solution, a characteristic of the light scattering caused by the cylindrical micelle assemblies. The final concentration was 0.17 mg/mL. TEM: 180 ± 120 nm (length) and 20 ± 2 nm (cross-sectional diameter).

Shell-crosslinked spherical and short cylindrical nanoparticle formation. The aqueous solutions of spherical and short cylindrical micellar assemblies of PAA_{128}-*b*-PS_{40} and PAA_{96}-*b*-PS_{48}, respectively, were individually mixed with O-bis-(aminoethyl)ethylene glycol (0.15 equiv., relative to the molar number of available COOH groups) and allowed to stir at room temperature. After 30 min, an aqueous solution of 1-[3'-(dimethylamino)propyl]-3-ethylcarbodiimide hydrochloride (EDCI) (1 equiv., relative to the molar number of available COOH groups) was added. The reaction mixture was allowed to stir overnight before being transferred to presoaked and rinsed dialysis tubing (MWCO 3 kDa) and dialyzed against nanopure water (18.0 MΩ·cm) for 3 days.

Long cylindrical shell-crosslinked nanoparticle formation. To a solution of triblock copolymer PAA_{94}-*b*-PMA_{103}-*b*-PS_{28} (8.4 mg) in THF (8.00 mL) with stirring was added a solution of THF (2.0 mL) containing O-bis-(aminoethyl)ethylene glycol (0.93 mg, 0.15 equiv., relative to COOH groups). The mixture was allowed to stir overnight at room temperature, and then H_2O (40 mL) was added at a rate of 7.50 mL/h to induce micellization. To this water-THF mixture, EDCI (5.6 mg) was added to crosslink the shell domain of the micelle and to lock the morphology (*27*). The pre-mixing of the diamine crosslinker with the triblock copolymer is essential to the formation of the desired morphology (*19*). After stirring overnight, the reaction mixture was transferred to presoaked and rinsed dialysis tubing (MWCO 6-8 kDa) and dialyzed against nanopure water (18.0 MΩ·cm) for 3 days to remove the organic solvent. The final volume was 61.3 mL of aqueous crosslinked long, cylindrical micelle solution for a final concentration of 0.14 mg/mL. TEM: 970 ± 900 nm (length) and 30 ± 2 nm (cross-sectional diameter).

Functionalization with fluorescent tag. The respective shell-crosslinked nanoparticle solutions were diluted to the same molar concentration (7.5 μM polymer) and each was placed into a round-bottom flask and cooled to 0 ˚C using an ice bath. A mixed solution of 1:1, EDCI:N-hydroxysulfosuccinimide (sulfo-NHS) was added to each nanoparticle solution (1.2:1 molar ratio, relative to the available COOH groups) to activate the acrylic acid residues. After 30 minutes, aliquots of Alexa Fluor 594 cadaverine stock solution were added to each flask and the mixtures and were allowed to react overnight. The solutions were then transferred to presoaked dialysis tubing (MWCO 6-8 kDa) and allowed to dialyze for 5 days against nanopure water.

Functionalization with PTD. Shell-crosslinked nanoparticle solutions pre-functionalized with Alexa Fluor 594 were each placed into a 25 mL round-bottom flask. Sodium chloride was placed into each flask to give a concentration of 5.0 mg/mL, to minimize particle-particle aggregation. The flask was then placed in an ice bath. A mixed solution of 1:1, EDCI:sulfo-NHS was added to each nanoparticle solution (1.2:1 molar ratio, relative to the available COOH groups) to activate the acrylic acid residues. A stock solution (18.21 mg/mL) of the ivDde-protected PTD peptide was made in nanopure water, and aliquots of the solution were added to the respective flasks 30 min after the addition of EDCI/NHS. The pH of each reaction mixture was adjusted to 7.40 using pH = 8.00 sodium phosphate buffer. The mixtures were allowed to react overnight. The solutions were then transferred to presoaked dialysis tubings (MWCO 12 kDa) and allowed to dialyze for 5 days against nanopure water. At the end of dialysis, the nanoparticle solutions were treated with 2.0% hydrazine for 20 minutes to remove the ivDde protecting groups, and then the pH was adjusted to 6.50 using pH = 6.34 sodium phosphate buffer. The solutions were then transferred to presoaked dialysis tubings (MWCO 100 kDa) for a second-stage dialysis over a period of 15 days. UV-Vis measurements confirmed coupling of the PTD peptide to the shell-crosslinked nanostructures (*18*). Removal of the ivDde protecting groups under these reaction conditions was confirmed by MALDI-ToF mass spectrometry for a model reaction performed upon non-conjugated PTD peptide (Fig. 2-3).

Cell Line and Fluorescence Confocal Microscopy. Chinese hamster ovary (CHO) cells (ATCC) were cultured, counted, and resuspended to a final concentration of 100 000 cells/mL. An aliquot of the cell suspension (3.00 mL) was deposited into each

well of a tissue culture treated six-well plate (Falcon, 3043), which contained a No. 1.5 glass cover slip (Corning). After 48 h, the cells (50-60% confluence) in each six-well plate were washed with PBS (2 × 5.00 mL). An aliquot of serum free RPMI 1640 media (1.00 mL) was added to each well, followed by the respective nanoparticle solutions (100 μL each). The plates were then returned to the incubator to incubate at 37 °C or 0 °C. Following desired incubation times, the nanoparticles were removed, and each well was washed with Hanks Balanced Salt Solution (HBSS) (3 × 5.00 mL) and viewed under bright field and fluorescent conditions using a Leica TCS SP2 inverted microscope.

Quantitative analysis of confocal images. The background levels of the red channel containing the signal of Alexa Fluor-labeled nanoparticles were determined by the following method: 1. Binary masks corresponding to nanoparticles-associated fluorescence were generated ($Mask_{NP0}$). Threshold levels were determined by visual inspection. 2. $Mask_{NP0}$ was inverted by applying a NOT-operation to generate a binary mask for the background ($Mask_{bg}$). 4. The inverted mask $Mask_{bg}$ was multiplied with the original red channel, Red_0, and the mean value of the resulting image was determined as the background level. Cell fluorescence intensities were determined by the following method: 1. Background noise was subtracted from the original signal, Red_0, giving Red_1. 2. Binary masks were generated ($Mask_{NP1}$) for Red_1. Threshold levels were determined by visual inspection. 3. $Mask_{NP1}$ was multiplied by Red_1. 4. Over the resulting image, individual cells were manually selected as regions of interest (ROI), and mean intensities were recorded for each cell. A minimum of 100 cells was measured for each time point of each sample. The mean intensity values and standard deviation values were calculated.

Results and Discussion

In order to validate size/shape effects of the nanoparticle carrier in their cell internalization characteristics, mediated by PTD peptide, two series of nanoparticle solutions were prepared. The first series included the same spherical structures with increasing loadings of PTD; the second series contained particles having the same amount of PTD but increasing particle length in one dimension (from 10 nm to several μm).

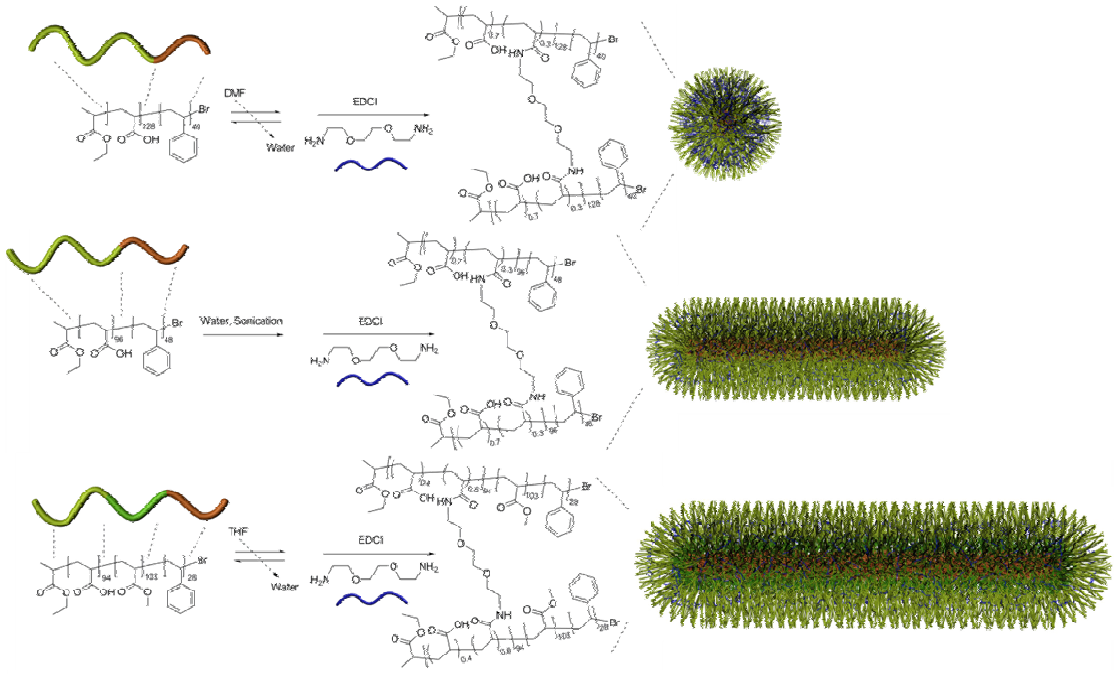

Scheme 2-1. Block copolymers (PAA_{128}-*b*-PS_{40}, PAA_{98}-*b*-PS_{48} and PAA_{94}-*b*-PMA_{103}-*b*-PS_{28}) were micellized by different procedures, to afford spherical and cylindrical nanoparticles of different cross-sectional diameters and lengths.

We designed and synthesized shell-crosslinked nanoparticles of different sizes and spherical or cylindrical shapes and then performed further functionalization for fluorescent labeling and PTD attachment to afford the two series of materials (Scheme 2-1). The spherical nanoparticle was assembled from a diblock copolymer (poly(acrylic

acid)$_{128}$-*b*-polystyrene$_{40}$, PAA$_{128}$-*b*-PS$_{40}$). The short and long cylindrical nanoparticles were assembled from a diblock and a triblock copolymer, PAA$_{98}$-*b*-PS$_{48}$ and poly(acrylic acid)-*b*-poly(methyl acrylate)-*b*-polystyrene (PAA$_{94}$-*b*-PMA$_{103}$-*b*-PS$_{28}$), respectively. All three particles were nominally 30% crosslinked in the shell domain, using standard procedures (*28*). The spherical particle had an average diameter of 11 ± 2 nm, as evidenced by transmission electron microscopy (TEM). The short cylinder had an average cross-sectional diameter of 20 ± 2 nm, and an average length of 180 ± 120 nm. The long cylinder had an average cross-sectional diameter of 30 ± 2 nm, and an average length of 970 ± 900 nm. The distinct size distributions of the nanoparticles are more clearly shown in Fig. 2-1. TEM images (Fig. 2-2) show the morphologies of the three nanostructures.

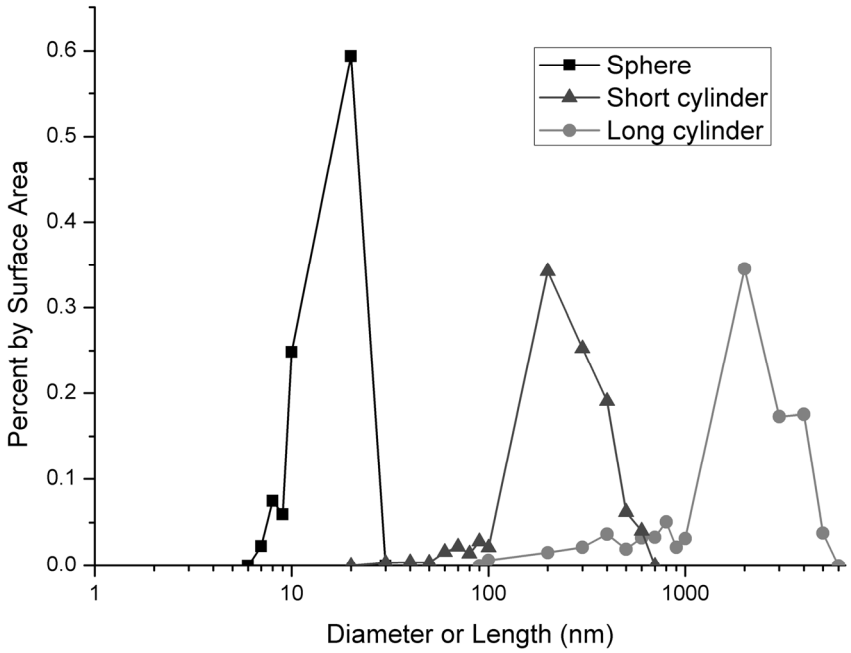

Figure 2-1. Size distribution by surface area. The size of the three nanostructures is each separated by an order of magnitude.

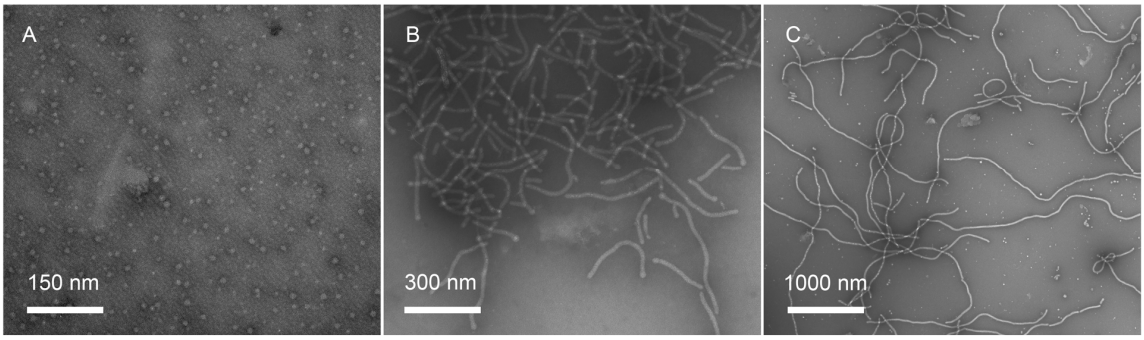

Figure 2-2. TEM of PAA_{128}-*b*-PS_{40} (A), PAA_{98}-*b*-PS_{48} (B) and PAA_{94}-*b*-PMA_{103}-*b*-PS_{28} (C) micelles in nanopure water.

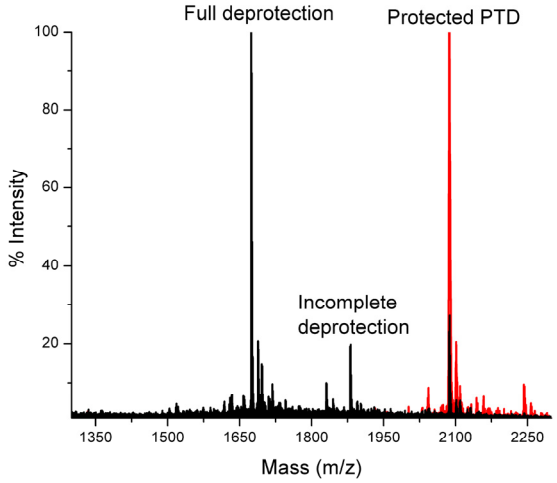

Figure 2-3. Overlaid MALDI-ToF spectra of ivDde-protected PTD before and after treatment with 2.0% hydrazine for 20 minutes in water. Adequate removal of ivDde (>70%) was achieved, despite the deprotection reaction being less efficient in water than in organic solvent.

Functionalization of the nanostructures with both the fluorescent tag (Alexa Fluor 594 cadaverine) for confocal microscopy and the Tat PTD peptide was achieved by using carbodiimide chemistry. Attachment of the Alexa Fluor 594 to the nanostructures was performed first. To ensure that all final solutions had the same amount of total

fluorescence, the solution of spherical particles was then split for further labeling with different amounts of PTD (at levels of 0.5, 1, and 2% consumption of total COOH groups of the PAA_{128}-*b*-PS_{40}), while the solutions of cylindrical nanostructures were functionalized at a level that coincided with the 1% labeling of the spheres. Because the Tat PTD has two lysine residues, whose side chain amine could compete with the terminal amine for the activated carboxylic acid on the nanoparticle, ivDde protecting groups were used to cap the lysine residues and were subsequently removed, after the Tat PTD was coupled to the nanoparticle (Scheme 2-2). A model study on aqueous ivDde removal by Matrix-Assisted Laser Desorption Ionization-Time of Flight (MALDI-ToF) mass spectrometry demonstrated adequate removal under reaction with 2% hydrazine in water (Fig. 2-3). These reaction conditions were fairly mild to the nanoparticle framework, although some amount of the AlexaFluor 594 cadaverine was cleaved. Therefore, all samples, even the control particles without PTD were treated to these deprotection reaction conditions. Extensive dialysis was used to remove unbound peptide, which previously has been reported to be effective (*18*). Both the fluorescent dye and the Tat PTD were loaded successfully within the nanoparticles, as evidenced by UV-Vis spectroscopy (Fig. 2-4), although it is not clear whether all detected peptide was covalently bound or electrostatically adsorbed onto or absorbed into the nanoparticles, due to their oppositely and highly positively-charged characteristics. For the cylindrical particles, accurate UV-Vis measurement was complicated by light scattering and, therefore, the assumption was made that the coupling yields for all particles were similar (Fig. 2-5). After functionalization, the morphologies of each nanostructure did not undergo discernible changes, as confirmed by TEM (images not shown).

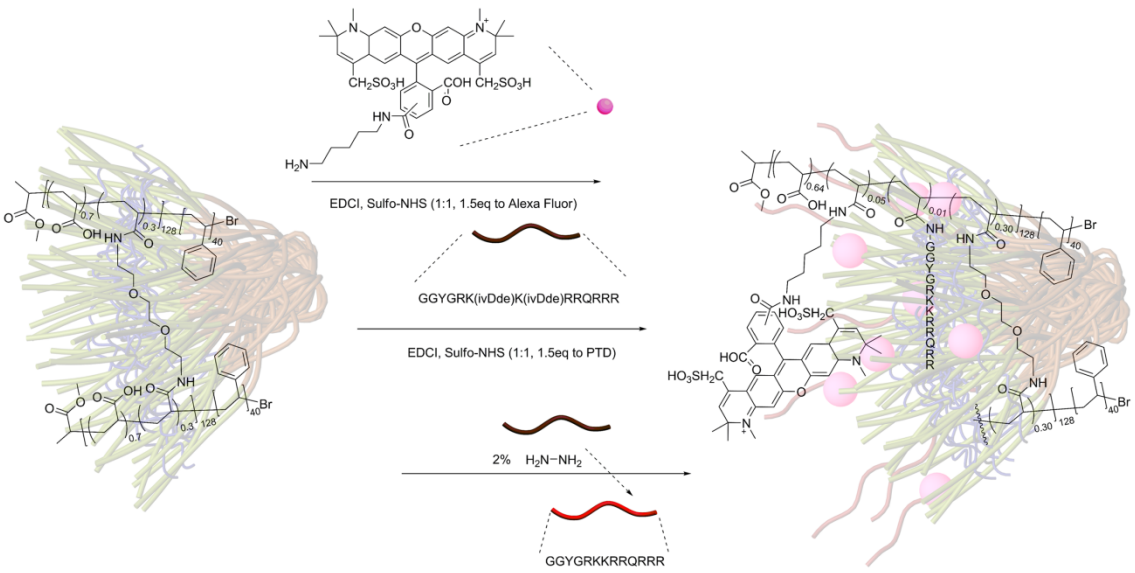

Scheme 2-2. Functionalization of the spherical nanoparticle sample was achieved through a three-step synthesis. Alexa Fluor 591 and protected PTD were respectively coupled to the nanoparticle *via* carbodiimide chemistry. The ivDde protecting groups were removed by treatment with a 2.0% hydrazine solution in water.

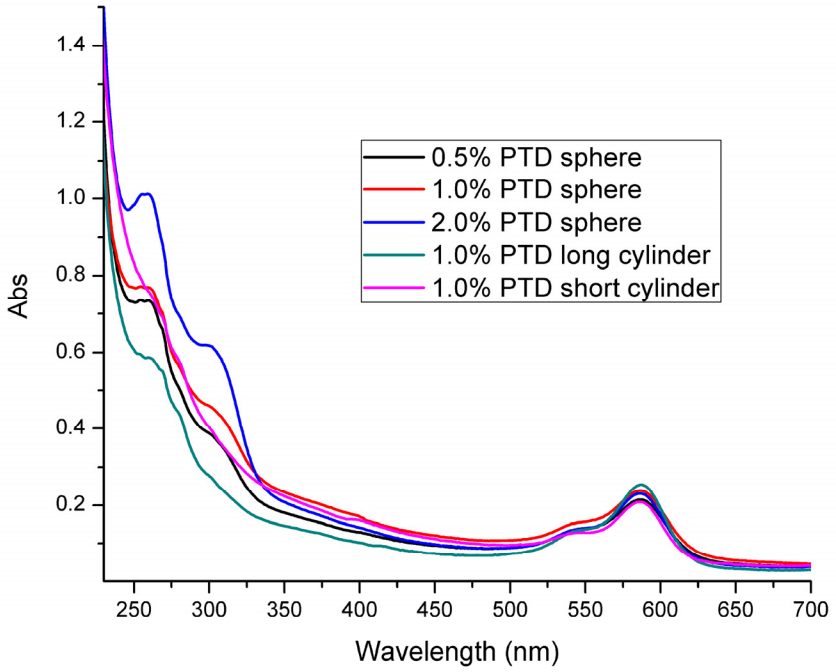

Figure 2-4. UV-Vis spectra of spheres and cylinders labeled with Alexa Fluor 594 cadaverine and PTD peptide.

Because the PTD peptides were conjugated after the micellization and crosslinking and should be present on the particles' surfaces, the surface areas of the nanostructures determine the number of peptides loaded onto each particle given the total amount of PTD peptide, assuming the particles' densities are similar (*29*). The three nanostructures each represented a unique size distribution, with the greatest percentage surface area for each morphology being separated by an order of magnitude (Fig. 2-1).

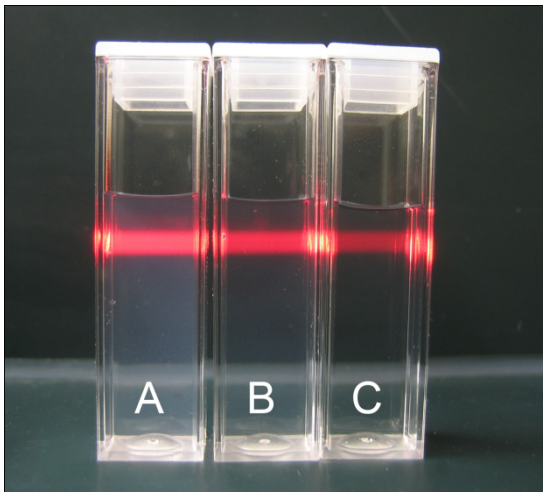

Figure 2-5. Light scattering of the long cylinders complicates accurate UV-Vis measurement. A: Long cylinders. B: Short cylinders. C: Spheres.

To verify the effectiveness of CPP, spherical particles of the same size loaded with different amounts of CPP (series 1) were incubated with CHO cells at a concentration of 0.68 μM (polymer) at 37 ˚C and 0 ˚C for 1 hour. Confocal microscopy imaging of non-fixed, live cells suggests that CPP had a pronounced enhancement in the uptake of the nanoparticles by the CHO cells (Fig. 2-6). The highest amount of PTD loading, 2.0%, gave nanoparticles that exhibited nearly a 5-fold increase in cell uptake at 37 ˚C, than the nanoparticles without PTD. Incubation at 0 ˚C, under otherwise the same

conditions, resulted in little cell uptake. The difference in cell uptake at different temperatures can be due to reduced membrane permeability at low temperatures, to the energy-dependency of the uptake process, or to both. An interesting phenomenon we noticed is that the PTD-nanoparticle conjugates were both contained within cellular vesicles and partly spread into the cytoplasm, with exclusion from the nucleus, whereas PTD alone has been reported to accumulate selectively in the cell nucleus (*30-31*). This observation is possibly due to the overall negatively-charged nature of the PTD-particle conjugate or may be due to comparisons between different cell lines.

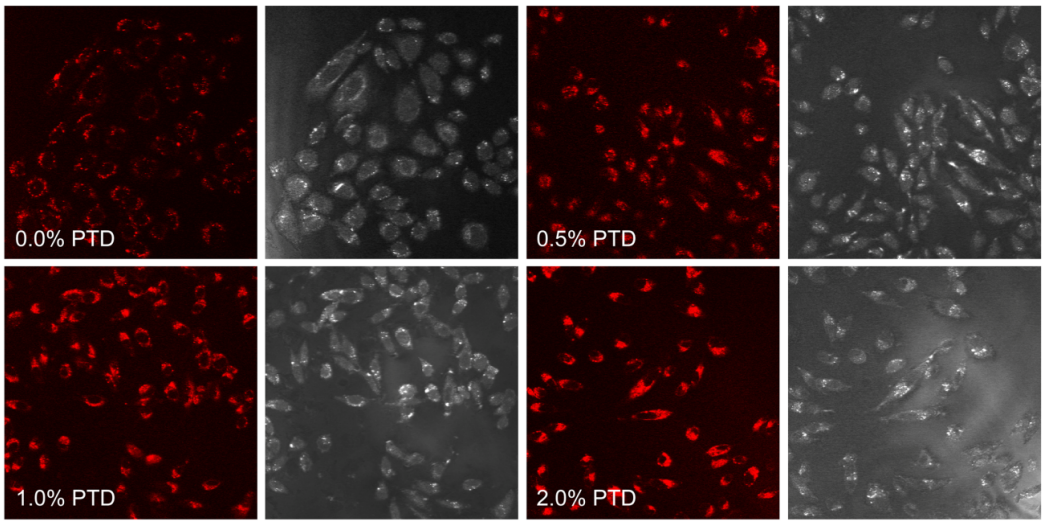

Figure 2-6. Confocal images of CHO cells incubated with the spherical nanoparticles having different amounts of PTD for 1 hour. Cell uptake of PTD-sphere conjugates increased by the action of increasing loadings of surface-bound PTD peptide.

To probe the size/shape effect, we loaded the three differently-shaped particles with a fixed amount of PTD (equivalent to 1% of the carboxylates of PAA_{128}-*b*-PS_{40}), and incubated CHO cells in their solutions under the same buffer condition as above at 37 ˚C for 1 hour. It was found that the smaller, spherical particle had higher cell uptake than

the larger, cylindrical nanoparticles (Fig. 2-7). Based on these results, we can speculate on the general mechanisms that govern the transduction of the PTD-functionalized nanomaterials. Many variables determine the uptake rate, including adhesion rate and receptor diffusion kinetics. Freund *et al* (*32*) and Bao *et al* (*33*) have modeled these factors and developed a hypothesis involving "wrapping time" of the membrane; the shorter the wrapping time, the faster is the uptake. It has been predicted theoretically by this model that through the competition between thermodynamic driving force and diffusion kinetics, there is an optimum radius for efficient "wrapping", which is 27-30 nm. Because the early endocytic vesicles are usually less than 100 nm in diameter (*6*), most short cylindrical particles (average length = 170 nm) would have to be curved or bent to be internalized, which requires additional energy. Therefore, although the cylindrical particles have higher surface area and hence more membrane-particle interaction (less diffusion), the system is not able to either overcome the overall lack of thermodynamic driving force caused by having to bend the cylinders to "fit" in the endosomes or to create larger endocytic vesicles to contain the cylindrical nanostructures. Another factor, for the higher uptake of the small, spherical particle by the cell at a given time, is the higher particle molar concentration for the spheres, which is the result of the lower aggregation number for the spherical particle, compared with the cylindrical particle. For example, the average short cylinder occupies *ca.* 80 times as much volume as does the sphere, based on calculations from TEM cross-sectional and longitudinal measurements.

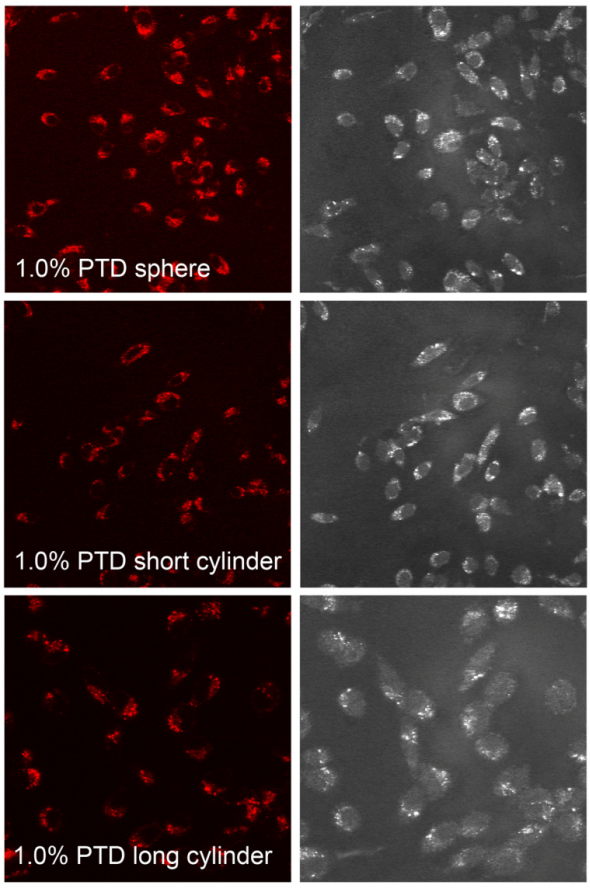

Figure 2-7. When conjugated with the same amount of PTD peptide, greater amounts of the smaller, spherical nanoparticles were internalized than were the larger, cylindrical nanoparticles. Images were taken after 1 hour of incubation.

Last, we investigated the release of the PTD-nanoparticle conjugates from CHO cells. CHO cells were incubated with 0.68 μM particle solutions for 1 h at 37 ˚C. Following the incubation period, the nanoparticle-containing solutions were removed, the cells were washed with PBS, and serum free RPMI 1640 media was introduced, followed by further incubation. Fluorescence monitoring of CHO cells immediately after buffer change, and at 2, 4 and 8 h time points revealed that fluorescence intensity decreased over time for spherical nanoparticles labeled with 2%, 1% and 0.5% PTD, suggesting particles being released from the cell (Fig. 2-8). The rates of release of spherical particles

appeared to be dependent on the amount of PTD loaded on the nanoparticle, for which the highest loading (2%) led to the fastest release. This result could suggest that PTD-assisted particle transduction works in a two-way fashion: both entry and exit seem to be facilitated by PTD (*34*). The cells that had been incubated with spheres having no PTD did not show apparent decrease of fluorescence over 8 h. Both the long and short cylinders behaved similarly as the spheres without the PTD peptide, showing little uptake and no measurable release. Other PTD-independent processes, such as peptide degradation are possible, and thus more detailed studies on cell uptake and release of differently-shaped nanostructures are needed to reveal a fuller picture of the mechanisms involved.

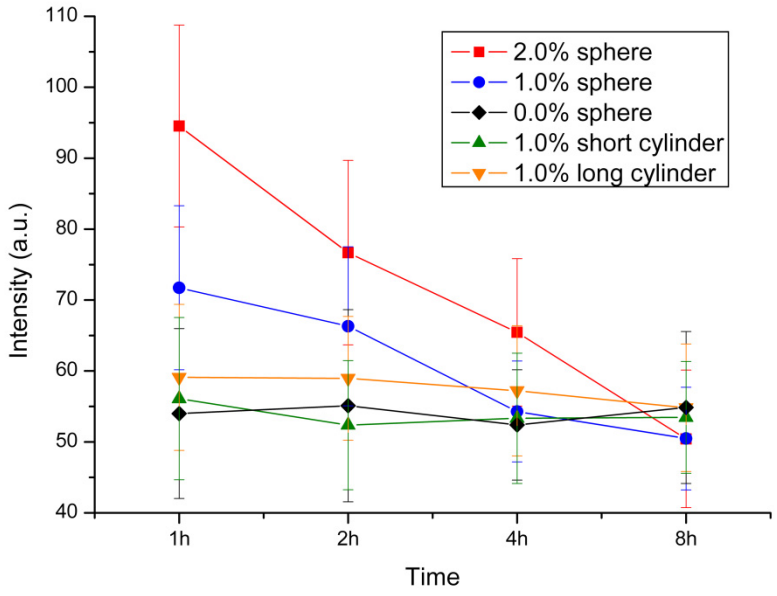

Figure 2-8. Release profile of series 1 nanoparticles (spherical in shape; different amounts of PTD peptide) and series 2 nanoparticles (different shapes; each with 1.0% PTD peptide conjugation).

Conclusions

The self assembly of block copolymers afforded spherical nanostructures and cylindrical nanostructures having distinctive lengths required to investigate the effects of different particle sizes and shapes, across a wide size range (10 nm - 1000 nm), upon cell transduction. Attachment of the Tat cell penetration peptide of HIV-1 improved cell internalization of the spheres. The amount of cell uptake was a function of PTD loading, with increasing amounts of PTD providing for increasing levels of cell internalization at a given time point. Attachment of PTD to the small cylinders (~200 nm) and long cylinders (~ 1000 nm) did not produce detectable increase in cell uptake. Once internalized, the PTD-spherical nanoparticle conjugates escaped from the cell at a rate that was a function of PTD loading. The observation of reversible cell transduction will become important as these nanostructures are functionalized also with ligands that are designed to probe intracellular targets, so that escape from cells lacking the target can be facilitated to allow for the nanostructures to accumulate in the designated cells.

The polymer micelle-based nanoparticles in this study have enabled comparison of size and shape on cellular uptake, for materials that have the same surface chemistry, differing only in their core composition, size and shape. Further studies are required to understand fully the mechanisms by which the particle characteristics lead to the observed differences in cellular uptake and release. Moreover, the particles and the methodologies for functionalization described herein can be employed for fundamental

studies that extend to systems involving ligand-receptor interactions to promote endocytosis, which will be important to gain new insights into the interface of biological systems with synthetic nanostructures. These results also serve as a guideline in engineering artificial nanoscale carrier particles for drug delivery, where the control of size/shape is of significance.

Acknowledgements

The authors gratefully acknowledge support from the National Heart Lung and Blood Institute of the National Institutes of Health as a Program of Excellence in Nanotechnology (NHLBI-PEN HL080729). The authors also thank senior microscopist G. Michael Veith of the Washington University Department of Biology Microscopy Facility for providing technical support with TEM and fluorescence confocal microscopy.

References and Notes

(1) Duchardt, F., Fotin-Mleczek, M., Schwarz, H., Fischer, R., and Brock, R. (2007) A comprehensive model for the cellular uptake of cationic cell-penetrating peptides. *Traffic 8*, 848-866.

(2) Chithrani, B. D., and Chan, W. C. W. (2007) Elucidating the mechanism of cellular uptake and removal of protein-coated gold nanoparticles of different sizes and shapes. *Nano Lett. 7*, 1542-1550.

(3) Hyunmin, K., Robert, D., H, F. M., and L, J. R. (2005) Tat-conjugated PAMAM dendrimers as delivery agents for antisense and siRNA oligonucleotides. *Pharm. Res. 22*, 2099-20106.

(4) Matthaeus, C., Kale, A., Chernenko, T., Torchilin, V., and Diem, M. (2008) New ways of imaging uptake and intracellular fate of liposomal drug carrier systems inside individual cells, based on Raman microscopy. *Mol. Pharmaceutics ASAP*.

(5) Kam, N. W. S., and Dai, H. (2005) Carbon nanotubes as intracellular protein transporters: Generality and biological funcitonality. *J. Am. Chem. Soc. 127*, 6021-6026.

(6) Osaki, F., Kannamori, T., Sando, S., Sera, T., and Aoyama, Y. (2004) A quantum dot conjugated sugar ball and its cellular uptake. On the size effects of endocytosis in the subviral region *J. Am. Chem. Soc. 126*, 6520-6521.

(7) Foerg, C., and Merkle, H. P. (2007) On the biomedical promise of cell penetrating peptides: limits *versus* prospects. *J. Pharm. Sci. 97*, 144-162.

(8) Chithrani, B. D., Chazani, A. A., and Chan, W. C. W. (2006) Determining the size and shape dependence of gold nanoparticle uptake into mammalian cells. *Nano Lett. 6*, 662-668.

(9) Champion, J. A., and Mitragotri, S. (2006) Role of target geometry in phargocytosis. *Proc. Natl. Acad. Sci. USA 103*, 4930-4934.

(10) Geng, Y., Dalhaimer, P., Cai, S., Tsai, R., Tewari, M., Miniko, T., and Discher, D. E. (2007) Shape effects of filaments *versus* spherical particles in flow and drug delivery. *Nature Nanotechnol. 2*, 249-255.

(11) Read, E. S., and Armes, S. P. (2007) Recent advances in shell cross-linked micelles. *Chem. Commun.*, 3021-3035.

(12) Krikorian, V., Kang, Y., and Thomas, E. L. (2007) Self-assembly and morphology diagrams for solution and bulk materials: Experimental aspects, in *Macromolecular Engineering* (Matyjaszewski, K., Gnanou, Y., and Leibler, L.,

Eds.) pp 1387-1430, Wiley-VCH Verlag GmbH & Co. KGaA, Weinheim, Germany.

(13) Hamley, I. (2005) Nanoshells and nanotubes from block copolymers. *Soft Matter 1*, 36-43.

(14) Sun, G. X., J., Hagooly, A., Rossin, R., Li, Z., Moore, D. A., Hawker, C. J., Welch, M. J., and Wooley, K. L. (2007) Strategies for optimized radiolabeling of nanoparticles for *in vivo* PET imaging. *Adv. Mater. ASAP*.

(15) Rossin, R., Pan, D., Qi, K., Turner, J. L., Sun, X., Wooley, K. L., and Welch, M. J. (2005) ^{64}Cu-labeled folate-conjugated shell cross-linked nanoparticles for tumor imaging and radiotherapy: Synthesis, radiolabeling, and biologic evaluation. *J Nucl. Med. 46*, 1210-1218.

(16) Yang, T.-F., Chen, C.-N., Chen, M.-C., Lai, C.-H., Liang, H.-F., and Sung, H.-W. (2006) Shell-crosslinked Pluronic L121 micelles as a drug delivery vehicle. *Biomaterials 28*, 725-734.

(17) Lazzari, M., Liu, G., and Lecommandoux, S. (2006) *Block Copolymers in Nanoscience*, Wiley-VCH Verlag GmbH & Co. KGaA, Weinheim, Germany.

(18) Becker, M. L., Remsen, E. E., Pan, D., and Wooley, K. L. (2004) Peptide-derivatized shell-cross-linked nanoparticles. 1. Synthesis and characterization. *Bioconjugate Chem. 15*, 699-709.

(19) Cui, H., Chen, Z., Wooley, K. L., and Pochan, D. J. (2006) Controlling micellar structure of amphiphilic charged triblock copolymers in dilute solution *via* coassembly with organic counterions of different spacer lengths. *Macromolecules 39*, 6599-6607.

(20) Cui, H., Chen, Z., Zhong, S., Wooley, K. L., and Pochan, D. J. (2007) Block copolymer assembly *via* kinetic control. *Science 317*, 647-650.

(21) Discher, D. E., and Eisenberg, A. (2002) Polymer vesicles. *Science 297*, 967-973.

(22) Pressly, E. D., Rossin, R., Hagooly, A., Fukukawa, K.-I., Messmore, B. W., Welch, M. J., Wooley, K. L., Lamm, M. S., Hule, R. A., Pochan, D. J., and Hawker, C. J. (2007) Structural effects on the biodistribution and positron emission tomography (PET) imaging of well-defined (64)Cu-labeled nanoparticles comprised of amphiphilic block graft copolymers. *Biomacromolecules 8*, 3126-3134.

(23) Pochan, D. J., Chen, Z., Cui, H., Hales, K., Qi, K., and Wooley, K. L. (2004) Toroidal triblock copolymer assemblies. *Science 306*, 94-97.

(24) Turner, J. L., Pan, D., Plummer, R., Chen, Z., Whittaker, A. K., and Wooley, K. L. (2005) Synthesis of gadolinium-labeled shell-crosslinked nanoparticles for magnetic resonance imaging applications. *Adv. Funct. Mater. 15*, 1248-1254.

(25) Pan, D., Turner, J. L., and Wooley, K. L. (2004) Shell cross-linked nanoparticles designed to target angiogenic blood vessels *via* $\alpha_v\beta_3$ receptor-ligand interactions. *Macromolecules 37*, 7109-7115.

(26) Ma, Q., and Wooley, K. L. (2000) The preparation of tbutyl acrylate, methyl acrylate, and styrene block copolymers by atom transfer radical polymerization: precursors to amphiphilic and hydrophilic block copolymers and conversion to complex nanostructured materials. *J. Polym. Sci. Part. A: Polym. Chem. 38*, 4805-4820.

(27) Ma, Q., Remsen, E. E., Christopher G. Clark, J., Kowalewski, T., and Wooley, K. L. (2002) Chemically induced supramolecular reorganization of triblock

copolymer assemblies: trapping of intermediate states *via* a shellcrosslinking methodology. *Proc. Natl. Acad. Sci. USA 99*, 5058-5063.

(28) Huang, H., Remsen, E. E., and Wooley, K. L. (1998) Amphiphilic core-shell nanospheres obtained by intramicellar shell crosslinking of polymer micelles with poly(ethylene oxide) linkers. *Chem. Commun.*, 1415-1416.

(29) Remsen, E. E., K. Bruce Thurmond, I., and Wooley, K. L. (1999) Solution and surface charge properties of shell-crosslinked knedel nanoparticles. *Macromolecules 32*, 3685-3689.

(30) Ziegler, A., Nervi, P., Durrenberger, M., and Seelig, J. (2005) The cationic cell-penetrating peptide CPP(TAT) derived from the HIV-1 protein TAT is rapidly transported into living fibroblasts: Optical, biophysical, and metabolic evidence. *Biochemistry 44*, 138-148.

(31) Ziegler, A., and Seelig, J. (2007) High affinity of the cell-penetrating peptide HIV-1 Tat-PTD for DNA. *Biochemistry 46*, 8138-8145.

(32) Gao, H., Shi, W., and Freund, L. B. (2005) Mechanics of receptor-mediated endocytosis. *Proc. Natl. Acad. Sci. USA 102*, 9469-9474.

(33) Bao, G., and Bao, X. R. (2005) Shedding light on the dynamics of endocytosis and viral budding. *Proc. Natl. Acad. Sci. USA 102*, 9997-9998.

(34) Hirano, K., Hirano, M., Nishimura, J., and Kanaide, H. (2004) A critical period requiring Rho proteins for cell cycle progression uncovered by reversible protein transduction in endothelial cells. *FEBS Letters 570*, 149-154.

Chapter 3

Folate-mediated cell uptake of shell-crosslinked spheres and cylinders

[Portions of this work have been published previously as Ke Zhang, Raffaella Rossin, Aviv Hagooly, Zhiyun Chen, Michael J. Welch and Karen L. Wooley *J. Polym. Sci. Part A Polym. Chem.* **2008**, 46(22), 7578-7583.]

Abstract

This chapter reports the synthesis of shell crosslinked nanoparticles (SCKs) of spherical and cylindrical shapes, and their functionalization with folate using a poly(ethylene glycol) (PEG) construct that has folate and an amine group as the opposing chain termini. By use of confocal microscopy, we demonstrate the selective delivery of folate conjugated SCKs to human KB cells, a cell line that overexpresses the folate receptor (FR). A higher extent of polymer uptake by the cells occurred with the cylindrical SCK morphology, relative to the spherical SCKs, when both samples had the same fluorescein-5-thiosemicarbazide and polymer concentrations. In both cases, by using excess free folic acid as a block or SCKs lacking the folate-PEG conjugate, cell uptake was significantly reduced. These results suggest that particle shape may play an important role in receptor-mediated cell uptake, and may be exploited in the targeted delivery of nanoscopic drugs.

Introduction

Thus far, most drugs approved for clinical use function in an indiscriminate fashion – they access pathologic and healthy tissues alike. As a result, the effect of the drug is systemic rather than specific. The ability of a therapeutic or diagnostic agent to preferentially localize at diseased tissues would, therefore, be of great value. Towards this end, polymeric nanoparticles have been designed and synthesized to augment the drug's local concentration. For example, Hubbell *et al.* have developed a nanoparticle drug delivery system with dual targeting moieties, which led to up to a 72-fold increase in targeting the extracellular compartment of articular cartilage in mice (*1*). Although significant progress has been made in terms of identifying the targets and construction of targeting nanoparticles, the shape effect of the nanoparticle platform *per se* on cell binding and internalization through receptor-ligand interactions has not yet been investigated thoroughly (*2-3*). Our interest here is to synthesize nanoparticles of different shapes and sizes, and use a well-known receptor-ligand pair to study whether the shape effects exist, and if they do, which shape is more favorable for this particular receptor-ligand pair.

In this chapter, folate was used as the model targeting ligand to be conjugated to the nanoparticles. Folate has received extensive study as a targeting device for proteins utilizing folate receptor (FR)-mediated endocytosis (*4*). By virtue of its high binding affinity towards the cell surface FR, which is overexpressed in a number of pathologic

cells, selective delivery of non-specific drugs that are conjugated to folate can be achieved. Derivatization of folate has been successfully exploited in the targeted delivery of proteins (*5-6*), liposomes (*7*), DNA nanoparticles (*8-9*), synthetic organic (*10-11*) and inorganic nanoparticles (*12-13*). As a targeting ligand, folate has many important advantages compared to monoclonal antibodies, such as low immunogenicity, high specificity and resistance to denaturation, *etc*. Moreover, FR targeting agents may continuously accumulate into the cells due to receptor recycling. Finally, folic acid has two carboxylic acid groups, one that is sterically blocked and the other that allows for simple and defined conjugation to a variety of organic molecules and nanoparticles through amidation chemistry. Herein, we report a method to create spherical and cylindrical polymer shell-crosslinked (SCK) nanoparticles of similar chemical compositions, and to functionalize these nanoparticles with folic acid through a PEG tether. We then further demonstrate that both nanoparticles received enhancement in uptake by human KB cells, surprisingly, with the cylindrical nanostructures being internalized to a greater extent than the spheres, and this enhancement could be competitively blocked partially by free folic acid.

Experimental Procedures

Polymer synthesis. The two amphiphilic block copolymers used in this study were prepared by atom transfer radical polymerization, using literature procedures (*14*).

Spherical SCK formation. The spherical polymer micelle sample was prepared by dissolving 18.6 mg of the block copolymer, poly(acrylic acid)$_{128}$-*b*-polystyrene$_{40}$ (PAA_{128}-b-PS_{40}) in 20 mL dimethylformamide (DMF) followed by slow addition (4.0 mL/h) of an equal volume of nonsolvent (H_2O) for the hydrophobic polystyrene to induce micellization. The micelles were stirred for 4 h before being transferred to presoaked dialysis tubing (MWCO 6-8 kDa) and dialyzed against nanopure water (18.0 MΩ·cm) for 3 days to remove the organic solvent. The final volume was 66 mL of aqueous micelle solution for a final concentration of 0.28 mg/mL. Transmission electron microscopy (TEM): 10 ± 1 nm (diameter). Dynamic light scattering (DLS): 14 ± 2 nm (diameter). The aqueous micelle solution was then mixed with *O*-bis-(aminoethyl)ethylene glycol (0.20 equiv., relative to the molar number of available COOH groups) and allowed to stir at room temperature. After 30 min, an aqueous solution of 1-[3'-(dimethylamino)propyl]-3-ethylcarbodiimide hydrochloride (EDCI) (1 equiv., relative to the molar number of available COOH groups) was added. The reaction mixture was allowed to stir overnight before being transferred to presoaked dialysis tubing (MWCO 3 kDa) and dialyzed against nanopure water (18.0 MΩ·cm) for 3 days.

Cylindrical SCK formation. To a stirring solution of 8.4 mg triblock copolymer, poly(acrylic acid)$_{94}$-*b*-poly(methyl acrylate)$_{103}$-*b*-polystyrene$_{28}$ (PAA_{94}-*b*-PMA_{103}-*b*-PS_{28}) in 8.00 mL tetrahydrofuran (THF) was added a solution of THF (2.0 mL) containing O-bis-(aminoethyl)ethylene glycol (0.20 equiv., relative to COOH

groups). The mixture was allowed to stir overnight at room temperature, and then H_2O (40 mL) was added at a rate of 7.00 mL/h to induce micellization. To this water-THF mixture, EDCI (6.3 mg) was added to crosslink the shell domain of the micelle and to lock the morphology (*15*). After stirring overnight, the reaction mixture was transferred to presoaked dialysis tubing (MWCO 6-8 kDa) and dialyzed against nanopure water (18.0 MΩ·cm) for 3 days to remove the organic solvent and other residues. The final volume was 62.6 mL of aqueous crosslinked long, cylindrical micelle solution for a final concentration of 0.13 mg/mL. TEM: 900 nm (length) and 30 ± 2 nm (cross-sectional diameter).

Functionalization with fluorescent tag. The SCK solutions were diluted to the same polymer concentration (6.9 μM) and each was placed into a round-bottom flask and cooled to 0 ˚C using an ice bath. A solution of 1:1 (mole : mole) EDCI : *N*-hydroxysulfosuccinimide (sulfo-NHS) was added to each nanoparticle solution (0.5 : 1 molar ratio, relative to the available COOH groups) to activate the acrylic acid residues. After 30 minutes, the pH of the reaction mixtures was adjusted to 7.7 using pH = 8.0 sodium bicarbonate solution. Then, aliquots of fluorescein-5-thiosemicarbazide stock solution were added to each flask and the mixtures were allowed to react overnight. The solutions were then transferred to presoaked dialysis tubings (MWCO 6-8 kDa) and allowed to dialyze for 3 days against 150 mM NaCl solution, then for 3 days against nanopure water.

Conjugation of folate-PEG(1.5 kDa)-amine to nanostructures. The folate-PEG(1.5 kDa)-amine construct was synthesized by coupling of bis-PEG-amine (MW 1.5 kDa) with folic acid, according to a literature procedure (*16-18*). Conjugation to the nanostructures was achieved by use of amidation chemistry. SCK solutions pre-functionalized with fluorescein-5-thiosemicarbazide were each placed into a 25 mL round-bottom flask. Sodium chloride was placed into each flask to give a concentration of 5.0 mg/mL, to minimize particle-particle aggregation. The flasks were then placed in an ice bath. A mixed solution of 1 : 1 (mole : mole), EDCI : sulfo-NHS was added to each nanoparticle solution (0.7 : 1 molar ratio, relative to the available COOH groups) to activate the acrylic acid residues. Aliquots of the folate-PEG-amine DMF solution (14.3 mg/mL, 10.0 equiv. to polymer) were added to the respective flasks 30 min after the addition of EDCI/NHS. The pH of each reaction mixture was adjusted to 7.4 using pH = 8.0 sodium bicarbonate solution. The mixtures were allowed to react overnight. The solutions were then transferred to presoaked dialysis tubings (MWCO 12 kDa) and allowed to dialyze against nanopure water for 5 days, then against pH =7.4 PBS buffer for 2 days. UV-Vis measurements confirmed coupling of the folate-PEG-amine to the SCKs.

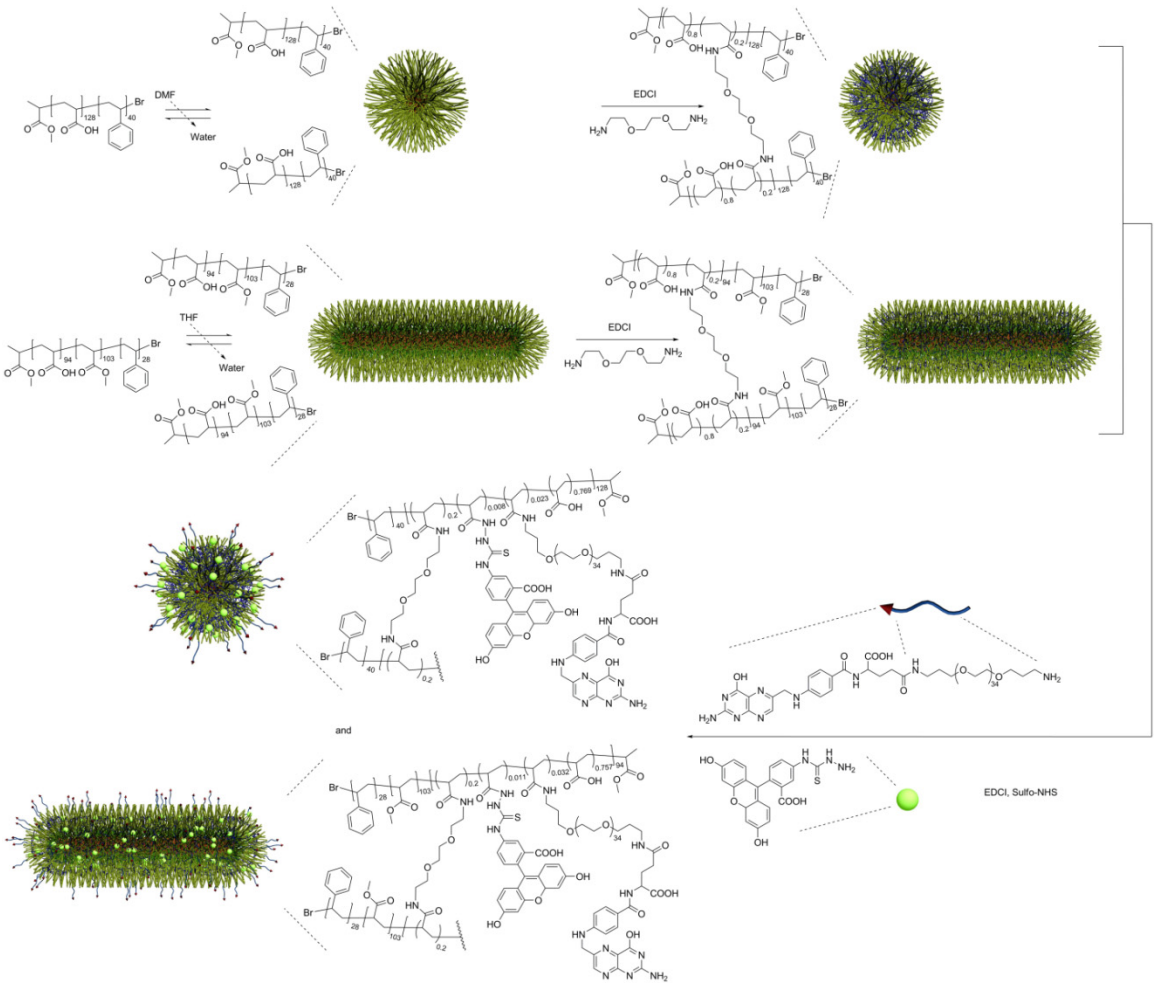

Scheme 3-1. Synthesis of folate-functionalized shell-crosslinked nanoparticles of two distinct shapes. A post-nanoparticle functionalization strategy was used, in which the spherical and cylindrical nanoparticles were constructed first from discrete polymer chains, and then a folate-PEG derivative was conjugated to the surface of the nanoparticles. The nanostructures were also labeled by reaction with fluorescein-5-thiosemicarbazide to enable particle tracking.

Results and Discussion

The overall design in this study involved the use of well-defined amphiphilic block copolymers to form micelles of a core-shell architecture. Due to the inherent

differences in the block copolymers and the micellization conditions, different morphologies of the resulting micelles could be obtained. After shell crosslinking of the micelles using a diamine crosslinker, their respective morphologies were locked (*15*). Then, a folic acid derivative, folate-PEG-amine, was conjugated to the shell-crosslinked nanoparticles, and the conjugates were evaluated in cells (Scheme 1). The syntheses of the amphiphilic diblock copolymer PAA_{128}-*b*-PS_{40} and triblock copolymer PAA_{94}-*b*-PMA_{103}-*b*-PS_{28}, were achieved using atom transfer radical polymerization, following previously reported methods (*14*). The block copolymers were then dissolved in a good solvent for both/all blocks (THF or DMF), followed by slow addition of water to induce micellization. The two resulting micelle samples exhibited distinctive morphologies, spherical and rod-shaped, from the diblock and triblock copolymers, respectively. To impart stability to these micelles, such that under cell incubation fluid conditions the micelles do not disassemble into discrete polymer chains, crosslinking in the shell domain of the micelle using 2, 2'-(ethylenedioxy)bis(ethylamine) was performed with the aid of EDCI, consuming 20% of available carboxylic acids on the micelle (*14*). The shell was also fluorescently labeled with fluorescein to enable particle tracking. The polymer and fluorescein concentrations for each sample were controlled to be approximately the same (Fig. 3-1), thus allowing direct comparison of cell uptake by examining the confocal fluorescent images. The shell-crosslinked nanoparticles were characterized by DLS and TEM (Fig. 3-2). DLS gave a mean diameter of 14 ± 2 nm for the spherical

SCK, while TEM gave 10 ± 1 nm. For the cylindrical SCK, TEM gave a mean length of 900 nm, and a mean cross-sectional diameter of 30 ± 2 nm.

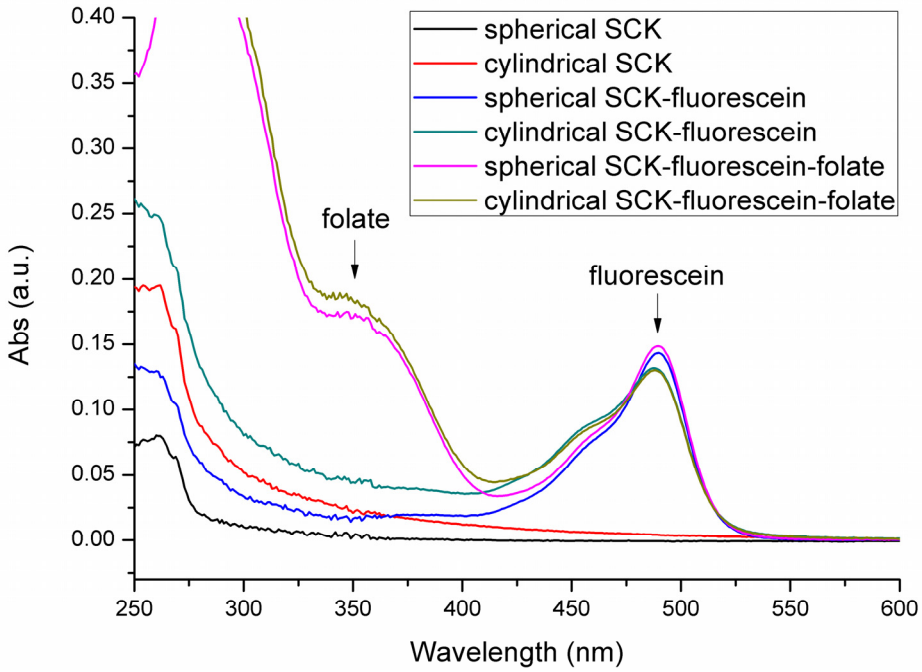

Figure 3-1. UV-Vis spectra of the nanostructure carriers functionalized with fluorescent tag and folate. The absorbance at 488 nm represents fluorescein-5-thiosemicarbazide, the fluorescent tag. Approximately the same amount of fluorescein was coupled to each of the samples. The absorbance at 363 nm indicate successful coupling of folate-PEG-amine to the nanostructures. Using fluorescein-tagged SCKs as background, the absorbances at 363 nm for the folate-fluorescein-SCKs were used to calculate the number of folates per polymer chain.

Attachment of folic acid to the surface of the SCKs was achieved through the same carbodiimide coupling chemistry as was employed for the crosslinking reactions. A PEG(1.5 kDa) linker was used to tether folate to the nanoparticle, since direct attachment of folic acid to nanostructures has been reported to result in reduced binding of folic acid to FR, possibly due to steric effects that limit folate from reaching the binding pockets of

FR (*19*). The synthesis of folate-PEG-amine followed previously reported methods (*16-18*). The conjugates showed UV absorptions at 363 nm, representative of folate. The extinction coefficient for folate in pH 7.4 PBS buffer at that wavelength is 6197 $M^{-1}cm^{-1}$. The number of folates per polymer can therefore be calculated as follows:

Folates/polymer = (Abs. at 363 nm/6197 $M^{-1}cm^{-1}$)/[polymer (mg/mL)]/(MW of polymer (g/mol))

For PAA_{128}-*b*-PS_{40}, which forms the spherical particle, the folate/polymer number was determined to be 3.2; for PAA_{94}-*b*-PMA_{103}-*b*-PS_{28}, which forms the cylindrical particle, the folate/polymer number was determined to be 3.0. As expected, no measurable changes were observed in particle morphology after conjugation with folate, as evidenced by TEM (images not shown).

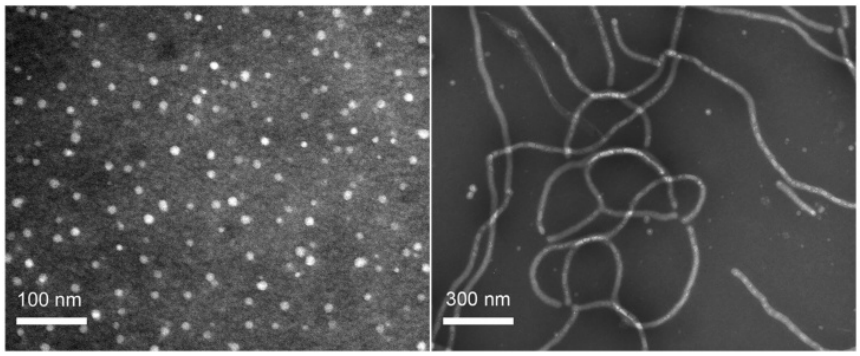

Figure 3-2. TEM images (obtained on a carbon-coated copper grid with negative staining by a mixture of uranyl acetate) of (left) the spherical supramolecular assembly of PAA_{128}-*b*-PS_{40} formed in DMF by slow addition of water and (right) the cylindrical supramolecular assembly of PAA_{94}-*b*-PMA_{103}-*b*-PS_{28} formed in THF/water (vol:vol = 1:1) by slow addition of water. Both particles were shell-crosslinked with 2, 2'-(ethylenedioxy)bis(ethylamine), consuming nominally 20% of available carboxylic acids in the micelle.

The folate-conjugated nanoparticles were incubated with KB cells, a human nasopharyngeal epidermal carcinoma cell line overexpressing the FR. As both samples contained the same molar concentrations of polymers and fluorescein probes, but different numbers of particles overall, quantification of cellular uptake on a polymer molar basis was observed. After 4 hours of incubation, confocal microscopy of the cells showed that the polymers were internalized to a higher extent when they were of a cylindrical morphology than when they were in the form of the spherical particles (Fig. 3-3, a and d), despite the fact that the cylinders are much larger in volume compared the spheres (*ca*. 700 times difference in volume for an average cylinder *vs*. sphere, based on TEM volume calculations). This result is somewhat surprising because previously we have observed an opposite trend in cell internalization of the same nanostructures, with the exception that they were instead functionalized with the cell transduction domain peptide sequence of the HIV Tat protein (PTD) (*20*). The different binding affinities between folate/FR and PTD/cell surface may contribute to the contrasting results for the folate- and PTD-decorated nanostructures. It is hypothesized that a larger structure may span across several FR binding sites and lead to an increase in polyvalent effect (*21*), and increased FR-mediated endocytosis. By contrast, the PTD-SCKs interact with the cell surface in a receptor-independent fashion (*22*) and, therefore, may not benefit from polyvalency. For both nanostructure shapes, an excess of free folate (1 mmol/L) was able to competitively inhibit the binding and internalization of folate-functionalized particles,

suggesting FR specific binding (Fig. 3-3, b and e). The control experiments using particles that lacked surface folate showed significantly reduced cell uptake for both spherical and cylindrical particles (Fig. 3-3, c and f).

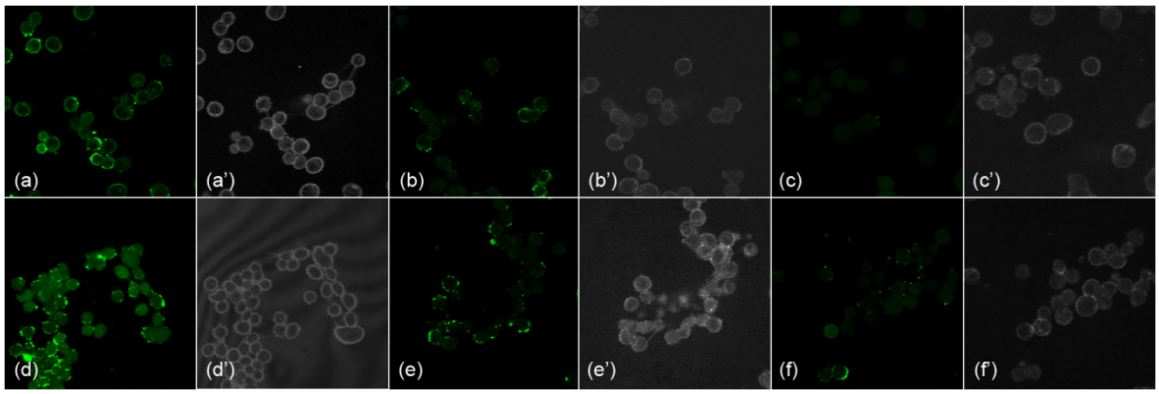

Figure 3-3. Fluorescent confocal microscopy images of KB cells incubated for 4 hours at 37 °C with spherical and cylindrical nanoparticles functionalized with and without folate (70 nM polymer per 33-mm culture dish, plated with 3×10^5 cells per dish 24 h before imaging). All particles were tagged with equal amount of fluorescein-5-thiosemicarbazide. (a) folate-labeled spherical particle; (b) folate-labeled spherical particle with the addition of 1 mmol/L free folate; (c) spherical particles with no folate; (d) folate-labeled cylindrical particle; (e) folate-labeled cylindrical particle with the addition of 1 mmol/L free folate; (f) cylindrical particle with no folate; (a')-(f') bright field images corresponding to the fluorescent images.

These preliminary results suggest that cylinders are a better candidate for cell internalization when the mechanism involves a receptor-mediated endocytotic process. This conclusion is valid, at least, for the folate-FR pair, which achieved a high degree of cell uptake; however, it may not be general. Each individual target-receptor pair deserves its own study on the nanoparticle shape effect due to the difference in binding affinity,

target density on cellular surfaces, *etc*. Knowing that shape plays important roles in cell internalization, as well as in overall biodistribution behavior *in vivo* (*23*), provides exciting opportunities to optimize another parameter in the design of drug delivery systems.

Acknowledgments

This material is based upon work supported by the National Heart Lung and Blood Institute of the National Institutes of Health as a Program of Excellence in Nanotechnology (HL080729). The authors thank Mr. G. M. Veith for TEM imaging.

References and Notes

(1) Rothenfluh, D. A., Bermudez, H., O'Neil, C. P., and Hubbell, J. A. (2008) Biofunctional polymer nanoparticles for intra-articular targeting and retention in cartilage. *Nature Nanotechnol. 7*, 248-254.

(2) Champion, J. A., and Mitragotri, S. (2006) Role of target geometry in phargocytosis. *Proc. Natl. Acad. Sci. USA 103*, 4930-4934.

(3) Chithrani, B. D., and Chan, W. C. W. (2007) Elucidating the mechanism of cellular uptake and removal of protein-coated gold nanoparticles of different sizes and shapes. *Nano Lett. 7*, 1542-1550.

(4) Rothberg, K. G., Ying, Y. S., Kolhouse, J. F., Kamen, B. A., and Anderson, R. G. (1990) The glycophospholipid-linked folate receptor internalizes folate without entering the clathrin-coated pit endocytic pathway. *J. Cell Biol. 110*, 637-649.

(5) Reddy, J. A., Leamon, C. P., and Low, P. S. (2006) Folate-mediated delivery of protein and peptide drugs into tumors, in *Delivery of Protein and Peptide Drugs in Cancer* pp 183-204.

(6) Turek, J. J., Leamon, C. P., and Low, P. S. (1993) Endocytosis of folate-protein conjugates: ultrastructural localization in KB cells. *J. Cell Sci. 106*, 423-430.

(7) Reddy, J. A., Abburi, C., Hofland, H., Howard, S. J., Vlahov, I., Wils, P., and Leamon, C. P. (2002) Folate-targeted, cationic liposome-mediated gene transfer into disseminated peritoneal tumors. *Gene Ther. 9*, 1542-1550.

(8) Guy, Z., Liliane, Z.-I., Emmanuel, D., and Jean-Paul, B. (2003) Targeted gene delivery to cancer cells: directed assembly of nanometric DNA particles coated with folic acid. *Angew. Chem., Int. Ed. 42*, 2666-2669.

(9) Zuber, G., Muller, C. D., and Behr, J.-P. (2005) Targeted gene delivery to cancer cells with nanometric DNA particles enveloped with folic acid using a polymerizable anchor. *Technol. in Cancer Res. & Treat. 4*, 637-643.

(10) Kukowska-Latallo, J. F., Candido, K. A., Cao, Z., Nigavekar, S. S., Majoros, I. J., Thomas, T. P., Balogh, L. P., Khan, M. K., and James R. Baker, J. (2005) Nanoparticle targeting of anticancer drug Improves therapeutic response in animal model of human epithelial cancer. *Cancer Res. 65*, 5317-5324.

(11) Rossin, R., Pan, D., Qi, K., Turner, J. L., Sun, X., Wooley, K. L., and Welch, M. J. (2005) ^{64}Cu-labeled folate-conjugated shell cross-linked nanoparticles for

tumor imaging and radiotherapy: Synthesis, radiolabeling, and biologic evaluation. *J. Nucl. Med. 46*, 1210-1218.

(12) Bharali, D. J., Lucey, D. W., Jayakumar, H., Pudavar, H. E., and Prasad, P. N. (2005) Folate-Receptor-Mediated Delivery of InP Quantum Dots for Bioimaging Using Confocal and Two-Photon Microscopy. *J. Am. Chem. Soc. 127*, 11364-11371.

(13) Dixit, V., Van den Bossche, J., Sherman, D. M., Thompson, D. H., and Andres, R. P. (2006) Synthesis and grafting of thioctic acid-PEG-folate conjugates onto Au nanoparticles for selective targeting of folate receptor-positive tumor cells. *Bioconjugate Chem. 17*, 603-609.

(14) Ma, Q., and Wooley, K. L. (2000) The preparation of tbutyl acrylate, methyl acrylate, and styrene block copolymers by atom transfer radical polymerization: precursors to amphiphilic and hydrophilic block copolymers and conversion to complex nanostructured materials. *J. Polym. Sci. Part A: Polym. Chem. 38*, 4805-4820.

(15) Ma, Q., Remsen, E. E., Christopher G. Clark, J., Kowalewski, T., and Wooley, K. L. (2002) Chemically induced supramolecular reorganization of triblock copolymer assemblies: trapping of intermediate states *via* a shellcrosslinking methodology. *Proc. Natl. Acad. Sci. USA 99*, 5058-5063.

(16) Guo, W., Hinkle, G. H., and Lee, R. J. (1999) ^{99m}Tc-HYNIC-folate: A novel receptor-based targeted radiopharmaceutical for tumor imaging. *J. Nucl. Med. 40*, 1563-1569.

(17) Pan, D., Turner, J. L., and Wooley, K. L. (2003) Folic acid-conjugated nanostructured materials designed for cancer cell targeting. *Chem. Commun. 19*, 2400.

(18) Shukla, S., Wu, G., Chatterjee, M., Yang, W., Sekido, M., Diop, L. A., Müller, R., Sudimack, J. J., Lee, R. J., Barth, R. F., and Tjarks, W. (2002) Synthesis and biological evaluation of folate receptor-targeted boronated PAMAM dendrimers as potential agents for neutron capture therapy *Bioconjugate Chem. 14*, 158-167.

(19) Gabizon, A., Horowitz, A. T., Goren, D., Tzemach, D., Mandelbaum-Shavit, F., Qazen, M. M., and Zalipsky, S. (1999) Targeting folate receptor with folate kinked to extremities of poly(ethylene glycol)-grafted liposomes: in vitro studies. *Bioconjugate Chem. 10*, 289-298.

(20) Zhang, K., Fang, H., Chen, Z., Taylor, J.-S. A., and Wooley, K. L. (2008) Shape effects of nanoparticles conjugated with cell-penetrating peptides (HIV Tat PTD) on CHO cell uptake. *Bioconjugate Chem.*, in press.

(21) Hong, S., Leroueil, P. R., Majoros, I. J., Orr, B. G., James R. Baker, J., and Holl, M. M. B. (2007) The binding avidity of a nanoparticle-based multivalent targeted drug delivery platform. *Chem. & Biol. 14*, 107-115.

(22) Duchardt, F., Fotin-Mleczek, M., Schwarz, H., Fischer, R., and Brock, R. (2007) A comprehensive model for the cellular uptake of cationic cell-penetrating peptides. *Traffic 8*, 848-866.

(23) Geng, Y., Dalhaimer, P., Cai, S., Tsai, R., Tewari, M., Miniko, T., and Discher, D. E. (2007) Shape effects of filaments *versus* spherical particles in flow and drug delivery. *Nature Nanotechnol. 2*, 249-255.

Chapter 4

Cationic shell-crosslinked knedel-like nanoparticles for highly efficient gene and oligonucleotide transfection of mammalian cells

[Portions of this work have been published previously as Ke Zhang, Huafeng Fang, Zhenghui Wang, John-Stephen A. Taylor and Karen L. Wooley *Biomaterials* **2009**, 30(5), 968-977.]

Abstract

In this chapter, a robust synthetic nanostructure was designed for the effective packaging of DNA and it was shown to be an efficient agent for cell transfection. An amphiphilic block copolymer, poly(acrylamidoethylamine)$_{128}$-*b*-polystyrene$_{40}$ (PAEA$_{128}$-*b*-PS$_{40}$), was synthesized, micellized in water and shell-crosslinked using a diacid-derivatized crosslinker, to give cationic shell-crosslinked nanoparticles (cSCKs) with a mean hydrodynamic diameter of 14 ± 2 nm. A series of discrete complexes of the cSCKs with plasmid DNA (pDNA) was able to be formed over a broad range of polymer amine:pDNA phosphate ratios (N/P ratio), 2:1 to 20:1. The sizes of the complexes and their ability to fully bind the pDNA were dependent upon the N/P ratio, as characterized by dynamic light scattering (DLS), transmission electron microscopy (TEM) and gel retardation assay. A luciferase activity assay and EGFP expression were used to evaluate

intracellular delivery of a splice-correcting phosphorothioate and genetic material, respectively, by the cSCKs, which indicated that an N/P ratio of 6:1 gave the highest transfection. It was shown by both luciferase activity assay (48 h) and EGFP transfection data that high transfection efficiencies were achieved for HeLa cells transfected by cSCK/CCUCUUACCUCAGUUACA and cSCK/pEGFP-N1 plasmid, respectively. The cSCK/pEGFP-N1 plasmid transfection efficiency of 27% far exceeded the performance of Polyfect® (PAMAM dendrimers), which achieved only 12% transfection efficiency, under the same conditions. Cytotoxicities for the cSCKs were evaluated for HeLa and CHO cells.

Introduction

Gene therapy has significant potential in the treatment, through the intracellular delivery of therapeutic gene-based materials, of many human diseases that are currently considered incurable. Viral vectors, such as adenovirus or retrovirus, are highly efficient in the delivery of genes. However, interests in developing non-viral vectors remain high because of both the advantages that synthetic materials offer and the concerns associated with human use of viral vectors, including bio-safety, large-scale production and immunogenicity (*1-3*). As an alternative to viral vectors, various cationic polymers and structures such as polyethylenimine (PEI), poly(L-lysine) (PLL), polyamidoamine dendrimers (PAMAM) and cationic liposomes have been studied as gene delivery agents (*4-5*). These cationic polymers condense DNA through electrostatic complexation and form nanoparticles on the order of *ca*. 100 nm. As a result, the DNA is protected from nuclease degradation (*5-6*), while the cationic polymers mediate cell uptake (*7*) and endosomal escape (*8*) to induce high transfection efficiencies.

The natural machinery for packaging of DNA are the histone core particles, that when wrapped by DNA form nucleosomes, responsible for storage of DNA within cell nuclei (*9-10*). Our interest has been in the development of synthetic nanoparticles that can mimic histone core particles in their dimensions (*ca*. 10 nm) and function for reversible DNA condensation, as a means to effect DNA packaging, protection, transport and release for gene therapy applications. Our initial design relied upon the robust

character of shell crosslinked knedel-like block copolymer micelles (SCKs) (*11-14*) constructed from amphiphilic block copolymers comprised of polystyrene and poly(4-vinylpyridine) (*15*). Quaternization of a portion of the 4-vinylpyridine repeat units with *p*-chloromethylstyrene provided sites for crosslinking reactions, to establish the robust SCK nanoparticle structures, and incorporated cationic character for electrostatic attractive interactions with the phosphodiester backbone of DNA. These nanoparticles (*ca*. 15 nm diameter) were shown to condense DNA and to protect it from enzymatic digestion, but they did not afford transfection above the level of naked DNA. The initial SCKs possessed several characteristics that could lead to their poor transfection properties, including limited number of cationic sites, low degree of cationic site accessibility because of the sterically-hindered aromatic quaternary nitrogens, and large diameter, relative to histone core particles. Therefore, our current efforts involved the design and synthesis of SCKs of smaller diameter and comprised of an amine-rich block copolymer amphiphile for gene delivery studies, borrowing concepts from the natural system and also from synthetic materials (*4-5, 16-17*).

Although SCKs comprised of poly(acrylic acid)-*block*-polystyrene (PAA-*b*-PS) block copolymers have been studied extensively, including their modification to achieve cell transduction (*18*), long blood circulation times *in vivo* (*19*) and targeting properties (*20*), the acrylic acid-based shell material imparts a constant negatively-charged surface (*21*). As a result, they do not complex with DNA in solution and produce little to no

transfection using plasmid DNA (pDNA) or oligonucleotides (ONs). Similar core-shell micellar structures, utilizing poly(ethylene glycol) (PEG)-*block*-polycation carrying ethylenediamine units in the side chain, have been exploited as successful biocompatible nanovectors for effective gene transfer to primary cells (*22*) and to vascular lesions without cytotoxicity and thrombus formation (*23*). It was, therefore, of interest to build upon the extensive understanding of PAA-based SCKs and borrow from the structural features of Kataoka's micellar systems to create well-defined nanoparticles that exhibit improved transfection rates *in vitro* and, ultimately, *in vivo*, with all of the advantages that a robust nanoparticulate form offers over a dynamic assembly.

This chapter describes a facile method to invert the surface charge of SCKs from negative to positive, through modification of the PAA-*b*-PS block copolymer precursor, to give cationic SCKs, or cSCKs. Complexation of cSCKs with pDNA and a phosphorothioate 2'-O-methyl oligoribonucleotide (ps-MeON) was then studied and the transfection efficiencies for each of the complexes toward CHO (Chinese hamster ovary cell line) and HeLa cells (human cervical cancer cell line) with EGFP pDNA were investigated.

Materials and Methods

Materials. All solvents and chemicals were purchased from Sigma-Aldrich and used without further purification, unless otherwise indicated. N-

hydroxybenzotriazole·H_2O (HOBt) and 2-(1H-benzotriazole-1-yl)-1, 1, 3, 3-tetramethylaminium hexafluorophosphate (HBTU) were purchased from EMD Chemicals, Inc. The amphiphilic block copolymer, PAA_{128}-*b*-PS_{40}, was prepared using atom transfer radical polymerization of (protected) monomer precursors followed by deprotection, according to literature reported methods (*24*). A luciferase splice-correcting phosphorothioate 2'-O-methyl-oligoribonucleotide (ps-MeON, CCUCUUACCUCAGUUACA) (*25*) was synthesized on an Expedite 8909 DNA synthesizer (Applied Biosystems, Inc.) using standard solid phase phosphoramidite chemistry and purified by 20% denaturing polyacrylamide gels, followed by extraction with phenol/chloroform and ethanol precipitation. CHO-K1 and HeLa cells were obtained from the American Type Culture Collection. The pLuc705 Hela cell line was a generous gift from Dr. R. Kole (University of North Carolina, Chapel Hill, NC). Oligofectamine and Lipofectamine™ 2000 were obtained from Invitrogen Co. Polyfect® was purchased from Qiagen Inc. pEGFP-N1 was obtained from Clontech Laboratories, Inc. Steady-Glo® Luciferase Assay reagent and CellTiter-Glo® Luminescent Cell Viability Assay Kit were purchased from Promega Co. All cell culture media was purchased from Invitrogen, Inc.

Measurements. ^1H NMR and ^{13}C NMR spectra were recorded on a Varian 300 MHz spectrometer interfaced to a UNIX computer using Mercury software. Chemical shifts were referred to the solvent resonance signals. IR spectra were recorded on a Perkin-Elmer Spectrum BX FT-IR system, and data were analyzed using Spectrum v2.0

software. Tetrahydrofuran-based gel permeation chromatography (THF GPC) was conducted on a Waters Chromatography, Inc. (Milford, MA) model 1515, equipped with a Waters model 5414 differential refractometer, a Precision Detectors, Inc. (Bellingham, MA) model PD-2026 dual-angle (15˚ and 90˚) light scattering detector and a three-column set of Polymer Laboratories, Inc. (Amherst, MA) gel mixed-bed styrene-divinylbenzene columns (PLgel 5μm Mixed C, 500 Å, and 104 Å, 300 x 7.5 mm columns). The system was equilibrated at 35 ˚C in tetrahydrofuran (THF), which served as the polymer solvent and eluent (flow rate set to 1.00 mL/min). An injection volume of 200 μL was used. System calibration was performed using polystyrene standards. Data were analyzed using Precision Detectors, Inc. Discovery 32 software. N, N-Dimethylformamide-based gel permeation chromatography (DMF GPC) was conducted on a Waters Chromatography, Inc. (Milford, MA) system equipped with an isocratic pump model 1515, a differential refractometer model 2414 and a two-column set of Styragel HR 4 and HR 4E 5 μm DMF 7.8 x 300 mm columns. The system was equilibrated at 70 ˚C in pre-filtered N, N-dimethylformamide (DMF) containing 0.05 M LiBr, which served as polymer solvent and eluent (flow rate set to 1.00 mL/min). Polymer solutions were prepared at concentrations of *ca.* 3 mg/mL and an injection volume of 200 μL was used. Data collection and analysis was performed with Empower Pro software. The system was calibrated with poly(ethylene glycol) standards (Polymer Laboratories, Amherst, MA) ranging from 615 to 442,800 Da. Samples for transmission electron microscopy (TEM) measurements were diluted with a 1 % phosphotungstic acid

(PTA) stain (v/v, 1:1). Carbon grids were exposed to oxygen plasma treatment to increase the surface hydrophilicity. Micrographs were collected at 50,000 and 100,000 × magnifications. Hydrodynamic diameters (D_h) and size distributions were determined by dynamic light scattering (DLS). The DLS instrumentation consisted of a Brookhaven Instruments Limited (Worcestershire, U.K.) system, including a model BI-200SM goniometer, a model BI-9000AT digital correlator, a model EMI-9865 photomultiplier, and a model 95-2 argon ion laser (Lexel Corp.) operated at 514.5 nm. Measurements were made at 25 ± 1 ˚C. Scattered light was collected at a fixed angle of 90˚. A photomulitplier aperture of 100 μm was used, and the incident laser intensity was adjusted to obtain a photon counting of between, 200 and 300 kcps. Only measurements in which the measured and calculated baselines of the intensity autocorrelation function agreed to within 0.1 % were used to calculate particle size. The calculations of the particle size distributions and distribution averages were performed with the ISDA software package (Brookhaven Instruments Company). All determinations were repeated 5 times.

Poly(acrylamidoethylamine-Boc)$_{128}$-*block*-polystyrene$_{40}$ (PAEA(Boc)$_{128}$-*b*-PS$_{40}$). PAA$_{128}$-*b*-PS$_{40}$ (50 mg, 3.7 μmol, 0.47 mmol carboxylic acid groups) was dissolved in DMF (5.0 mL) and stirred for 3 h, before 1.0 mL DMF solution containing HOBt (79 mg, 0.59 mmol) and HBTU (222 mg, 0.585 mmol) was added. After 30 min, *tert*-butyl 2-aminoethylcarbamate (117 mg, 0.727 mmol) and diisopropylethylamine

(DIPEA, 102 μL, 0.585 mmol) were added. The reaction mixture was allowed to stir overnight, diluted by the addition of DMF (10.0 mL), transferred to pre-soaked dialysis tubing (MWCO = 6 - 8 kDa), and was dialyzed against 150 mM NaCl solution for 2 days, then against nanopure water (18.0 MΩ·cm) for 5 days. Precipitation occurred shortly after the dialysis began. After the dialysis period, the polymer was collected by suction filtration and then dried *in vacuo* overnight. M_n^{NMR} = 31.9 kDa; M_n^{GPC} (DMF) = 10.5 kDa, M_w/M_n = 1.27. IR (cm^{-1}): 3600-3200, 3082, 2977, 2932, 1693, 1659, 1537, 1453, 1392, 1343, 1366, 1274, 1252, 1172, 1003, 858, 737, 699. ^{1}H NMR (300 MHz, CD_2Cl_2): 1.05-2.52 (br, Boc protons and polymer backbone protons), 2.85-3.65 (br, NHC***H*****$_2$**C***H*****$_2$**NH_2), 5.60-6.33 (br, N***H***), 6.35-6.80 and 6.88-7.40 (br, Ar***H***) ppm. ^{13}C NMR (75 MHz, CD_2Cl_2): 28.8 (br), 31.8-48.0 (multiple overlapping br), 79.7 (br), 126.2 (br), 128.4 (br), 145.9 (br), 157.1 (br), 176.4 (br) ppm.

Poly(acrylamidoethylamine)$_{128}$-*block*-polystyrene$_{40}$ (PAEA$_{128}$-*b*-PS$_{40}$). PAEA(Boc)$_{128}$-*b*-PS$_{40}$ (80 mg, 2.5 μmol) was dissolved in TFA (6 mL) and stirred for 2 h. The TFA was then removed *in vacuo* over two days. M_n^{NMR} = 19.0 kDa. IR (cm^{-1}): 3700-2600, 1681, 1556, 1434, 1204, 1135, 1026, 839, 801, 723, 700. ^{1}H NMR (300 MHz, DMSO-d_6): 0.95-2.24 (br, polymer backbone protons), 3.00-3.47 (br, NHC***H*****$_2$**C***H*****$_2$**NH_2), 6.20-6.80 and 6.81-7.33 (br, Ar***H***), 7.82-8.49 (br, N***H***) ppm. ^{13}C NMR (75 MHz, DMSO-d_6): 31.3, 32.5-45.0 (multiple overlapping br), 125.7 (br), 127.4 (br), 128.0 (br), 145.7 (br), 175.0 (br) ppm.

Synthesis of diacid crosslinker, 14-oxo-7,10-dioxa-4,13-diazaheptadecane-1,17-dioic acid. 1, 2-Bis(2-aminoethoxy)ethane (74 mg, 0.50 mmol) was dissolved in DMF (1 mL), to which a DMF solution (1 mL) containing succinic anhydride (100 mg, 1.00 mmol) and DIPEA (174 μL, 1.00 mmol) was added slowly. The reaction mixture was stirred overnight and then the product was precipitated into diethyl ether containing 1% TFA, then pure diethyl ether (4 ×), and collected by centrifugation and decanting of the supernatant, and was dried *in vacuo* overnight (yield: 132 mg, 76%). IR (cm^{-1}): 3700-2200, 2928, 1716, 1651, 1557, 1418, 1201, 1134. ^{1}H NMR (300 MHz, DMSO-d_6): 2.33 (t, J = 6 Hz, 4H, $CH_2C\boldsymbol{H_2}CONH$), 2.41 (t, J = 6 Hz, 4H, $C\boldsymbol{H_2}CH_2CONH$), 3.20 (t, J = 5.4 Hz, 4H, $NHC\boldsymbol{H_2}CH_2O$), 3.40 (t, J = 5.4 Hz, 4H, $NHCH_2C\boldsymbol{H_2}O$), 3.52 (s, 4H, $OC\boldsymbol{H_2}C\boldsymbol{H_2}O$) ppm. ^{13}C NMR (75 MHz, DMSO-d_6): 29.8, 30.5, 39.3, 70.1, 70.5, 171.9, 174.8 ppm.

Formation of cSCK. $PAEA_{128}$-*b*-PS_{40} (43 mg, 2.2 μmol) was dissolved in 20 mL dimethylsulfoxide (DMSO) and stirred for 2 h, before being transferred to a pre-soaked dialysis tube (8 kDa MWCO) and being allowed to dialyze against nanopure water (18.0 MΩ·cm) to remove organic solvent. After 4 days of dialysis, a clear solution (59 mL) containing the micelle precursors for the cSCKs was obtained. To crosslink the micelles, the diacid crosslinker (5.0 mg, 14 μmol) was activated by mixing with 2.2 equiv. of HOBt/HBTU (4 mg/12 mg, 1:1, mole:mole) in DMF (400 μL) and allowing to stir for 1 h. This solution was then added slowly with stirring to the micelle solution,

which had undergone adjustment of the pH to 8.0, using 1.0 M aqueous sodium carbonate, and reduction of the temperature to 0 ˚C, using an ice bath. The reaction mixture was allowed to stir overnight, and was then transferred to dialysis tubing (8 kDa MWCO) and dialyzed against nanopure water (18 MΩ·cm) for 2 days. A clear solution containing the cSCKs with a final concentration of 0.70 mg/mL was obtained. TEM: D_n = 9 ± 1 nm, DLS: $(D_h)_{vol}$ = 14 ± 2 nm. ζ potential: 21.3 ± 1.3 mV.

Gel retardation assay. An agarose gel (1%, w/v) was prepared in TAE (Tris−acetate−EDTA) buffer. cSCK/pDNA (pEGFP-N1 plasmid, 4.7 kbp) complexes at predetermined N/P ratios were incubated in PBS buffer for 30 min, before being mixed with loading buffer (6 ×) and then loaded onto the agarose gel. The gel was run at 120 V for 20 min and stained by incubating in TAE buffer with 0.5 μg/mL ethidium bromide (EtBr) for 30 min. The locations of DNA bands were visualized using a UV illuminator.

Cell culture. cSCK mediated transfection was evaluated on CHO-K1 (Chinese hamster ovary cell line, ATCC CCL-61) and pLuc705 HeLa cells (human cervical cancer cell line) by using the pEGFP-N1 as reporter gene. Cells were maintained in F-12K (CHO-K1) or DMEM (HeLa) containing 10% FBS, streptomycin (100 μg/mL), and penicillin (100 units/mL) at 37 ˚C in a humidified atmosphere with 5% CO_2. For pLuc705 HeLa cells, additional G418 (100 μg/mL) and hygromycin B (100 μg/mL) were also added.

Fluorescence confocal microscopy. CHO cells (5×10^5) were plated in 35 mm MatTek glass bottom microwell dishes (MatTek Co.) 24 h prior to transfection. pEGFP-N1 (5.0 μg) was complexed with cSCKs at predetermined N/P ratios in 500 μL opti-MEM solution and incubated for 30 min before use. Prior to transfection, the medium in each well was replaced with 2.0 mL of fresh medium with 10 % FBS, to which cSCK/DNA complexes were added. The plates were then returned to the incubator to incubate at 37 ˚C for another 24 or 48 h. Each plate was washed 3 times with PBS buffer and viewed under bright field and fluorescent conditions using a Leica TCS SP2 inverted microscope, with excitation by an argon laser (488 nm).

Flow cytometry. The cell culture used for flow cytometry was the same as above. Prior to analysis, cells were washed 3 times with 2.0 mL PBS, collected by trypsinisation, pelleted, and resuspended in 0.5 mL PBS. Flow cytometric analysis for the transfection using cSCKs was performed using an FACS-calibur (Becton Dickinson) equipped with an argon laser exciting at 488 nm. For each sample, 20,000 events were collected by list-mode data that consisted of side scatter, forward scatter, and fluorescence emission centered at 530 nm (FL1). The fluorescence was collected at a logarithmic scale with a 1024 channel-resolution. CellQuest software (Becton Dickinson) was applied for the analyses.

Luciferase antisense splicing correction assay. pLuc705 HeLa cells were seeded in a 96-well microtiter plate at a density of 1×10^4 cells/well and cultured for 24 h

in 100 μL DMEM containing 10% FBS. ps-MeON (phosphorothioate 2'-O-methyl-oligoribonucleotide: CCUCUUACCUCAGUUACA) was complexed with cSCKs at predetermined N/P ratios in 20 μL opti-MEM solution and incubated for 30 min before use. At the time of the transfection experiment, the medium was replaced with 80 μL of fresh medium, to which the cSCK/ps-MeON complexes were added. Following 24 h and 48 h incubation periods, 100 μL Steady-Glo® Luciferase assay reagent were added. The contents were mixed and the plate was allowed to incubate at room temperature for 10 min to stabilize the luminescence signal. Luminescence intensities were recorded on a Luminoskan Ascent® luminometer (Thermo Scientific) with an integration time of 1 second per well.

Cytotoxicity assay. The cytotoxicity of the cSCKs was examined by CellTiter-Glo Luminescent Cell Viability Assay (Promega Co.). CHO and HeLa cells were each seeded in a 96-well plate at a density of 1×10^4 cells/well and cultured for 24 h in 100 μL F-12K (CHO-K1) or DMEM (HeLa) containing 10% FBS. Thereafter, the medium was replaced with 100 μL of fresh medium containing various concentrations of cSCKs, Polyfect (positive control), or no additive (negative control). After 24 h incubation at 37 ˚C, 100 μL CellTiter-Glo reagent was added. The contents were mixed and the plate was allowed to incubate at room temperature for 10 min to stabilize luminescence signals. Luminescence intensities were recorded on a Luminoskan Ascent® luminometer (Thermo

Scientific) with an integration time of 1 second per well. The relative cell viability was calculated by the following equation:

$$\text{Cell viability (\%)} = (\text{luminescence}_{(\text{sample})} / \text{luminescence}_{(\text{negative control})}) \times 100$$

Where $\text{luminescence}_{(\text{negative control})}$ was obtained in the absence of particles and $\text{luminescence}_{(\text{sample})}$ was obtained in the presence of cSCKs or Polyfect. Data are shown as mean ± SD (n = 6).

Results and Discussion

To improve cell transfection, we designed and prepared the cSCKs as robust nanostructures that mimic the natural nucleosome core particle in terms of its DNA binding capability and size (*ca.* 10 nm). The cSCKs originated from the supramolecular assembly and covalent stabilization of an amine-rich block copolymer $PAEA_{128}$-*b*-PS_{40}, which was afforded by chemical modification of a common amphiphilic block copolymer of acrylic acid and styrene. A key step in the preparation $PAEA_{128}$-*b*-PS_{40} was the complete conversion of carboxylic acids on PAA_{128}-*b*-PS_{40} to amides using mono-Boc-protected 1,2-ethylene diamine, which was achieved by using a large excess of the amine component. The choice of the segment lengths and block ratio is based on previous findings that the block copolymer PAA_{128}-*b*-PS_{40} gave SCKs of ~ 10 nm in diameter (*18*). It was reasoned that, with maintenance of the hydrophilic:hydrophobic balance, polymers derived from PAA_{128}-*b*-PS_{40} would be likely to result in spherical micelles of similar size

upon micellization. Polystyrene continues to be the choice of core material for the cSCK, as it has been shown to provide sufficient rigidity to the poly(4-vinylpyridine)-based SCKs such that the electrostatic interaction between the SCK and DNA did not deform or destroy the particles' spherical morphology. With poly(acrylamidoethylamine) as the particle shell, the success of PAMAM dendrimers in cell transfection was drawn upon by use of the same surface unit (amidoethylamine). It was expected that the basic primary amines of the cSCK, and the positive charge resulting from their protonation, would promote its cell uptake and endosomal release through the proton-sponge effect (*26*). To crosslink the $PAEA_{128}$-*b*-PS_{40} micelles and form cSCKs, a diacid crosslinker (14-oxo-7,10-dioxa-4,13-diazaheptadecane-1,17-dioic acid) was employed.

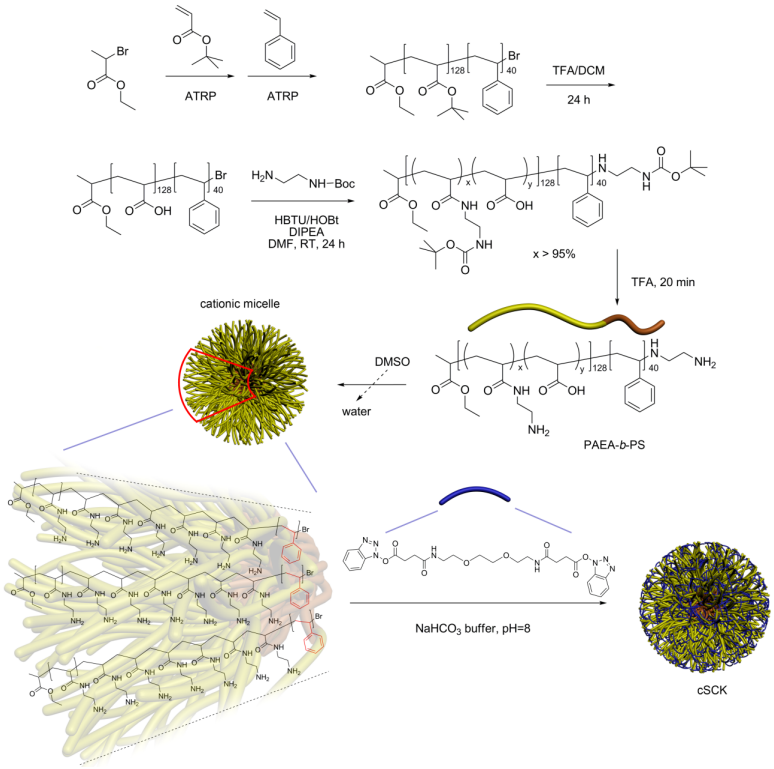

Scheme 4-1. Preparation of cSCK.

The amphiphilic polymer component of cSCK, $PAEA_{128}$-*b*-PS_{40} was prepared by using atom transfer radical polymerization to give poly(*t*-butyl acrylate)-*b*-polystyrene ($PtBA_{128}$-*b*-PS_{40}), followed by removal of the *t*-butyl protecting groups, coupling of mono-Boc protected 1,2-bis(2-aminoethoxy)ethane, and deprotection to remove the Boc groups (Scheme 1). Complete consumption of acrylic acid residues of PAA_{128}-*b*-PS_{40} during the amidation reaction was achieved, as demonstrated by the disappearance of the carboxylic acid protons in the ^{1}H NMR spectrum (12.22 ppm, DMSO-d_6). The resulting polymer, $PAEA(Boc)_{128}$-*b*-PS_{40}, showed only two kinds of carbonyl carbons by ^{13}C NMR spectroscopy, resonating at 157.5 ppm and 175.0 ppm (CD_2Cl_2), corresponding to the Boc carbamate carbons and the polymer amide carbons, respectively. This result again confirmed the successful and complete conversion of the carboxylic acids to amides, a key step in this work. Because the parent polymer ($PtBA_{128}$-*b*-PS_{40}, M_n^{NMR}: 20.7 kDa, M_n^{GPC} (THF): 20.0 kDa, PDI: 1.06) had a narrow molecular weight distribution, typical for polymers obtained from controlled radical polymerization, $PAEA(Boc)_{128}$-*b*-PS_{40} also exhibited adequate polydispersity in molecular weight (M_n^{NMR}: 31.9 kDa, M_n^{GPC} (DMF): 10.5 kDa, PDI: 1.27), even after three chemical modification steps. The molecular weight calculation by GPC using DMF as eluent for $PAEA(Boc)_{128}$-*b*-PS_{40} is not expected to be accurate, primarily because the molecular weight determinations were based PEG standards. Deprotection of $PAEA(Boc)_{128}$-*b*-PS_{40} was accomplished by stirring with an excess of TFA for 2 h at room temperature with no additional solvent

being required. Quantitative removal of the Boc protecting groups was evidenced by loss of signals from Boc-related protons (^{1}H NMR, CD_2Cl_2, 1.50 ppm) and carbons (^{13}C NMR, CD_2Cl_2, 28.7 and 79.7 ppm).

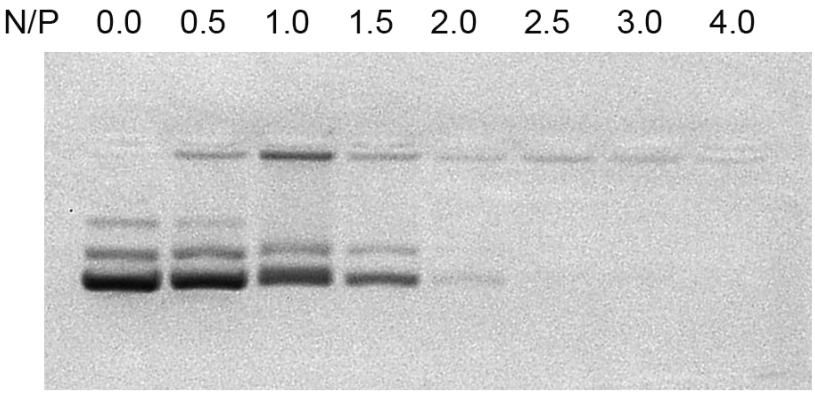

Figure 4-1. Gel retardation assay of cSCK/pDNA complexes at different N/P ratios ranging from 0:1 to 4:1. A fixed amount of pEGFP-N1 pDNA was used. The cSCK was shown to fully bind to pDNA and prevent its migration on the agarose gel at an N/P ratio of 2:1.

Self assembly of the block copolymer into micelles was achieved by direct dialysis of the DMSO solution of $PAEA_{128}$-*b*-PS_{40} against nanopure water, where gradual exchange of DMSO by water occurred (Scheme 1). Due to the nanoscopic size of the assemblies, the micelle solution remained clear at 0.70 mg/mL. The volume-average hydrodynamic diameter ($(D_h)_{vol}$) of the particle was determined by DLS to be 14 ± 2 nm, and the number-average dry state diameter was determined by TEM to be 9 ± 1 nm. The size of these cationic micelles is very close to that of the micelles comprised of PAA_{128}-*b*-PS_{40} ($(D_h)_{vol}$ = 12 ± 3 nm (DLS), D_n = 11 ± 2 nm (TEM)) due to their same polymer block lengths and segment ratio, and to that of nucleosome core particles (*ca*. 10 nm).

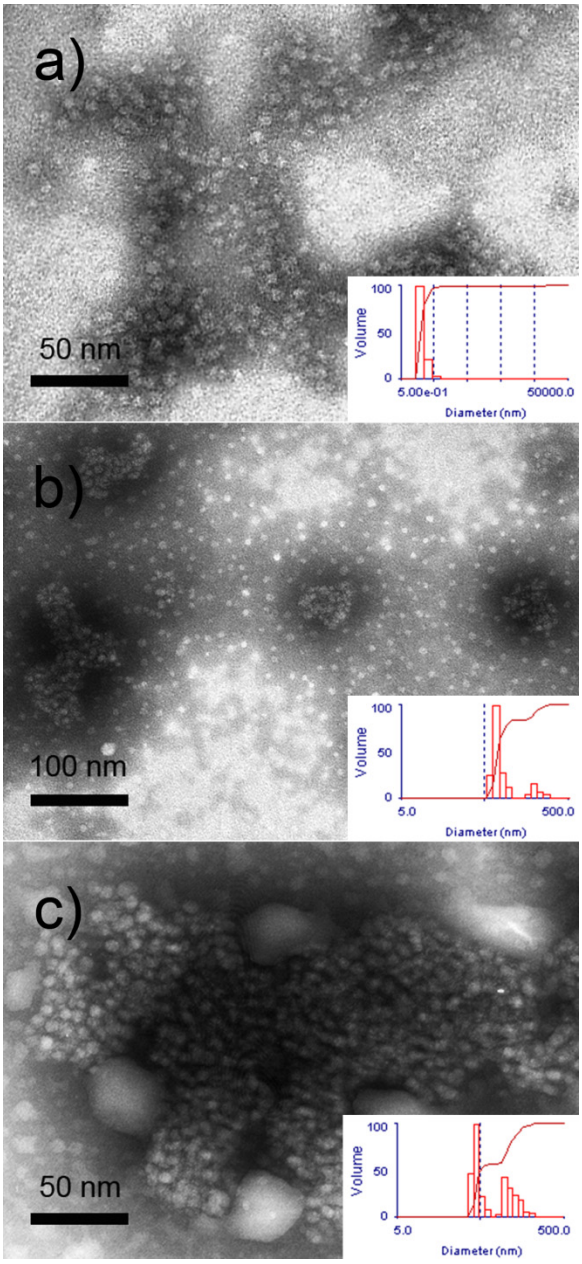

Figure 4-2. TEM images of cSCK and cSCK/pDNA complexes at different N/P ratios. a) cSCK alone, without pDNA. b) cSCK/pDNA complex at N/P ratio of 6:1. c) cSCK/pDNA complex at N/P ratio of 2:1. At an N/P ratio of 6:1, the majority of the complex nanoparticles were 50-100 nm in diameter. Below 4:1, larger aggregates of hundreds of nanometers in size were also formed. Insets: DLS measurement of volume-average hydrodynamic diameter ($(D_h)_{vol}$) of cSCK and complexed particles.

Furthermore, ζ potential measurements of the micelles based on $PAEA_{128}$-*b*-PS_{40} showed that the amidation step had inverted the charge of the particles to be cationic, with ζ = 22.9 mV, relative to the negative-charge character of PAA_{128}-*b*-PS_{40} micelles with ζ = -31.5 mV.

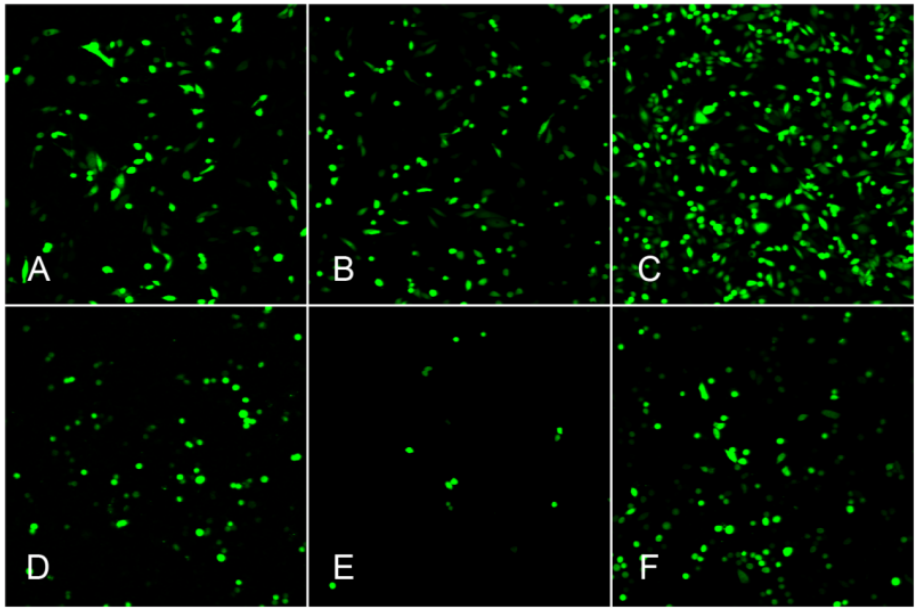

Figure 4-3. Confocal laser scanning microscopy of HeLa cells (A-C) and CHO-K1 cells (D-F), transfected with pEGFP. In A and D, cSCK was used as the transfection agent with pEGFP-N1 at an N/P ratio of 6:1. B/E and C/F were positive controls using Polyfect and Lipofectamine2000 as the transfection agent, respectively, at N/P ratios recommended by manufacturer.

In order to crosslink the micelles, a diacid crosslinker, 14-oxo-7,10-dioxa-4,13-diazaheptadecane-1,17-dioic acid, was prepared. When activated with carbodiimide, the carboxylic acids of the crosslinker react readily with amines. Activation of the crosslinker was achieved by mixing with 2.2 equiv. of HOBt/HBTU (1:1, mol:mol) in

DMF and allowing to stir for 1 h. The DMF solution containing the activated crosslinker, equivalent to 5% of the available amines, was then added to a solution of the $PAEA_{128}$-*b*-PS_{40} micelles with stirring, over a period of 10 min. The crosslinking process resulted in no discernible change in DLS and TEM sizes.

To mediate endocytosis and endosomal escape of DNA, the cSCK was designed to complex with the DNA and form supramolecular aggregates (larger composite nanostructures comprised of smaller cSCK and pDNA sub-units), *via* electrostatic interactions between the positively-charged cSCK and the negatively-charged DNA. Agarose gel retardation assays verified that the EGFP pDNA underwent complete complexation with cSCK at polymer/pDNA amine/phosphate (N/P) ratios of 2:1 (mol:mol) and above, as demonstrated by retardation of DNA migration in electrophoresis (Fig. 4-1). A low value of the N/P ratio to retard DNA migration is often desired as it not only suggests strong binding between the positively-charged transfection agent and the DNA, but also means that less transfection agent can be used in the cell experiments, which reduces toxic stress on the cells. Because the cSCKs contain only closely-spaced primary amines, which have a higher binding affinity to DNA than tertiary amines, due to their lack of steric hindrance, optimal DNA complexes with cSCK are expected to require lower N/P values than cationic polymers containing secondary, tertiary amines, or aromatic amines. For example, poly(amido amine) (pAPOL) requires a polymer:DNA wt:wt ratio of 24:1 (which corresponds to an approximate N/P ratio of

27:1, assuming an average MW of a deoxynucleotide base unit to be 330 Da) to fully retard DNA migration during electrophoresis (*27*). Poly(4-vinylpyridine) only allows for incomplete complexation at room temperature with pDNA at 5:1 N/P ratio, due to the weakly interacting quaternary nitrogen (*15*). Therefore, the cSCKs were found to be effective agents for condensing pDNA, even at relatively low N/P ratios.

The sizes of the complexed pDNA/cSCK nanoparticles were measured by DLS, which allowed for determination of the hydrodynamic diameters for the aggregates while suspended in aqueous solution, and by TEM, which provided visualization of the components within those pDNA/cSCK clusters. At an N/P ratio of 6:1, the majority of the aggregates were 50-100 nm in diameter, as measured by DLS, and had irregular shapes, as observed by TEM (Fig. 4-2b). Mixing at N/P ratios of 4:1 and 2:1 resulted also in a significant volume of the material being organized into 50-100 nm-sized assemblies, but also with a population that had hydrodynamic diameters of several hundred nm (Fig. 4-2c). In each case, it was observed that the rigidity of the cSCKs, imparted by their PS core material, allowed for retention of their globular morphology (Fig. 4-2a) when complexed with pDNA, as suggested by the approximately circular two-dimensional shapes of the cSCKs in the TEM images (Fig. 4-2b and 2c). In contrast, liposomes lose their particulate characteristic when complexed with DNA, and as a result, their binding is usually non-specific resulting in a heterogeneous mixture of particles. Based on TEM measurements of particle size, and on the stoichiometry of particle/DNA

ratios, an average pDNA/cSCK supramolecular aggregate with a diameter of 50 nm is estimated to comprise *ca.* 43 cSCKs and *ca.* 16 pDNAs.[1] These results indicate that the cSCK has a relatively high efficiency in DNA packaging per gram of cSCK (1:1, pDNA/cSCK, wt:wt), similar to that of some commercially used agents such as bPEI (25 kDa) (1:1).

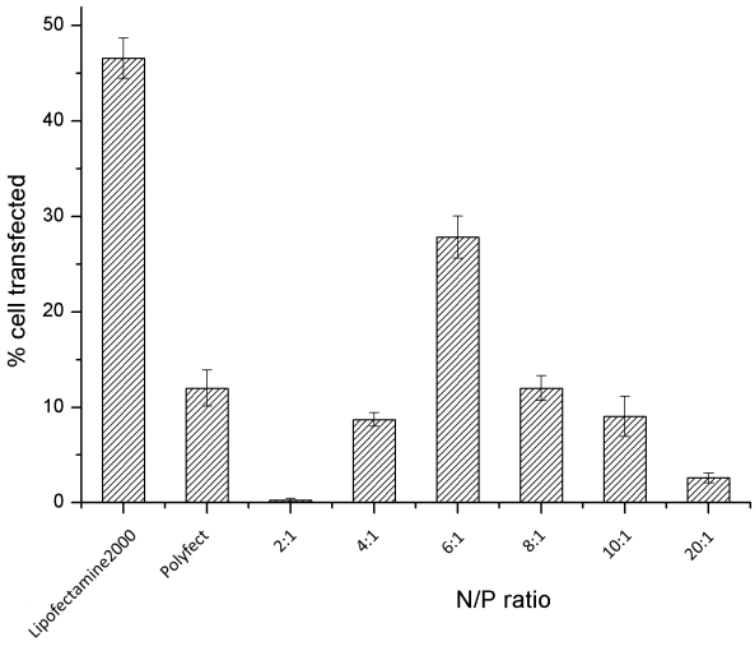

Figure 4-4. Quantification of pEGFP-N1 transfection for HeLa cells by flow cytometry. The reported transfection efficiency is the ratio of the number of cells producing fluorescent signal to the number of total cells.

[1] The cSCK/DNA molar ratio for the complex is calculated to be 2.7:1 (mol:mol), based on an N/P ratio of 2:1 as determined by gel electrophoresis. This molar ratio was calculated by taking into account the double-stranded pDNA having 9466 b, interacting with 18932 amino groups of the cSCK, which requires 2.7 cSCKs, as each cSCK contains *ca*. 7080 amines (based upon a $PAEA_{128}$-*b*-PS_{40} block copolymer aggregation number of 60, as expected from the TEM-measured particle diameter [19]). The theoretical cSCK and pDNA numbers (43 and 16, respectively) within the complexes were calculated by using the buoyant volume of pDNA, calculated to be 3030 nm^3 based on an average buoyant density of 1.7 g/mL and 4733 bp/pDNA, with each base unit being an average of 330 Da in MW, and the volume occupied by cSCKs having diameter of 9 nm.

To evaluate the *in vitro* transfection efficiency of the cSCK, its complexes with pDNA and ps-MeON were produced and assayed by using confocal microscopy/flow cytometry and a luciferase activity assay, respectively. To demonstrate delivery of pDNA, cSCK was complexed with reporter gene pEGFP-N1 expressing green fluorescent protein and incubated with two cell lines (HeLa cells and CHO cells), at six different N/P ratios ranging from 2:1 to 20:1 with no serum added. Polyfect and Lipofectamine2000 were used as positive controls. Confocal microscopy confirmed successful transfection in both cell lines (Fig. 4-3). cSCK appeared to have transfected a similar proportion of cells as did Polyfect for CHO cells, and a higher proportion for HeLa cells. The transfection efficiency was also quantitatively measured by flow cytometry, by the ratio of fluorescent cells to total cells, which showed that cSCK indeed achieved higher transfection (27%) than Polyfect (12%) for HeLa cells (Fig. 4-4), at an N/P ratio of 6:1. Particles at lower N/P ratios did not produce the same level of transfection, possibly due to the size effect of the complexed nanoparticle on cell uptake. It has been reported that particles of 50 - 100 nm in diameter were most efficiently internalized by the cell (*28-30*), compared to larger particles having at least in one dimension a length of 200 to 1000 nm (*18*). The correlation of the transfection efficiencies of cSCK/pDNA complexes at different N/P ratios with their respective average hydrodynamic diameters seems to agree with these literature reports.

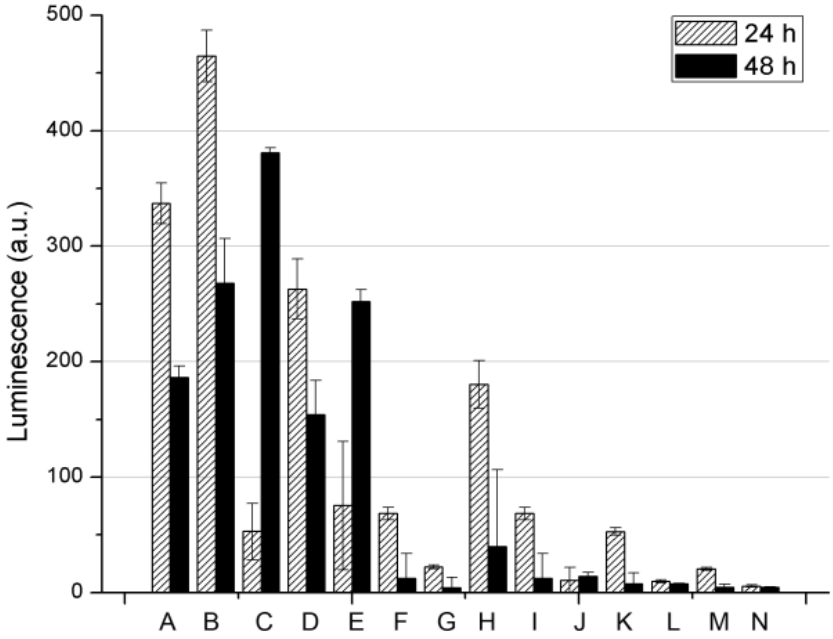

Figure 4-5. Luciferase activity assay of cSCK at different cSCK and ps-MeON concentrations, compared to commercially available transfection agents (Oligofectamine and Polyfect), after 24 h and 48 h incubations. A: Oligofectamine 1.0 µg, ODN 1.0 µmol; B: Polyfect 2.0 µg, ps-MeON 1.0 µmol; C: cSCK 0.3 µg, ps-MeON 1.0 µmol; D: cSCK 0.6 µg, ps-MeON 1.0 µmol; E: cSCK 1.2 µg, ps-MeON: 1.0 µmol; F: cSCK 2.4 µg, ps-MeON: 1.0 µmol; G: cSCK 4.8 µg, ps-MeON 1.0 µmol; H: cSCK 2.4 µg, ps-MeON 0.5 µmol; I :cSCK 2.4 µg, ps-MeON 1.0 µmol; J: cSCK 2.4µg, ps-MeON 2.0 µmol; K:cSCK 2.4 µg, ps-MeON 5.0 µmol; L: ps-MeON 1.0 µmol; M: ps-MeON 5.0 µmol; N: cells only.

To demonstrate delivery of an oligonucleotide, ps-MeON, a 18-mer 2'-O-methyl phosphorothioate oligoribonucleotide that corrects luciferase pre-mRNA splicing in an engineered HeLa cell line was complexed with cSCK in two series of cSCK/ps-MeON ratios. The first series contained a fixed amount of ps-MeON (1 µmol) and various

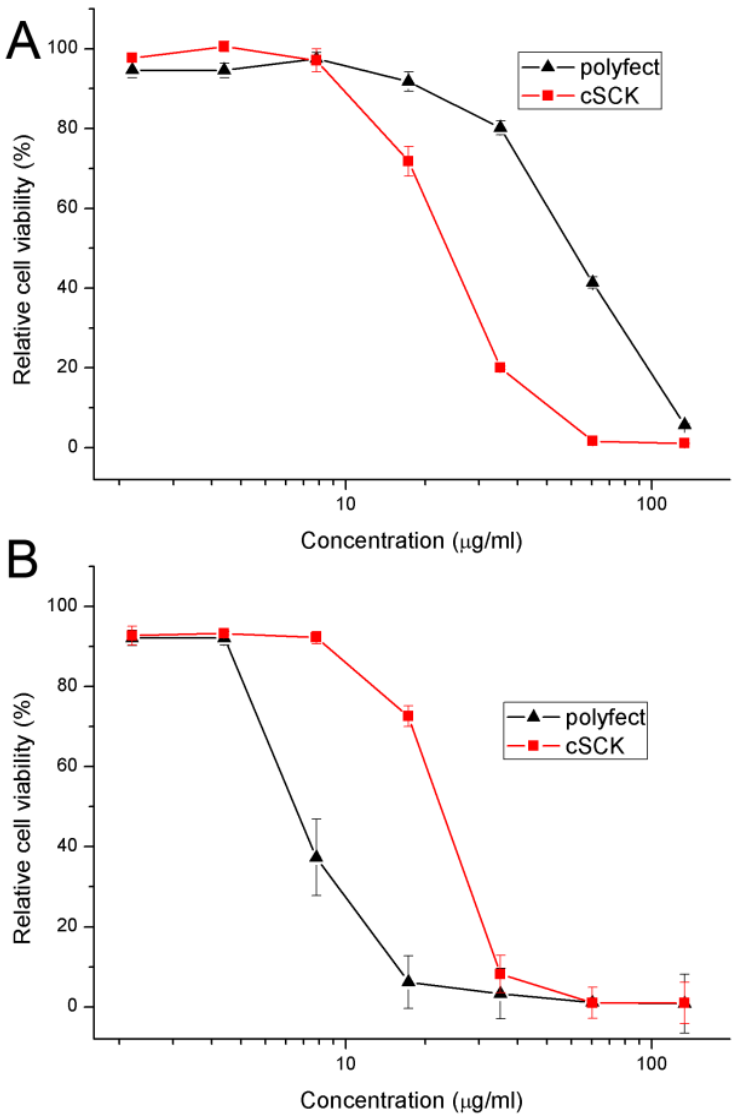

Figure 4-6. Relative cell viability of CHO-K1 cells and HeLa cells in the presence of cSCK and polyfect dendrimer. Data are shown as mean ± SD (n = 6). cSCK showed higher toxicity towards HeLa cells and lower toxicity towards CHO cells, when compared with Polyfect.

amounts of cSCK (0.3-4.8 μg). The second series involved a fixed amount of cSCK (2.4 μg) and various amounts of ps-MeON (0.5 to 5 μmol). Polyfect and Oligofectamine at their respective manufacturer-recommended transfection agent/pDNA ratios were used as

positive controls, using an equal amount of ps-MeON as used in series 1. The ps-MeON-complexes were incubated with pLuc705 HeLa cells for 24 h and 48 h, to allow for expression of luciferase, which was then quantified by measurement of luminescence after the Steady-Glo Luciferase assay reagent was added. In series 1 with 24 h incubation, an optimum ratio of cSCK 0.6 μg/ps-MeON 1.0 μmol was found (Fig. 4-5). After 48 h incubation, the best performing ratio was cSCK 0.3 μg/ps-MeON 1.0 μmol, which led to a higher amount of luminescence than that produced by complexes containing Polyfect and Oligofectamine. It is worth noting that, for the data point where cSCK and Polyfect gave comparable transfection at 48 h (Fig. 4-5, C), only 0.3 μg cSCK was used compared to the 2.0 μg of Polyfect. In series 2, the best performing ratio is cSCK 2.4 μg/ps-MeON 0.5 μmol, for both 24 and 48 h incubations. In both series, a non-linear relationship between cSCK:ps-MeON ratio and total luminescence was observed, a result for which multiple factors might be in effect, such as cell internalization rate, cell proliferation rate (due to cytotoxicity) and intracellular cSCK/ps-MeON dissociation rate.

In vitro cytotoxicity of cSCK was evaluated using CellTiter-Glo Luminescent Cell Viability Assay (Promega Co.) on CHO and HeLa cells. Compared to Polyfect, cSCK maintained > 70% cell viability for CHO cells at 18 μg/mL while < 10% cells were viable under the same conditions and for the same weight concentration of Polyfect (Fig. 4-6). For HeLa cells, the cSCK exhibited higher toxicity than Polyfect, but still

maintained >70% cell viability at 18 μg/mL. Cell death is often caused by the aggregation and accumulation of the multivalent transfection agents in various cellular organelles after dissociation with DNA. To reduce the problem of cytotoxicity, various strategies have been applied including incorporation of degradable moieties in the backbone of the cationic polymers, such as disulfide or ester linkages (*31*-*32*). The cSCK is expected to have lowered cytotoxicity when a degradable crosslinker and/or degradable polymer structure is used, due to disassembly of the nanostructure into discrete polymer chains below critical micelle concentrations and/or small molecules, and subsequent removal from the cell. Amine density also plays a role on cytotoxicity and DNA delivery efficiency. A high amine density may not significantly increase transfection efficiency but could lead to an increase in cytotoxicity (*33*). Therefore, by modulating amine densities of the cSCK through incorporation of diamines containing longer alkyl spacers, a reduction in cytotoxicity while maintaining efficient transfection is expected.

Conclusions

In this work, we have constructed cSCKs that contain closely-spaced primary amines by facile post-polymerization modification of PAA_{128}-*b*-PS_{40}. These nanoparticles formed supramolecular composite assemblies with plasmid DNA at N/P ratios of 2:1 and above. At an N/P ratio of 6:1, the complexes exhibited equal or higher EGFP plasmid transfection efficiencies than that of Polyfect, for CHO and HeLa cells.

Additionally, the cSCK showed higher transfection of a splice-correcting 18-mer oligonucleotide at 48 h than did Polyfect and Lipofectamine2000 while only using a relatively small weight amount of cSCK (0.3 μg cSCK *vs.* 2.0 μg Polyfect). Further increase in transfection efficiency is expected when multiple factors, including polymer molecular weight, block ratio and/or particle morphology and size are optimized. For CHO cells, Polyfect exhibits higher toxicity than cSCK, and for HeLa cells the trend is opposite. However, higher than 90% cell viability at 24 h was observed for cSCK at concentrations of 10 μg/mL or below for both cell lines. It is expected that by incorporation of degradable crosslinkers and/or by use of degradable block copolymer, cytotoxicity would be reduced.

Acknowledgements

This work is supported by the National Heart Lung and Blood Institute of the National Institutes of Health as a Program of Excellence in Nanotechnology (NHLBI-PEN HL080729). The authors thank G. Michael Veith of the Washington University Department of Biology Microscopy Facility for providing technical support with TEM and fluorescence confocal microscopy. We also thank Dr. R. Kole (University of North Carolina, Chapel Hill, NC) for the pLuc705 Hela cell line.

References and Notes

(1) Raper, S. E., Yadkoff, M., Chirmule, N., Gao, G. P., Nunes, F., Haskal, Z. J., Furth, E. E., Propert, K. J., Robinson, M. B., Magosin, S., Simoes, H., Speicher, L., Hughes, J., Tazelaar, J., Wivel, N. A., Wilson, J. M., and Batshaw, M. L. (2002) A pilot study of in vivo liver-directed gene transfer with adenoviral vector in partial ornithine transcarbamylase deficiency. *Hum. Gene Ther. 13*, 163-175.

(2) Verma, I. M., and Somia, N. (1997) Gene therapy - promises, problems and prospects. *Nature 389*, 239-242.

(3) Li, S., and Huang, L. (2000) Nonviral gene therapy: promises and challenges. *Gene Ther. 7*, 31-34.

(4) Taira, K., Kataoka, K., and Niidome, T. (2005) *Non-Viral Gene Therapy*, Springer Tokyo, Tokyo, Japan.

(5) Pack, D. W., Hoffman, A. S., Pun, S., and Stayton, P. S. (2005) Design and development of polymers for gene delivery. *Nat. Rev. Drug Discovery 4*, 581-593.

(6) Boussif, O., Lezoualc'h, F., Zanta, M. A., Mergny, M. D., Scherman, D., Demeneix, B., and Behr, J. P. (1995) A versatile vector for gene and oligonucleotide transfer into cells in culture and in vivo: polyethylenimine. *Proc. Natl. Acad. Sci. U. S. A. 92*, 7297-7301.

(7) Chung, T.-H., Wu, S.-H., Yao, M., Lu, C.-W., Lin, Y.-S., Hung, Y., Mou, C.-Y., Chen, Y.-C., and Huang, D.-M. (2007) The effect of surface charge on the uptake and biological function of mesoporous silica nanoparticles in 3T3-L1 cells and human mesenchymal stem cells *Biomaterials 28*, 2959-2966.

(8) Cho, Y. W., Kim, J. D., and Park, K. (2003) Polycation gene delivery systems: escape from endosomes to cytosol. *J. Pharm. Pharmacol. 55*, 721-734.

(9) Luger, K., Mäder, A. W., Richmond, R. K., Sargent, D. F., and Richmond, T. J. (1997) Crystal structure of the nucleosome core particle at 2.8 Å resolution. *Nature 389*, 251-260.

(10) Suto, R. K., Clarkson, M. J., Tremethick, D. J., and Luger, K. (2000) Crystal structure of a nucleosome core particle containing the variant histone H2A.Z. *Nat. Struct. Mol. Biol. 7*, 1121-1124.

(11) Pan, D., Turner, J. L., and Wooley, K. L. (2004) Shell cross-linked nanoparticles designed to target angiogenic blood vessels *via* $\alpha_v\beta_3$ receptor-ligand interactions. *Macromolecules 37*, 7109-7115.

(12) Rossin, R., Pan, D., Qi, K., Turner, J. L., Sun, X., Wooley, K. L., and Welch, M. J. (2005) ^{64}Cu-labeled folate-conjugated shell cross-linked nanoparticles for tumor imaging and radiotherapy: Synthesis, radiolabeling, and biologic evaluation. *J. Nucl. Med. 46*, 1210-1218.

(13) Sun, G. X., J., Hagooly, A., Rossin, R., Li, Z., Moore, D. A., Hawker, C. J., Welch, M. J., and Wooley, K. L. (2007) Strategies for optimized radiolabeling of nanoparticles for *in vivo* PET imaging. *Adv. Mater. 19*, 3157-3162.

(14) Turner, J. L., Pan, D., Plummer, R., Chen, Z., Whittaker, A. K., and Wooley, K. L. (2005) Synthesis of gadolinium-labeled shell-crosslinked nanoparticles for magnetic resonance imaging applications. *Adv. Funct. Mater. 15*, 1248-1254.

(15) Thurmond, K. B. I., Remsen, E. E., Kowalewski, T., and Wooley, K. L. (1999) Packaging of DNA by shell crosslinked nanoparticles. *Nucleic Acids Res. 27*, 2966-2971.

(16) Green, J. J., Langer, R., and Anderson, D. G. (2008) A combinatorial polymer library approach yields Insight into nonviral gene delivery. *Acc. Chem. Res. 41*, 749-759.

(17) Peer, D., Jeffery, M. K., Hong, S., Farokhzad, O. C., Margalit, R., and Langer, R. (2007) Nanocarriers as an emerging platform for cancer therapy. *Nat.Nanotechnol. 2*, 751-760.

(18) Zhang, K., Fang, H., Chen, Z., Taylor, J.-S. A., and Wooley, K. L. (2008) Shape effects of nanoparticles conjugated with cell-penetrating peptides (HIV Tat PTD) on CHO cell uptake. *Bioconjugate Chem.*, in press.

(19) Sun, G., Hagooly, A., Xu, J., Nyström, A. M., Li, Z., Rossin, R., Moore, D. A., Wooley, K. L., and Welch, M. J. (2008) Facile, efficient approach to accomplish

tunable chemistries and variable biodistributions for shell cross-linked nanoparticles. *Biomacromolecules 9*, 1997-2006.

(20) Pan, D., Turner, J. L., and Wooley, K. L. (2003) Folic acid-conjugated nanostructured materials designed for cancer cell targeting. *Chem. Commun. 19*, 2400-2401.

(21) Remsen, E. E., Thurmond II, K. B., and Wooley, K. L. (1999) Solution and surface charge properties of shell-crosslinked knedel nanoparticles. *Macromolecules 32*, 3685-3689.

(22) Kanayama, N., Fukushima, S., Nishiyama, N., Itaka, K., Jang, W.-D., Miyata, K., Yamasaki, Y., Chung, U.-i., and Kataoka, K. (2006) A PEG-based biocompatible block catiomer with high buffering capacity for the construction of polyplex micelles showing efficient gene transfer toward primary cells. *ChemMedChem 1*, 439-444.

(23) Akagi, D., Oba, M., Koyama, H., Nishiyama, N., Fukushima, S., Miyata, T., Nagawa, H., and Kataoka, K. (2007) Biocompatible micellar nanovectors achieve efficient gene transfer to vascular lesions without cytotoxicity and thrombus formation. *Gene Ther. 14*, 1029-1038.

(24) Ma, Q., and Wooley, K. L. (2000) The preparation of tbutyl acrylate, methyl acrylate, and styrene block copolymers by atom transfer radical polymerization: precursors to amphiphilic and hydrophilic block copolymers and conversion to

complex nanostructured materials. *J. Polym. Sci., Part A: Polym. Chem. 38*, 4805-4820.

(25) Kang, S., Cho, M., and Kole, R. (1998) Up-regulation of luciferase gene expression with antisense oligonucleotides: implications and applications in functional assay development. *Biochemistry 37*, 6235-6239.

(26) Lee, Y., Miyata, K., Oba, M., Ishii, T., Fukushima, S., Han, M., Koyama, H., Nishiyama, N., and Kataoka, K. (2008) Charge-conversion ternary polyplex with endosome disruption moiety: a technique for efficient and safe gene delivery. *Angew. Chem., Int. Ed. 47*, 5163-5166.

(27) Lin, C., Zhong, Z., Lok, M. C., Jiang, X., Hennink, W. E., Feijen, J., and Engbersen, J. F. (2007) Novel bioreducible poly(amindo amine)s for highly efficient gene delivery. *Bioconjugate Chem. 18*, 138-145.

(28) Chithrani, B. D., and Chan, W. C. W. (2007) Elucidating the mechanism of cellular uptake and removal of protein-coated gold nanoparticles of different sizes and shapes. *Nano Lett. 7*, 1542-1550.

(29) Gao, H., Shi, W., and Freund, L. B. (2005) Mechanics of receptor-mediated endocytosis. *Proc. Natl. Acad. Sci. U. S. A. 102*, 9469-9474.

(30) Osaki, F., Kannamori, T., Sando, S., Sera, T., and Aoyama, Y. (2004) A quantum dot conjugated sugar ball and its cellular uptake. On the size effects of endocytosis in the subviral region *J. Am. Chem. Soc. 126*, 6520-6521.

(31) Ou, M., Wang, X.-L., Xu, R., Chang, C.-W., Bull, D. A., and Kim, S. W. (2008) Novel biodegradable poly(disulfide amine)s for gene delivery with high efficiency and low cytotoxicity. *Bioconjugate Chem. 19*, 626-633.

(32) Anderson, D. G., Akinc, A., Hossain, N., and Langer, R. (2005) Structure/property studies of polymeric gene delivery using a library of poly(beta-amino esters). *Mol. Ther. 11*, 426-434.

(33) Lee, C.-C., Liu, Y., and Reineke, T. M. (2008) General structure-activity relationship for poly(glycoamidoamine)s: the effect of amine density on cytotoxicity and DNA delivery efficiency. *Bioconjugate Chem. 19*, 428-440.

Chapter 5

Structure-activity relationships of cationic shell-crosslinked knedel-like nanoparticles: Shell composition and transfection efficiency/cytotoxicity

[Portions of this work have been published previously as Ke Zhang, Huafeng Fang, Zhenghui Wang, Zhou Li, John-Stephen A. Taylor and Karen L. Wooley *Biomaterials* **2009**, published online]

Abstract

Cationic nanoparticles are a promising class of transfection agents for oligonucleotide and gene delivery, but vary greatly in their effectiveness and cytotoxicity. In the last chapter, we described a new class of cationic transfection agents based on cationic shell-crosslinked nanoparticles (cSCKs) that efficiently transfect mammalian cells with both oligonucleotides and plasmid DNA. In an effort to further improve transfection efficiency without increasing cytotoxicity, we examined the effects of the composition of primary amine (pa), tertiary amine (ta) and carboxylic acid (ca) groups in the shell of these nanoparticles. A series of discrete complexes of the cSCKs with plasmid DNA (pDNA) or phosphorothioate 2'-OMe oliogonucleotides (ps-MeON) were prepared over a broad range of amine to phosphate ratios (N/P ratio) of 0:1 to 32:1. The sizes of the complexes and the ability of the nanoparticles to completely bind ODNs were

found to depend on the cSCK amine to DNA phosphate (N/P) ratio and the cSCK buffering capacity. The cSCKs were then evaluated for their ability to transfect cells with plasmid DNA by monitoring fluorescence from an encoded EGFP, and for delivery of ps-MeON by monitoring luminescence from luciferase resulting from ps-MeON-mediated splicing correction. Whereas the cationic cSCK-pa_{25}-ta_{75} was found to be best for transfecting plasmid DNA into HeLa cells at an N/P ratio of 20:1, cSCK-pa_{50}-ta_{50}, at an N/P ratio 10:1 was best for ps-MeON delivery. We also found that increasing the proportion of tertiary relative to primary amine reduced the cytotoxicity. These results demonstrate that a dramatic improvement in gene and oligonucleotide delivery efficiency with decreased cytotoxicity in HeLa cells can be achieved by incorporation of tertiary amines into the shells of cSCKs.

Introduction

Gene therapy and antisense and antigene agents are widely believed to have tremendous potential for the treatment of many diseases currently considered incurable. One major stumbling block in the implementation of these therapeutic strategies is the lack of a suitable method for efficient intracellular delivery of the nucleic acid-based agents. Compared with viral vectors, synthetic materials, such as cationic liposomes, polymers and nanoparticles, are spared from many biosafety issues inherent to viral systems, and are amenable to large scale production and chemical modifications (*1-5*). Though progress has been made in the development of such non-viral vectors (*6-9*), the better transfection materials usually exhibit higher toxicities, and show high variation in effectiveness depending on cell type. Therefore, materials for efficient and non-cytotoxic transfection of nucleic acid-based agents is one of the most urgent and important issues in the field of biomedicine.

Current methods for effecting delivery of nucleic acid therapeutics are often based on liposome- or polymersome-mediated membrane fusion (*10-12*) and ligand-mediated endocytosis (*13-14*). Cationic liposomes have been widely used to transfect DNA in cell culture but its use *in vivo* is oftentimes compromised by its cytotoxicity and poor biodistribution. Addition of polyethylene glycol (PEG) moieties to the transfection agents generally improves their biocompatibility but often leads to significantly reduced transfection efficiency. Surface-conjugated PEG has also been found to hinder the ability

of the cationic functional groups to interact with cell surface receptors (*15-16*). Intricate designs are required to retain effectiveness in transfection while improving biodistribution (*17*). Cationic peptides, polymers, and nanoparticles have been used to enhance endocytosis of nucleic acids through macropinocytosis, and various ligands have been used for receptor-mediated endocytosis. In all cases, the transfection agents must form stable complexes with the nucleic acid therapeutic to protect it from enzymatic degradation and ensure delivery to the target site. The complexes also need to be of appropriate size, shape, flexibility and surface composition for optimal biodistribution and efficient intracellular delivery. For complexes entering cells by endocytosis, a mechanism for endosome rupture or leakage is required to release the complexed nucleic acid therapeutic into the cytosol, such as membrane disruption by endosome disrupting peptides, or the proton sponge effect, which is triggered during endosomal acidification (*18*). Each of the steps, if problematic, can lead to poor performance of the transfection agent. It is, therefore, not surprising that the structure and properties of the transfection agent play important roles in the formation and cell uptake of the complexes, and timely release of the nucleic acid therapeutic (*19-20*).

We have shown that cationic shell-crosslinked knedel-like nanoparticles (cSCKs) can form electrostatic complexes with plasmid DNA and antisense phosphorothioate 2'-OMe oligonucleotides (ps-MeON) and efficiently transfect them into cells (*21*). Similar to the cationic micellar structures (*6, 22-24*) studied by Kataoka *et al*, the cSCKs

represent an example of an emerging class of nanoscale materials composed of amphiphilic block copolymers, each consisting of a hydrophobic section linked to a hydrophilic section (*25-30*). The block copolymers are first assembled into micelles and then crosslinked through chemical conjugation between functional groups in the shell. Compared to the dynamic assemblies of micellar structures, the cSCKs are rigid, robust nanoparticles and resemble natural histones in size and DNA packaging ability (*31*). The particular cSCK used for the transfection experiments consisted of a hydrophobic polystyrene (PS) polymer joined to a polyacrylamidoethylamine (PAEA) that were subsequently micellized and then crosslinked through amide bond formation. The cationic nature of the cSCK, resulting from the protonated primary amines of the PAEA in the shell, facilitates electrostatic binding to negatively charged nucleic acids. The cationic shell is capable of enhancing endocytosis through electrostatic interaction with the membrane surface and subsequent macropinocytosis. The presence of amines is also likely to promote subsequent endosomal release through the proton-sponge effect, due to their ability to neutralize protons (buffering capacity) in the pH 5.5-7.0 range during endosomal acidification.

cSCKs of PAEA-*b*-PS composition were found to transfect plasmid DNA into HeLa cells efficiently. These same particles were also shown to deliver peptide nucleic acids (PNAs) with very high efficiency, through electrostatic binding to a partially complementary DNA, or with even greater efficiency through conjugation *via* a

bioreductively cleavable linker (*32*). The different efficiencies observed for transfection of the electrostatically and covalently bound PNAs suggested that it might still be possible to improve the DNA/ODN binding and release properties of the cSCK by manipulating the structures of the functional groups in the shell. We, therefore, synthesized a series of cSCKs with different shell compositions, and found that their binding capacity, transfection efficiency, and cytotoxicity could be manipulated and improved by varying the relative amounts of primary amines (pa), tertiary amines (ta) and carboxylic acids (ca).

Materials and Methods

Materials. All solvents and chemicals were purchased from Sigma-Aldrich and used without further purification, unless otherwise indicated. *N*-hydroxybenzotriazole·H_2O (HOBt) and 2-(1H-benzotriazole-1-yl)-1, 1, 3, 3-tetramethylaminium hexafluorophosphate (HBTU) were purchased from EMD Chemicals, Inc. The amphiphilic block copolymer, PAA_{128}-*b*-PS_{40}, was prepared using atom transfer radical polymerization of (protected) monomer precursors followed by deprotection, according to literature reported methods (*33*). A luciferase splice-correcting phosphorothioate 2'-O-methyl-oligoribonucleotide (ps-MeON, CCUCUUACCUCAGUUACA) was synthesized on an Expedite 8909 DNA synthesizer (Applied Biosystems, Inc.) using standard solid phase phosphoramidite chemistry and

purified by 20% denaturing polyacrylamide gels, followed by extraction with phenol/chloroform and ethanol precipitation. HeLa cells were obtained from the American Type Culture Collection. The pLuc705 Hela cell line was a generous gift from Dr. R. Kole (University of North Carolina, Chapel Hill, NC). Oligofectamine and Lipofectamine™ 2000 were obtained from Invitrogen Co. Polyfect® was purchased from Qiagen Inc. pEGFP-N1 was obtained from Clontech Laboratories, Inc. Steady-Glo® Luciferase Assay reagent and CellTiter-Glo® Luminescent Cell Viability Assay Kit were purchased from Promega Co. All cell culture media was purchased from Invitrogen, Inc.

Measurements. ^{1}H NMR and ^{13}C NMR spectra were recorded on a Varian 300 MHz spectrometer interfaced to a UNIX computer using Mercury software. Chemical shifts were referenced to the solvent resonance signals. IR spectra were recorded on a Perkin-Elmer Spectrum BX FT-IR system, and data were analyzed using Spectrum v2.0 software. Samples for transmission electron microscopy (TEM) measurements were diluted with a 1 % phosphotungstic acid (PTA) stain (v/v, 1:1). Micrographs were collected at 50,000 and 100,000 × magnifications on a Hitachi-600. Hydrodynamic diameters (D_h) and size distributions were determined by dynamic light scattering (DLS). The DLS instrumentation consisted of a Brookhaven Instruments Limited (Worcestershire, U.K.) system, including a model BI-200SM goniometer, a model BI-9000AT digital correlator, a model EMI-9865 photomultiplier, and a model 95-2 argon ion laser (Lexel Corp.) operated at 514.5 nm. Measurements were made at 25 ± 1 ˚C.

Scattered light was collected at a fixed angle of 90˚. A photomulitplier aperture of 100 μm was used, and the incident laser intensity was adjusted to obtain a photon counting of between, 200 and 300 kcps. Only measurements in which the measured and calculated baselines of the intensity autocorrelation function agreed to within 0.1 % were used to calculate particle size. The calculations of the particle size distributions and distribution averages were performed with the ISDA software package (Brookhaven Instruments Company). All determinations were repeated 5 times and the standard deviations reported were calculated as the error between DLS runs. Zeta potential (ζ) values for the nanoparticle solution samples were determined with a Brookhaven Instrument Co. (Holtsville, NY) model Zeta Plus zeta potential analyzer. Data were acquired in the phase analysis light scattering (PALS) mode following solution equilibration at 25 °C. Potentiometric titration of various cSCKs was performed using a Brinkmann Bottletop Buret 25 and a Corning pH meter 440. cSCK solutions containing 0.5 μmol polymers were diluted in 20 mL 38.94 mM HCl and titrated with 0.010 M NaOH.

Poly(acrylamidoethylamine(Boc)-*co*-acrylamidoethyldimethylamine)-*block*-polystyrene (PAEA(Boc)-*co*-PAEDMA-*b*-PS). PAA_{128}-*b*-PS_{40} (100 mg, 7.4 μmol, 0.94 mmol carboxylic acid groups) was dissolved in DMF (8.0 mL) and stirred for 3 h. Aliquots (2.0 mL) of the solution containing 25 mg polymer were transferred to 3 flasks. Then, 2.0 mL DMF solution containing HOBt (44 mg, 0.33 mmol) and HBTU (125 mg, 0.330 mmol) was added to each flask. After 30 min, 2.0 mL DMF solution containing

various molar ratios of *tert*-butyl 2-aminoethylcarbamate and *N*-(2-aminoethyl) acrylamide (1:3, 2:2 and 3:1, 1.5 eq. to COOH total) and diisopropylethylamine (DIPEA, 35 μL, 0.20 mmol) was slowly added to each flask at 4.0 mL/h using a syringe pump. The reaction mixtures were then sealed, allowed to stir overnight, diluted by the addition of DMF (5.0 mL), transferred to pre-soaked dialysis tubing (MWCO = 6 - 8 kDa), and were dialyzed against 150 mM NaCl solution for 2 days, then against nanopure water (18.0 MΩ·cm) for 5 days. After the dialysis period, the polymers were collected by lyophilization. Characterization data shown below are for PAEA(Boc)$_{64}$-*co*-PAEDMA$_{64}$-*b*-PS$_{40}$. IR (cm^{-1}): 3281, 3060, 2931, 2685, 1660, 1538, 1392, 1366, 1273, 1252, 1170, 1026, 1005, 824, 759. ^{1}H NMR (300 MHz, DMSO-d_6, ppm): δ 1.05-2.30 (br, Boc protons and polymer backbone protons), 2.85-3.65 (br, NHC***H*****$_2$**C***H*****$_2$**NH, NHC***H*****$_2$**C***H*****$_2$**N(C***H*****$_3$**)$_2$), 6.35-6.80 and 6.88-7.40 (br, Ar***H***), 7.50-9.00 (br, CON***H***). ^{13}C NMR (75 MHz, CD_2Cl_2, ppm): δ 28.9 (br), 31.8-46.0 (multiple overlapping br), 56.6 (br), 78.4 (br), 126.4 (br), 127.9 (br), 128.7 (br), 145.3 (br), 156.8 (br), 175.3 (br).

Poly((acrylic acid)-*co*-acrylamidoethylamine(Boc))-*block*-polystyrene (PAA-*co*-PAEA(Boc)-*b*-PS) and poly((acrylic acid)-*co*-acrylamidoethyldimethylamine)-*block*-polystyrene (PAA-*co*-PAEDMA-*b*-PS). Steps leading to the formation of activated polymers were the same as above. Afterwards, 1.0 mL DMF solutions of *tert*-butyl 2-aminoethylcarbamate (180, 96 and 64 equivalents to polymer) and *N*-(2-aminoethyl) acrylamide (180, 96, 64, and 32 equivalents to polymer) were added to the

polymer solutions. Following 24 h reaction time, the polymers were purified using above procedures. PAA_{64}-*co*-$PAEA(Boc)_{64}$-*b*-PS_{40}. IR (cm^{-1}): 3316, 2931, 1704, 1660, 1531, 1392, 1366, 1252, 1170, 823, 760, 668. ^{1}H NMR (300 MHz, DMSO-d_6, ppm): δ 1.05-2.30 (br, Boc protons and polymer backbone protons), 2.80-3.20 (br, NHC$\boldsymbol{H_2}$C$\boldsymbol{H_2}$NH), 6.22-6.83 and 6.83-7.27 (br, Ar$\boldsymbol{H}$), 7.40-8.00 (br, CON$\boldsymbol{H}$). ^{13}C NMR (75 MHz, DMSO-d_6, ppm): δ 28.3 (br), 31.8-44.0 (multiple overlapping br), 79.7 (br), 126.2 (br), 127.3 (br), 128.4 (br), 145.9 (br), 155.9 (br), 174.0 (br), 176.4 (br). PAA_{64}-*co*-$PAEDMA_{64}$-*b*-PS_{40}. IR (cm^{-1}): 3283, 3027, 2927, 2715, 2359, 1727, 1678, 1553, 1382, 1199, 1138, 799, 703. ^{1}H NMR (300 MHz, DMSO-d_6 with 1% TFA-*d*, ppm): δ 0.80-2.49 (br, polymer backbone protons), 2.52-4.20 (br, NHC$\boldsymbol{H_2}$C$\boldsymbol{H_2}$N(C$\boldsymbol{H_3}$)$_2$), 6.35-6.80 and 6.88-7.40 (br, Ar$\boldsymbol{H}$), 8.18-8.84 (br, CON$\boldsymbol{H}$). ^{13}C NMR (75 MHz, DMSO-d_6, ppm): δ 28.8 (br), 31.9-48.0 (multiple overlapping br), 56.4 (br), 126.4 (br), 128.0 (br), 145.9 (br), 175.7 (br).

Removal of Boc groups. Polymers containing Boc protecting groups (1.0 μmol) were dissolved in TFA (3 mL) and stirred for 6 h. The TFA was then removed *in vacuo*. ^{1}H NMR and ^{13}C NMR (DMSO-d_6) confirmed the loss of Boc protons (1.42 ppm) and carbons (28.9 ppm, 79.7 ppm, 155.9 ppm), respectively. $PAEA_{64}$-*co*-$PAEDMA_{64}$-*b*-PS_{40}. IR (cm^{-1}): 3277, 3063, 2956, 2705, 1648, 1553, 1467, 1394, 1366, 1274, 1165, 1024, 748, 701, 660, 630. ^{1}H NMR (300 MHz, DMSO-d_6, ppm): δ 1.05-2.30 (polymer backbone protons), 2.85-3.65 (br, NHC$\boldsymbol{H_2}$C$\boldsymbol{H_2}$NH, NHC$\boldsymbol{H_2}$C$\boldsymbol{H_2}$NH^{+}(C$\boldsymbol{H_3}$)$_2$), 6.20-6.80 and 6.82-7.40 (br, Ar$\boldsymbol{H}$), 7.80-8.40 (br, $CH_2CH_2N\boldsymbol{H_3}^{+}$, CON$\boldsymbol{H}$), 9.70-10.20 (br,

$CH_2CH_2N\boldsymbol{H}^+(CH_3)_2$). ^{13}C NMR (75 MHz, CD_2Cl_2, ppm): δ 31.8-46.0 (multiple overlapping br), 56.6 (br), 126.4 (br), 127.9 (br), 128.6 (br), 145.3 (br), 175.6 (br).

General procedure for the formation of primary-amine containing cSCK-pa-ta, and cSCK-pa-ca from PAEA-*co*-PAEDMA-*b*-PS and PAA-*co*-PAEA-*b*-PS, respectively. Each polymer (1.0 μmol) was dissolved in 7.0 mL dimethylsulfoxide (DMSO) and stirred for 2 h, before being transferred to a pre-soaked dialysis tube (8 kDa MWCO) and being allowed to dialyze against nanopure water (18.0 MΩ·cm) to remove organic solvent. After 4 days of dialysis, clear solutions containing the micelle precursors for the modified cSCKs were obtained. To crosslink each micelle sample, a diacid crosslinker (6.4 μmol, corresponding to 5% crosslinking) was activated by mixing with 2.2 equiv. of HOBt/HBTU (mole:mole) in DMF (400 μL) and allowing to stir for 1 h. This solution was then added slowly with stirring to the micelle solution, which had undergone adjustment of the pH to 8.0, using 1.0 M aqueous sodium carbonate, and reduction of the temperature to 0 ˚C, using an ice bath. The reaction mixture was allowed to stir overnight, and was then transferred to dialysis tubing (8 kDa MWCO) and dialyzed against nanopure water (18 MΩ·cm) for 3 days. All particles showed a mean hydrodynamic diameter (D_h) in the14-18 nm range by DLS, and a mean dry-state diameter of 9 ± 3 nm, estimated from multiple (>3) TEM images.

General procedure for the formation of cSCK-ta-ca from PAA-*co*-PAEDMA-*b*-PS. PAA-*co*-PAEDMA-*b*-PS polymers (1.0 μmol) were assembled into micelles using

the procedures above. To crosslink the micelles, O-bis-(aminoethyl)ethylene glycol (6.4 μmol, corresponding to 5% crosslinking) was added and the solution was allowed to stir at room temperature. After 30 min, an aqueous solution of 1-[3'-(dimethylamino)propyl]-3-ethylcarbodiimide hydrochloride (EDCI) (1.0 equiv., relative to the molar number of available COOH groups) was added. The reaction mixture was allowed to stir overnight before being transferred to presoaked and rinsed dialysis tubing (MWCO 3 kDa) and dialyzed against nanopure water (18.0 MΩ·cm) for 3 days.

Gel retardation assay. The oligodeoxynucleotide d(CCTCTTACCTCAGTTACA) was 5'-labeled by p32-γ-ATP with T4 Polynucleotide Kinase. Serial amounts of cSCKs were mixed with 0.5 μM radiolabeled ODN at N/P ratio of 0, 0.5:1, 1:1, 2:1, 4:1, 8:1, 16:1, 32:1, in PBS buffer for 30 min, which were then mixed with loading buffer (6 ×), and loaded to 15% native polyamide gel.

Cell culture. cSCKs mediated transfection was evaluated on HeLa cells (human cervical cancer cell line) by using the pEGFP-N1 as reporter gene or on pLuc705 Hela cells by luciferase expression. Cells were maintained in DMEM containing 10% FBS, streptomycin (100 μg/mL), and penicillin (100 units/mL) at 37 ˚C in a humidified atmosphere with 5% CO_2. For pLuc705 HeLa cells, additional G418 (100 μg/mL) and hygromycin B (100 μg/mL) were also added.

Luciferase antisense splicing correction assay. pLuc705 HeLa cells were seeded in a 96-well microtiter plate at a density of 2×10^4 cells/well and cultured for 24 h

in 100 μL DMEM containing 10% FBS. ps-MeON (phosphorothioate 2'-O-methyl-oligoribonucleotide: CCUCUUACCUCAGUUACA) was complexed with cSCKs at predetermined N/P ratios in 20 μL opti-MEM solution and incubated for 30 min before use. At the time of the transfection experiment, the medium was replaced with 80 μL of fresh medium, to which the cSCK/ps-MeON complexes were added. Following 24 h incubation periods, 100 μL Steady-Glo® Luciferase assay reagent were added. The contents were mixed and the plate was shaken for 3 min at 600 rpm, and then allowed to incubate at room temperature for 10 min to stabilize the luminescence signal. Luminescence intensities were recorded on a Luminoskan Ascent® luminometer (Thermo Scientific) with an integration time of 1 second per well.

Fluorescence confocal microscopy. HeLa cells (5×10^5) were plated in 35 mm MatTek glass bottom microwell dishes (MatTek Co.) 24 h prior to transfection. pEGFP-N1 (5.0 μg) was complexed with cSCKs at predetermined N/P ratios in 500 μL opti-MEM solution and incubated for 30 min before use. Prior to transfection, the medium in each well was replaced with 2.0 mL of fresh DMEM, to which cSCK/pDNA complexes were added. 6h later, 10 % FBS was added. The plates were then incubated at 37 ˚C for another 24. Each plate was washed 3 times with PBS buffer and viewed under bright field and fluorescent conditions using a Leica TCS SP2 inverted microscope, with excitation by an argon laser (488 nm).

Flow cytometry. The cell culture used for flow cytometry was the same as above. Prior to analysis, cells were washed 3 times with 2.0 mL PBS, collected by trypsinization, pelleted, and resuspended in 0.5 mL PBS. Flow cytometric analysis for the transfection using cSCKs was performed using an FACS-calibur (Becton Dickinson) equipped with an argon laser exciting at 488 nm. For each sample, 20,000 events were collected by list-mode data that consisted of side scatter, forward scatter, and fluorescence emission centered at 530 nm (FL1). The fluorescence was collected at a logarithmic scale with a 1024 channel-resolution. CellQuest software (Becton Dickinson) was applied for the analyses.

Cytotoxicity assay. The cytotoxicity of the cSCKs was examined by CellTiter-Glo Luminescent Cell Viability Assay (Promega Co.). HeLa cells were each seeded in a 96-well plate at a density of 2×10^4 cells/well and cultured for 24 h in 100 μL DMEM containing 10% FBS. Thereafter, the medium was replaced with 100 μL of fresh medium containing various concentrations of cSCKs, Lipofectamine 2000,Polyfect (positive control), or no additive (negative control). After 24 h incubation at 37 ˚C, 100 μL CellTiter-Glo reagent was added. The contents were mixed and the plate was allowed to incubate at room temperature for 10 min to stabilize luminescence signals. Luminescence intensities were recorded on a Luminoskan Ascent® luminometer (Thermo Scientific) with an integration time of 1 second per well. The relative cell viability was calculated by the following equation:

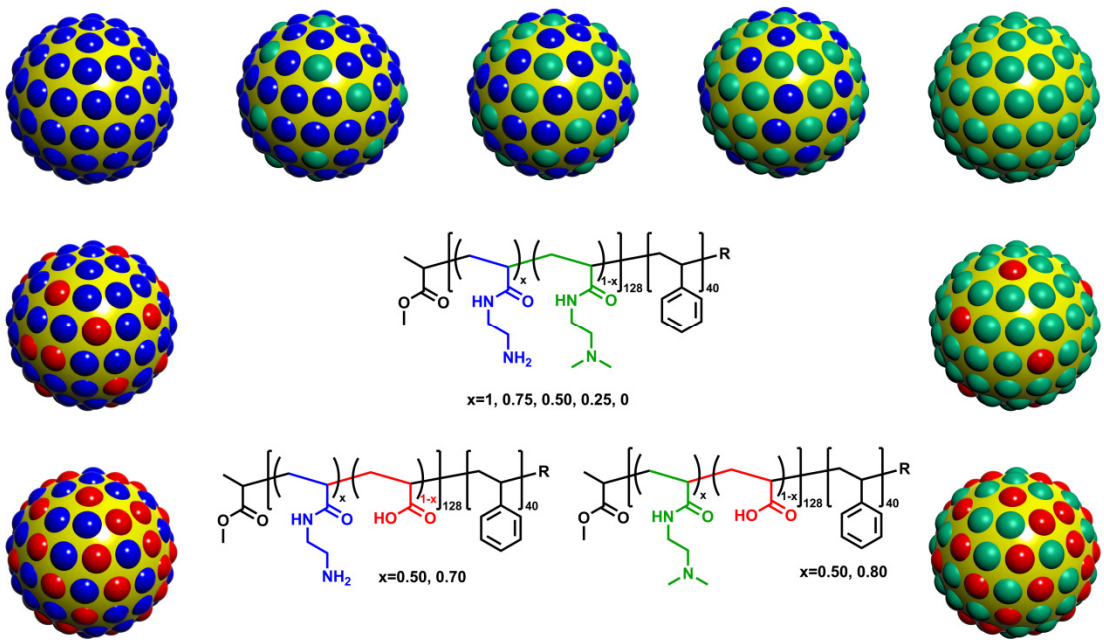

Scheme 5-1. cSCKs with various shell compositions, including mixtures of primary/tertiary amines, mixtures of primary amines/carboxylic acids and mixtures of tertiary amines/carboxylic acids.

$$\text{Cell viability (\%)} = (\text{luminescence}_{(\text{sample})} / \text{luminescence}_{(\text{negative control})}) \times 100$$

Where $\text{luminescence}_{(\text{negative control})}$ was obtained in the absence of particles and $\text{luminescence}_{(\text{sample})}$ was obtained in the presence of cSCKs, Lipofectamine 2000, or Polyfect. The LC50 was determined by non-linear least squares fitting to a Hill Slope function % viability = % $\text{viability}_{\text{max}}$/(1+([NP]/LC50)^slope).

Results and Discussion

The cSCK that we had originally designed consisted of a shell bearing primary amines. To determine the extent to which the structure and basicity of the amines, as well as the net charge and buffering capacity of the shell would affect nucleic acid

binding and transfection, we prepared two general classes of modified cSCKs (Scheme 1). One class consisted of cSCKs with differing ratios of primary and tertiary amines, to maintain the same charge and the buffering capacity in the pH 5.5-7 range, but change the phosphate binding properties of the amines. The second class consisted of cSCKs with differing ratios of amines and carboxylic acids, to change the net charge of the cSCK as well as its buffering capacity. The required cSCKs were prepared by creating a library of modified precursor block copolymers, each of which was separately assembled into micelles and then chemically crosslinked. The particles were 9-11 nm in diameter, as observed by TEM, and 14-18 nm in hydrodynamic diameter, as measured by DLS. All particles were positively charged at pH 5.5 or pH 7.0, as determined by zeta potential measurements. The positively-charged nature of the cSCKs was utilized to form cSCK/DNA complexes through electrostatic interactions.

Binding affinity of the cSCKs for DNA. The binding affinity of the cSCKs for DNA was measured by a gel retardation assay with a 5‘-^{32}P-labeled oligodeoxynucleotide (ODN) at increasing N/P (cSCK nitrogen to DNA phosphate) ratios (Fig. 5-1). While complete binding of the ODN could be achieved at an N/P ratio of 4:1 with the primary amine modified cSCK-pa$_{100}$ (100% primary amine), an N/P ratio of 16:1 was required for the tertiary amine-modified cSCK-ta$_{100}$. The higher N/P ratio required for the tertiary amine-modified cSCK may result from steric hindrance to phosphate binding caused by the methyl groups. Increasing the fraction of tertiary amines from cSCK-pa$_{100}$ to cSCK-

ta_{100} caused an increase in the N/P ratio for complete binding. cSCKs containing carboxylic acids (cSCK-ca) required even higher N/P ratios for complete DNA binding. For example, cSCK-ta_{80}-ca_{20} only showed a small degree of DNA binding at N/P of 32, while cSCK-pa_{50}-ca_{50} showed no binding at all. This is perhaps due to intra-nanoparticle ammonium-carboxylate salt bridge interactions that reduced the availability of the ammonium ions for interacting with the DNA phosphates.

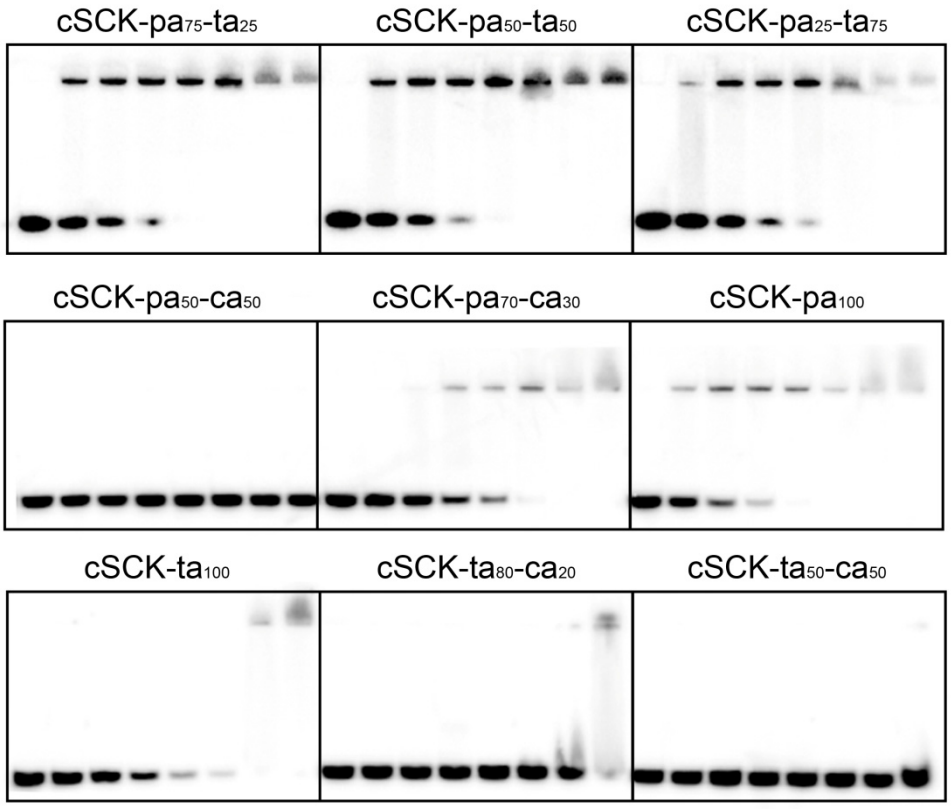

Figure 5-1. Gel retardation essay of cSCKs/ODN complexes at different N/P ratios ranging from 0:1 to 32:1. Radioactively 5'-^{32}P-labeled d(CCTCTTACCTCAGTTACA) (0.5 μM) was incubated with cSCK at N/P ratios of 0, 0.5:1, 1:1, 2:1, 4:1, 8:1, 16:1, 32:1 in PBS buffer for 30 min and then loaded to 15% native polyacrylamide gel

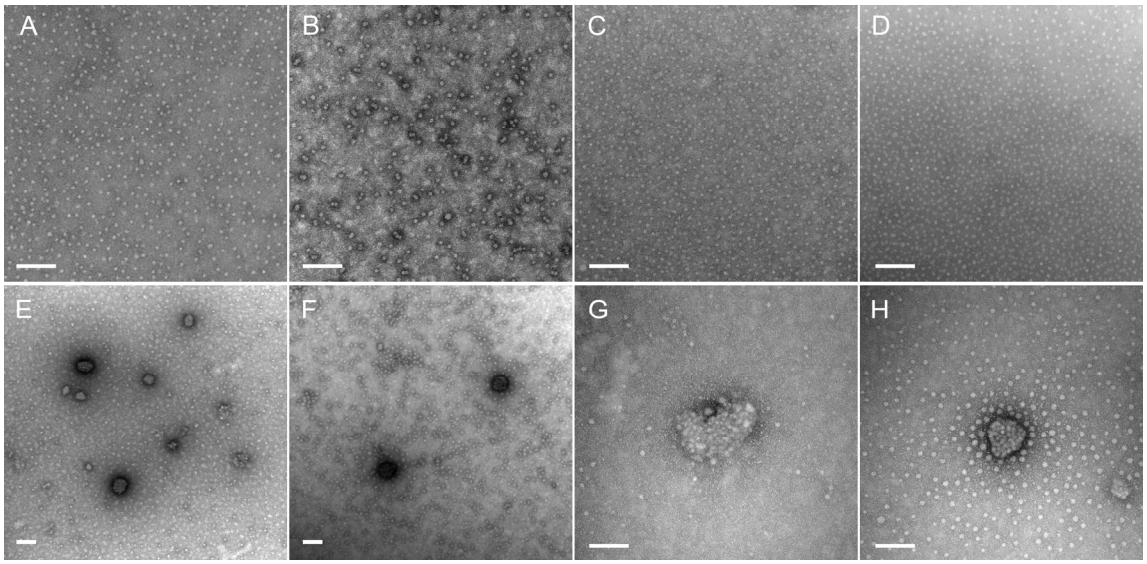

Figure 5-2. TEM images of cSCKs/ps-ODN and cSCK/pDNA complexes at different N/P ratios. A) cSCK-pa_{100}/ps-ODN, N/P 6:1; B) cSCK-pa_{50}-ta_{50}/ps-ODN, N/P 20:1; C) cSCK-ta_{100}/ps-ODN, N/P 20:1; D) cSCK-pa_{70}-ca_{30}/ps-ODN, N/P 30:1; E) cSCK-pa_{100}/pEGFP, N/P 6:1; F) cSCK-pa_{50}-ta_{50} /pEGFP, N/P 20:1; G) cSCK-ta_{100}/pEGFP, N/P 20:1; H) cSCK-pa_{70}-ca_{30}/pEGFP, N/P 30:1.

The binding of pDNA and ps-ODN to various cSCKs was also visualized by TEM (Fig. 5-2). Whereas cSCK-pa-ta, cSCK-ta and cSCK-pa all formed complexes with pDNA or ps-ODN, the size of cSCK/ps-ODN complexes were much smaller than were the cSCK/pDNA complexes. The larger size of the cSCK/pDNA complexes results from multiple cSCKs being required to bind to the large number of phosphates on the plasmid DNA. With an excess of cSCK (N/P>6), the complexes of cSCK/pDNA are generally 50-100 nm in diameter with irregular shapes, while the cSCK/ps-ODN complexes are *ca*. 10 nm in diameter, appear circular in the two-dimensional TEM images, which suggests that the particles adopt a three-dimensional spherical morphology. Decreasing the N/P

ratio below to 2 led to the formation of large aggregates (>800 nm) and further decrease resulted in macroscopic precipitation of the pDNA-cSCK complexes. These large aggregates have been shown to be inefficient for cell transfection, perhaps due to difficulty in endocytosing large structures (*21*).

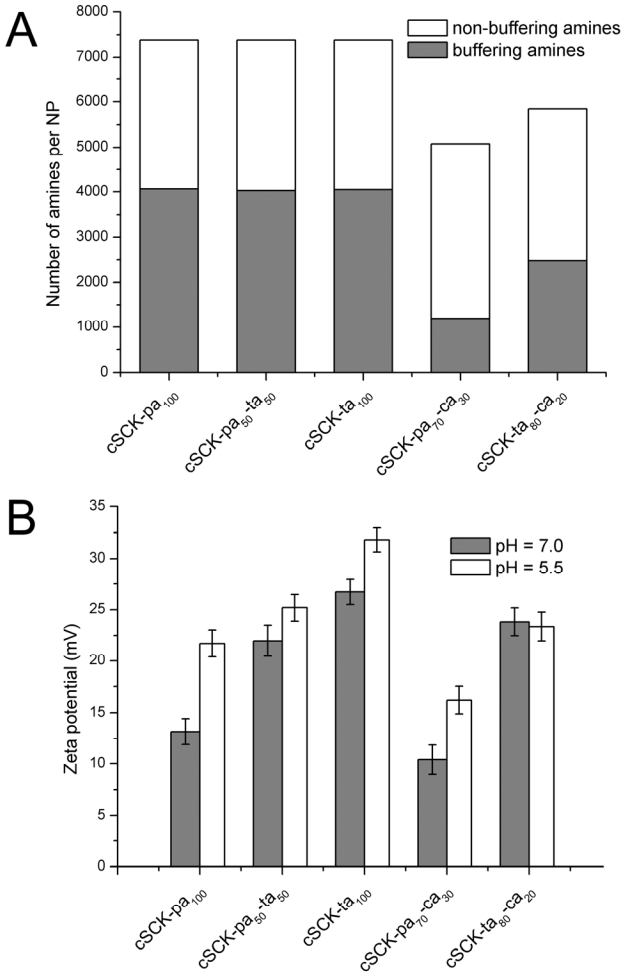

Figure 5-3. A) Relative buffering capacity for the cSCKs. Each bar represents the number of amines per NP, as expected from the particle size and composition. Grey area represents the fraction of amines that absorb protons when pH is changed from 7.0 to 5.5, calculated from potentiometric titration. Other amines (white area) are either already protonated at pH 7.0, or are unable to be protonated at pH 5.5. B) Zeta potential of the particles at pH 7.0 and 5.5.

Buffering capacity and charge of the cSCKs. To determine the buffering capacity of the shells of each type of cSCK, potentiometric titration experiments were conducted. The particles were found to have buffering ability across a pH region of *ca*. 4-9, though only ability to absorb protons in the pH 5.5-7 range during endosomal acidification contributes to endosomal destabilization through the proton sponge effect. We calculated the total number of amines in the shell of each particle based on the particle size and composition, and the number of protons that each NP can absorb when pH is reduced from 7.0 to 5.5, using previously established methods (Fig. 5-3A) (*21, 34*).[1] The cSCKs with 100% amine modification (cSCK-pa_{100}, cSCK-pa-ta and cSCK-ta_{100}), showed almost equal buffering capacity over this pH range, taking up approx. 4000 protons per NP, while incorporation of carboxylic acids significantly decreased this number. For example, cSCK-pa_{70}-ca_{30} could only capture *ca*. 1200 protons. Because all of the particles each have more than 5000 amines, those amines not participating in buffering could be either already protonated at pH 7.0, or unable to be protonated due to being close to the interior of the NP even at pH 5.5. Calculations based on the titration curves over the range of pH from 4-9 support the former explanation.

[1] The total number of amines per particle is estimated based on the mean core size of the particles as measured from TEM images. The number of protontated amines is calculated from the potentiometric titration curve.

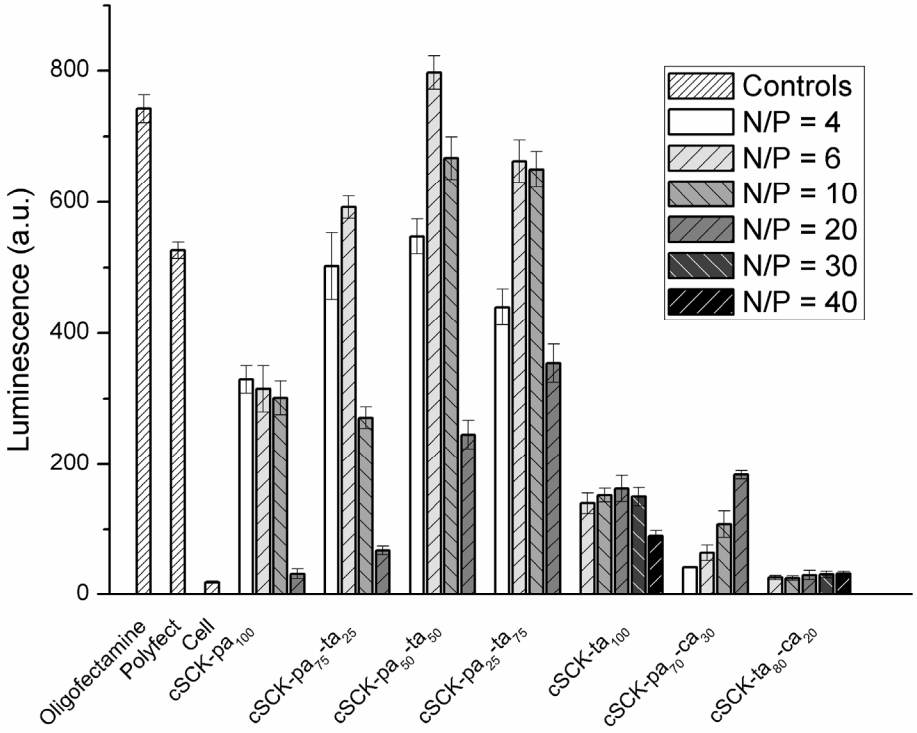

Figure 5-4. Luciferase splice correction activity of cSCK-psON at different N/P ratios, compared to the commercially available transfection agents Oligofectamine and Polyfect, after 24 h incubations with 0.5 μM ps-ODN. From left to right: Polyfect (2 μg), Oligofectamine (0.5 μg), no transfection agent controls; cSCK-pa_{100} at 4:1, 6:1, 10:1, 20:1, cSCK-pa_{75}-ta_{25}, cSCK-pa_{50}-ta_{50}, and cSCK-pa_{25}-ta_{75} at 6:1; 10:1;20:1 ;30:1; cSCK-ta_{100} at 6:1; 10:1; 20:1; 30:1, 40:1; cSCK-pa_{100} and cSCK-pa_{70}-ca_{30} at 4:1, 6:1, 10:1, 20:1; cSCK-ta_{80}-ca_{20} at 6:1, 10:1, 20:1, 30:1, 40:1.

Zeta potential values of the cSCKs were obtained at pH 7.0 and pH 5.5 (Fig. 5-3B). All particles were found to be positively charged at both pHs. However, at pH 5.5, the zeta potential was generally 5-10 mV above that at pH 7.0, except for cSCK-ta_{80}-ca_{20}, which showed very little difference (23.4 mV at pH 5.5 and 23.8 mV at pH 7.0). For the cSCK-pa-ta series, increasing zeta potential was observed with increasing tertiary amine

content at both pH 5.5 and pH 7.0; cSCK-ta_{100} showed the highest charge (31.8 mV at pH 5.5 and 26.7 mV at pH 7.0), and cSCK-pa100 showed the lowest charge (21.7 mV at pH 5.5 and 13.2 mV at pH 7.0). Despite being more charged, cSCK-ta_{100} did not have higher binding affinity for DNA compared with cSCK-pa_{100}, as evidenced in the gel retardation assay (*vide supra*), which is likely due to the steric hindrance of the N-methyl groups.

Transfection of ps-ODN by cSCKs. To rapidly and quantitatively compare the cell transfection efficiences of the modified cSCKS using ps-ODN, we adopted the luciferase splice correction assay developed by Kole and coworkers. This assay relies on a luciferase gene (pLuc705) that results in a longer, mis-spliced mRNA that encodes a defective luciferase. In the presence of a phosphorothioate 2'-O-methyl-oligodeoxyribonucleotide (ps-MeON) CCUCUUACCUCAGUUACA, complementary to the aberrant splice site, correct splicing is restored in a dose-dependent and sequence-specific manner, resulting in an active luciferase. To determine the optimal N/P ratio for a given type of cSCK, we tested the splice correcting efficiciency of a range of cSCK/ps-MeON ratios, using Oligofectamine and Polyfect as positive controls and cells with no additives as a negative control (Fig. 5-4). The highest luciferase activities were observed for the 100% amine-containing cSCKs with 50:50 and 25:75 primary:tertiary amine ratios at N/P ratios of 10:1~20:1. The best among these was cSCK-pa_{50}-ta_{50} at an N/P 10:1 which gave higher levels of transfection than both Polyfect and Oligofectamine. The N/P ratio at which a given cSCK achieved its maximum luciferase activity coincided

with the N/P ratio required to bind all the ps-ODN in the gel retardation assay. This indicates that to achieve maximum luciferase activity, all the ps-ODN must be bound to the cSCK. Differences in the maximum values suggest differences in endocytosis and/or endosomal release efficiencies, since the better-performing particles (cSCK-pa-ta) all have similar buffering capacities in the pH 5.5-7.0 range and,therefore, should all be able to disrupt the endosomes. It may be that the cSCK with a 50:50 mix of primary and tertiary amines has an optimal binding affinity for the ps-MeON for delivery and subsequent release from the cSCK. cSCKs with more tertiary amines may not bind the ps-MeON tightly enough for transport during endocytosis, or may not be endocytosed as efficiently. Conversely, cSCKs with more primary amine may be better at endocytosis and/or bind too tightly to the ps-MeON and prevent release during endosomal disruption. These results agree well with the finding that acetylation of polyethylenimine enhances gene delivery by weakening polymer/DNA interactions (*35*).

Introduction of carboxylates into the shell greatly reduced luciferase activity at all N/P ratios. For cSCK-pa_{70}-ca_{30} at an N/P ratio of 4:1, the luciferase activity was only 7% of the Oligofectamine control and only increased to about 25% at its maximum activity at an N/P ratio of 20:1. For cSCK-ta_{80}-$ca_{20,}$ maximum luciferase activity occurred at an N/P ratio of 20:1 and was only about 5% compared with Oligofectamine. The poor efficiency of the particles containing carboxylic acids can be explained by their reduced buffering capacity in the pH 5.5-7 range, and lower affinity for binding the ps-MeON.

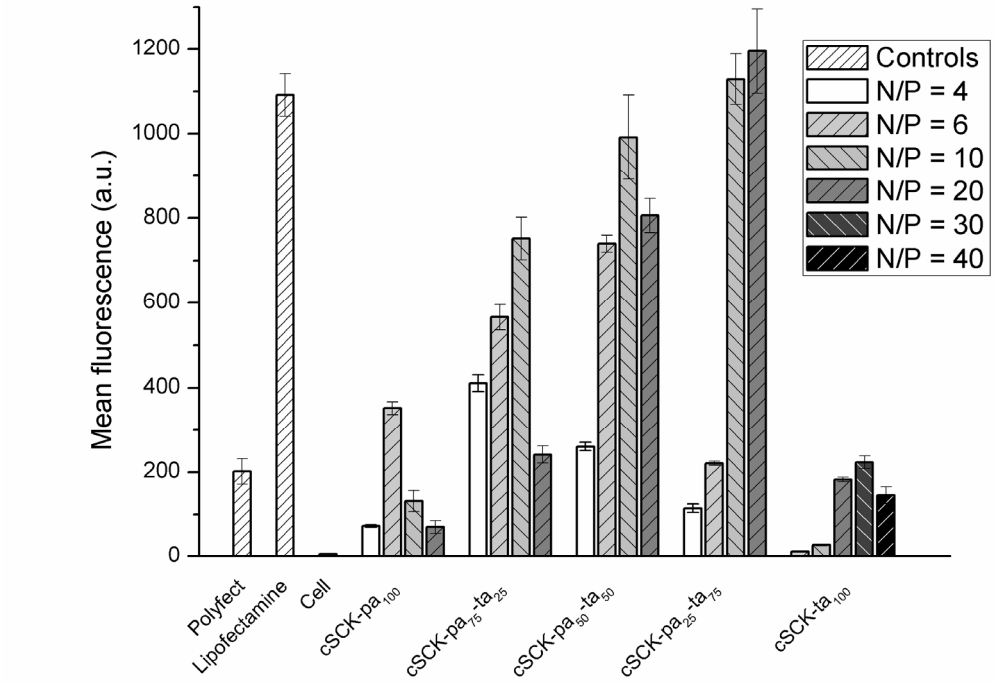

Figure 5-5. Flow cytometry analysis of transfection of plasmid DNA by the cSCKs. The green fluorescent protein encoding pEGFP-N1 (0.8 μg) was transfected into HeLa cells with various N/P ratios.

Transfection of plasmid DNA by cSCKs. To quantify the delivery of plasmid DNA by the cSCKs, we assayed the fluorescence of HeLa cells transfected with the EGFP expressing plasmid pEGFP-N1 by flow cytometry (Fig. 5-5). In general, the higher the percentage of tertiary amine in the cSCK, the higher the EGFP expression level. The highest level of EGFP expression was observed for cSCK-pa_{25}-ta_{75} at N/P of 20:1 to 30:1, which exceeded that for Lipofectamine 2000 and Polyfect, and the lowest level for cSCK-ta_{100} and cSCK-pa_{100}. The trend paralleled what was observed for ps-ODN delivery. Confocal microscopy showed similar results with cSCK-pa_{50}-ta_{50} and

cSCK-pa_{25}-ta_{75} at N/P ratios of 20:1 producing the highest numbers of transfected cells (Fig. 5-6). The number of transfected cells appeared higher with the cSCKs than with Liopfoectamine 2000, although the mean of fluorescence of the cells is almost same. We attribute this effect to the increased cytotoxicity of Lipofectamine 2000 (*vide infra*). Compared with Lipofectamine 2000, Polyfect showed low plasmid delivery, giving *ca*. 20% mean fluorescence, although it outperformed Lipofectamine 2000 in oligo delivery. It is worth noting that the cSCKs with 50-75% tertiary amines gave higher transfection than both Polyfect and Lipofectamine 2000, in both oligo and plasmid delivery experiments.

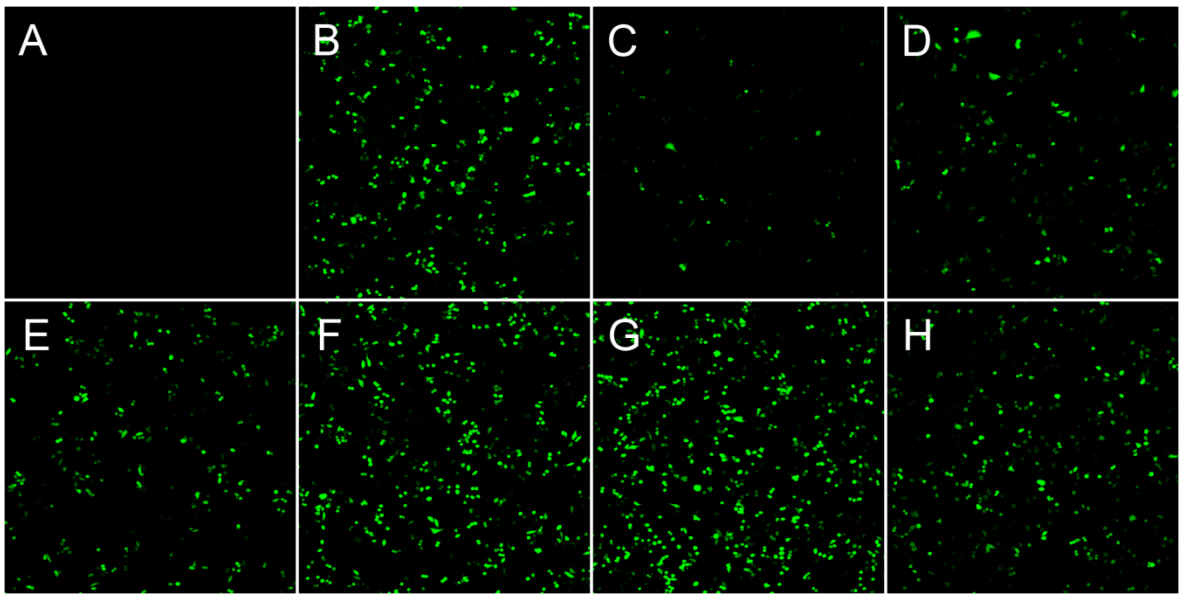

Figure 5-6. Confocal laser scanning microscopy of HeLa cells transfected with pEGFP-N1 (4.0 μg) by cSCKs at specific N/P ratios. A) No transfection agent, B) Lipofectamine 2000 (10 μg), C) Polyfect (20 μg), D) cSCK-pa_{100} at N/P = 10:1, E) cSCK-pa_{75}-ta_{25} at N/P = 10:1, F) cSCK-pa_{50}-ta_{50} at N/P=20:1, G) cSCK-pa_{25}-ta_{75} at N/P=20:1, H) cSCK-ta_{100} at N/P=20:1.

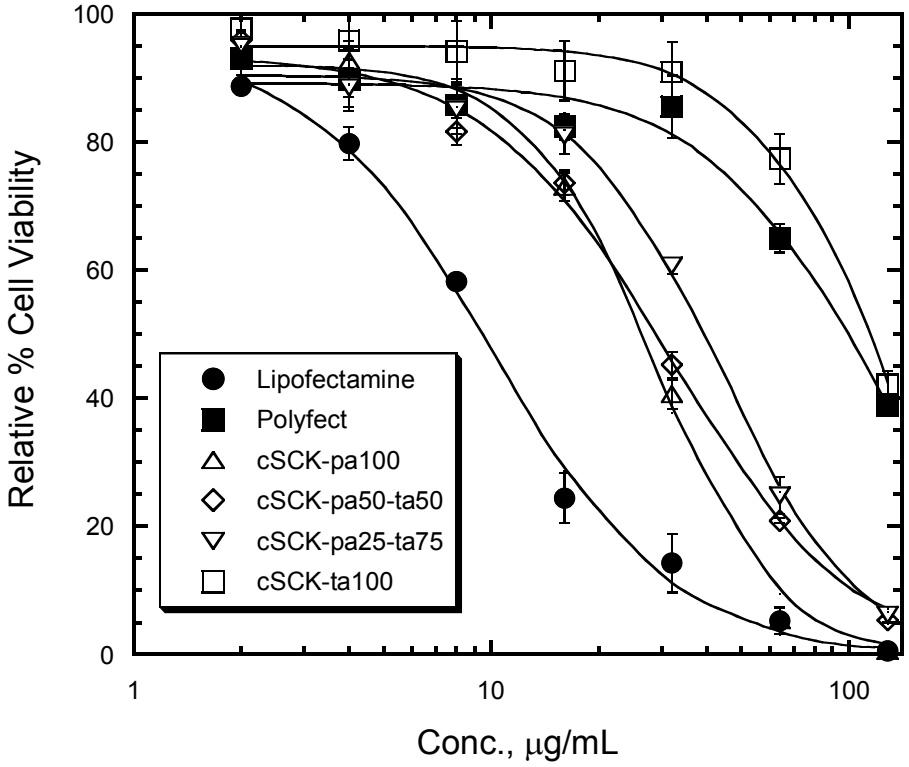

Figure 5-7. Relative cell viability of HeLa cells in the presence of cSCKs and commercial transfection agents.

cSCK cytotoxicity. We evaluated the cytotoxicity of the modified cSCK in HeLa cells by a fluorescence assay for measuring cellular ATP concentration (Fig. 5-7). All of the cSCKs were less toxic than Lipofectamine 2000 (LC50 = 10 ± 1 μg/mL), with the cSCK bearing all primary amines (cSCK-pa100) being the most toxic (28 ± 1.5 μg/mL). In contrast the cSCK bearing all tertiary amines (cSCK-ta100) was the least toxic (117 ± 4 μg/mL) and was similar in toxicity to Polyfect (111 ± 9 μg/mL). The cSCKs that

showed the best transfection efficiencies for ps-ON and plasmid (cSCK-pa50-ta50 and cSCK-pa25-ta75) were of similar or slightly less cytotoxicity (31 ± 2 and 42 ± 2 μg/mL respectively) to cSCK-pa100. All cSCKs showed better than about a 25% loss in viability at 20 μg/mL compared to a 75% loss of viability with the same concentration of Lipofectamine 2000. The results clearly show that the tertiary amines confer less cytotoxicity than the primary amines.

Conclusions

In summary, we have been able to increase the plasmid DNA- and ps-MeON-transfection efficiency and minimize the cytotoxicity of cSCKs by introducing tertiary amines into the shell by chemical modification of the precursor block copolymer. cSCKs with tertiary/primary amine ratios of 50:50 and 75:25 achieved equal or better transfection efficiency for ps-MeON at N/P ratios of ~10:1 - 20:1 compared to Oligofectamie or Polyfect, the current gold standards, with lower cytotoxicity than Lipofectamine 2000. These same cSCKs also showed high plasmid transfection efficiencies, comparable to Lipofectamine 2000, at N/P ratios of ~20:1 - 30:1. We ascribe the high efficiency of these particles to an optimum nucleic acid binding affinity, required to transport the pDNA or ps-MeON into the cell through endocytosis, and buffering capacity in the pH 5.5-7 range, to achieve endosomal disruption and subsequent release of nucleic acid. These modifications and the resulting changes in transfection

efficiency have also helped to better elucidate the structure-activity relationships of the cSCKs. Even higher efficiencies are expected when the particles are conjugated with appropriate ligands for receptor-mediated endocytosis such as the tripeptide RGD for integrin receptors, and moieties for enhancing endosomal release, which are currently under study.

Acknowledgments

This work is supported by the National Heart Lung and Blood Institute of the National Institutes of Health as a Program of Excellence in Nanotechnology (NHLBI-PEN HL080729). We thank Dr. R. Kole (University of North Carolina, Chapel Hill, NC) for the pLuc705 HeLa cell line. We also thank Professor Donald Elbert for use of the Brookhaven Zeta Plus zeta potential analyzer.

References and Notes

(1) Pack, D. W., Hoffman, A. S., Pun, S., and Stayton, P. S. (2005) Design and development of polymers for gene delivery. *Nat. Rev. Drug Discovery 4*, 581-593.

(2) Reineke, T. M., and Grinstaff, M. W. (2005) Designer materials for nucleic acid delivery. *MRS. Bull. 30*, 635-638.

(3) Verma, I. M., and Somia, N. (1997) Gene therapy - promises, problems and prospects. *Nature 389*, 239-242.

(4) Taira, K., Kataoka, K., and Niidome, T. (2005) *Non-viral gene therapy*, Springer Tokyo, Tokyo, Japan.

(5) Raper, S. E., Yadkoff, M., Chirmule, N., Gao, G. P., Nunes, F., Haskal, Z. J., Furth, E. E., Propert, K. J., Robinson, M. B., Magosin, S., Simoes, H., Speicher, L., Hughes, J., Tazelaar, J., Wivel, N. A., Wilson, J. M., and Batshaw, M. L. (2002) A pilot study of in vivo liver-directed gene transfer with adenoviral vector in partial ornithine transcarbamylase deficiency. *Hum. Gene Ther. 13*, 163-175.

(6) Lee, Y., Ishii, T., Cabral, H., Kim, H. J., Seo, J.-H., Nishiyama, N., Oshima, H., Osada, K., and Kataoka, K. (2009) Charge-conversion polyionic complex micelles - efficient nanocarriers for protein delivery into cytoplasm. *Angew. Chem., Int. Ed. 48*, 5309-5312.

(7) Green, J. J., Langer, R., and Anderson, D. G. (2008) A combinatorial polymer library approach yields Insight into nonviral gene delivery. *Acc. Chem. Res. 41*, 749-759.

(8) Peer, D., Jeffery, M. K., Hong, S., Farokhzad, O. C., Margalit, R., and Langer, R. (2007) Nanocarriers as an emerging platform for cancer therapy. *Nat.Nanotechnol. 2*, 751-760.

(9) Li, S., and Huang, L. (2000) Nonviral gene therapy: promises and challenges. *Gene Ther. 7*, 31-34.

(10) Lomas, H., Canton, I., MacNeil, S., Du, J., Armes, S. P., Ryan, A. J., Lewis, A. L., and Battaglia, G. (2007) Biomimetic pH sensitive polymersomes for efficient DNA encapsulation and delivery. *Adv. Mater. 19*, 4238-4243.

(11) Ewert, K. K., Ahmad, A., Bouxsein, N. F., Evans, H. M., and Safinya, C. R. (2008) Non-viral gene delivery with cationic liposome-DNA complexes, in *Methods in molecular biology*, Humana Press Inc., Totowa, NJ United States.

(12) Blanazs, A., Armes, S. P., and Ryan, A. J. (2009) Self-assembled block copolymer aggregates: from micelles to vesicles and their biological applications. *Macromol. Rapid Commun. 30*, 267-277.

(13) Kichler, A., Frisch, B., Lima de Souza, D., and Schuber, F. (2000) Receptor-mediated gene delivery with non-viral DNA carriers. *J. Liposome Res. 10*, 443-460.

(14) Guy, J., Drabek, D., and Antoniou, M. (1995) Delivery of DNA into mammalian cells by receptor-mediated endocytosis and gene therapy. *Mol. Biotechnol. 3*, 237-248.

(15) Sung, S.-J., Min, S. H., Cho, K. Y., Lee, S., Min, Y.-J., Yeom, Y. I., and Park, J.-K. (2003) Effect of polyethylene glycol on gene delivery of polyethylenimine. *Biol. Pharm. Bull. 26*, 492-500.

(16) Mishra, S., Webster, P., and Davis, M. E. (2004) PEGylation significantly affects cellular uptake and intracellular trafficking of non-viral gene delivery particles. *Eur. J. Cell. Biol. 83*, 492-500.

(17) Han, M., Oba, M., Nishiyama, N., Kano, M. R., Kizaka-Kondoh, S., and Kataoka, K. (2009) Enhanced percolation and gene expression in tumor hypoxia by PEGylated polyplex micelles. *Mol. Ther. 17*, 1404-1410.

(18) Cho, Y. W., Kim, J. D., and Park, K. (2003) Polycation gene delivery systems: escape from endosomes to cytosol. *J. Pharm. Pharmacol. 55*, 721-734.

(19) Lee, C.-C., Liu, Y., and Reineke, T. M. (2008) General structure-activity relationship for poly(glycoamidoamine)s: the effect of amine density on cytotoxicity and DNA delivery efficiency. *Bioconjugate Chem. 19*, 428-440.

(20) Yezhelyev, M. V., Qi, L., O'Regan, R. M., Nie, S., and Gao, X. (2008) Proton-sponge coated quantum dots for siRNA delivery and intracellular imaging. *J. Am. Chem. Soc. 130*, 9006-9012.

(21) Zhang, K., Fang, H., Wang, Z., Taylor, J.-S. A., and Wooley, K. L. (2009) Cationic shell-crosslinked knedel-like nanoparticles for highly efficient gene and oligonucleotide transfection of mammalian cells. *Biomaterials 30*, 968-977.

(22) Lee, Y., Miyata, K., Oba, M., Ishii, T., Fukushima, S., Han, M., Koyama, H., Nishiyama, N., and Kataoka, K. (2008) Charge-conversion ternary polyplex with

endosome disruption moiety: A technique for efficient and safe gene delivery. *Angew. Chem. Int. Ed. 47*, 5163-5166.

(23) Honda, M., Kataoka, K., Seki, T., and Takeoka, Y. (2009) Intelligent polymeric micelles from functional poly(ethylene glycol)-poly(amino acid) block copolymers. *Adv. Drug Delivery Rev. 61*, 768-784.

(24) Oba, M., Aoyagi, K., Miyata, K., Matsumoto, Y., Itaka, K., Nishiyama, N., Yamasaki, Y., Koyama, H., and Kataoka, K. (ASAP) Polyplex micelles with cyclic RGD peptide ligands and disulfide cross-links directing to the enhanced transfection via controlled intracellular trafficking. *Mol. Pharmaceutics*.

(25) Huang, H., Remsen, E. E., and Wooley, K. L. (1998) Amphiphilic core-shell nanospheres obtained by intramicellar shell crosslinking of polymer micelles with poly(ethylene oxide) linkers. *Chem. Commun. 13*, 1415-1416.

(26) Thurmond, K. B. I., Remsen, E. E., Kowalewski, T., and Wooley, K. L. (1999) Packaging of DNA by shell crosslinked nanoparticles. *Nucleic Acids Res. 27*, 2966-2971.

(27) Read, E. S., and Armes, S. P. (2007) Recent advances in shell cross-linked micelles. *Chem. Commun. 29*, 3021-3035.

(28) Zhang, K., Fang, H., Chen, Z., Taylor, J.-S. A., and Wooley, K. L. (2008) Shape effects of nanoparticles conjugated with cell-penetrating peptides (HIV Tat PTD) on CHO cell uptake. *Bioconjugate Chem. 19*, 1880-1887.

(29) Pochan, D. J., Chen, Z., Cui, H., Hales, K., Qi, K., and Wooley, K. L. (2004) Toroidal triblock copolymer assemblies. *Science 306*, 94-97.

(30) Zhang, K., Rossin, R., Hagooly, A., Chen, Z., Welch, M. J., and Wooley, K. L. (2008) Folate-mediated cell uptake of shell-crosslinked spheres and cylinders. *J. Polym. Sci., Part A: Polym. Chem. 46*, 7578-7583.

(31) Luger, K., Mäder, A. W., Richmond, R. K., Sargent, D. F., and Richmond, T. J. (1997) Crystal structure of the nucleosome core particle at 2.8 Å resolution. *Nature 389*, 251-260.

(32) Fang, H., Zhang, K., Shen, G., Taylor, J.-S. A., and Wooley, K. L. (2009) Cationic shell-crosslinked knedel-like (cSCK) nanoparticles for highly efficient PNA delivery. *Mol. Pharmaceutics 6*, 615-626.

(33) Ma, Q., and Wooley, K. L. (2000) The preparation of tbutyl acrylate, methyl acrylate, and styrene block copolymers by atom transfer radical polymerization: precursors to amphiphilic and hydrophilic block copolymers and conversion to complex nanostructured materials. *J. Polym. Sci., Part A: Polym. Chem. 38*, 4805-4820.

(34) Sun, G., Hagooly, A., Xu, J., Nyström, A. M., Li, Z., Rossin, R., Moore, D. A., Wooley, K. L., and Welch, M. J. (2008) Facile, efficient approach to accomplish tunable chemistries and variable biodistributions for shell cross-linked nanoparticles. *Biomacromolecules 9*, 1997-2006.

(35) Gabrielson, N. P., and Pack, D. W. (2006) Acetylation of polyethylenimine enhances gene delivery via weakened polymer/DNA interactions. *Biomacromolecules 7*, 2427-2435.

Chapter 6

Cationic shell-crosslinked knedel-like (cSCK) nanoparticles for highly efficient PNA delivery

[Portions of this work have been published previously as Huafeng Fang, Ke Zhang, Gang Shen, Karen L Wooley and John-Stephen A. Taylor *Mol. Pharm.* **2009**, 6(4), 615-626.]

Abstract

Peptide nucleic acids have a number of features that make them an ideal platform for the development of *in vitro* biological probes and tools. Unfortunately, their inability to pass through membranes has limited their *in vivo* application as diagnostic and therapeutic agents. Herein, we describe the development of cationic shell-crosslinked knedel-like (cSCK) nanoparticles as highly efficient vehicles for the delivery of PNAs into cells, either through electrostatic complexation with a PNA•ODN hybrid, or through a bioreductively cleavable disulfide linkage to a PNA. These delivery systems are better than the standard lipofectamine/ODN-mediated method and much better than the Arg_9-mediated method for PNA delivery in HeLa cells, showing lower toxicity and higher bioactivity. The cSCKs were also found to facilitate both endocytosis and endosomal release of the PNAs, while themselves remaining trapped in the endosomes.

Introduction

Peptide nucleic acid (PNA) has a number of properties that make it an ideal platform for the development of antisense- and antigene-based diagnostic and therapeutic agents.(*1-5*) PNA is highly resistant to degradation by biological systems, hybridizes to a complementary DNA or RNA strand with higher affinity than DNA, is able to invade regions of secondary structure, and does not activate RNase H, which would otherwise degrade a target mRNA sequence. It is also readily amenable to synthesis by solid phase automated peptide synthesis, which allows the facile preparation of PNA-peptide hybrids and the incorporation of a wide variety of amino acid analogs and auxiliary agents. Despite these advantages, its poor membrane permeability has limited its widespread application for *in vitro* and *in vivo* purposes. There have been numerous attempts to improve PNA's ability to enter cells, which have largely focused on the use of cationic lipids in conjunction with a complementary ODN, (*6, 7*) and covalently attached cell penetrating peptides and lipids.(*5, 8-10*).

Since their inception, nanoparticles have been investigated as carriers and intracellular delivery agents for antisense oligonucleotides, siRNA, and DNA with varying degrees of success.(*11-15*) We have previously shown that shell crosslinked knedel-like nanoparticles (SCKs) can be made to efficiently enter cells when derivatized with a cell penetrating peptide.(*14, 16, 17*) SCKs are a member of a large family of cross-linked block copolymer micelles that have shown great potential and versatility for

biotechnology and medicine due to the ease by which the shape, composition, functionality, and properties can be tailored for a particular purpose.(*18*) Herein, we report the use of a newly developed class of SCK nanoparticles, called cationic SCKs, or cSCKs, to deliver PNAs into cells without the need to attach cell penetrating peptides.

cSCKs are nanoparticles consisting of a hydrophobic core and a positively charged, highly functionalizable crosslinked shell. We have recently found that these nanoparticles greatly facilitate the entry of plasmid DNA and phosphorothioate 2-O-methyloligoribonucleotides into cells through a likely endocytotic mechanism mediated by the positively charged shell.(*19*) cSCKs are prepared in a multistep process involving the synthesis of an amphiphilic block copolymer, in this particular example, consisting of a polystyrene block linked to a poly(acrylic acid) segment, the carboxylic acids of which are then elaborated into primary amines by coupling to a mono-protected diamine, followed by deprotection. At pH 7, these amines are largely protonated, facilitating the formation of a micelle consisting of a hydrophobic polystyrene core and a hydrophilic, positively-charged shell. The micelle is then stabilized by covalently crosslinking of the shell by amide formation between chains with an activated diester. In this paper, we will show how cSCKs can be used to efficiently deliver PNAs into cells *via* electrostatic complexation with a negatively charged PNA•ODN hybrid, and *via* covalent attachment of a PNA through a bioreductively cleavable disulfide bond (Fig. 6-1). We also show that cSCKs are able to both facilitate endocytosis and endosomal release of the PNAs.

Experimental Procedures

Materials. All solvents and chemicals were purchased from Sigma-Aldrich and used without further purification, unless otherwise indicated. N-hydroxybenzotriazole·H_2O (HOBt) and 2-(1H-benzotriazole-1-yl)-1, 1, 3, 3-tetramethyluronium hexafluorophosphate (HBTU) were purchased from EMD Chemicals, Inc. The amphiphilic block copolymer, poly(acrylic acid)$_{128}$-*block*-polystyrene$_{40}$ (PAA_{128}-*b*-PS_{40}), was prepared using atom transfer radical polymerization of (protected) monomer precursors followed by deprotection, according to literature reported methods.(*20*) This polymer was then transformed into poly(acrylamidoethylamine)$_{128}$-*block*-polystyrene$_{40}$ ($PAEA_{128}$-*b*-PS_{40}) and used for the creation of the cSCKs, according to the literature reported sequence of procedures.(*19*) The pLuc705 HeLa cell line was a generous gift from Dr. R. Kole (University of North Carolina, Chapel Hill, NC). Lipofectamine 2000 was obtained from Invitrogen Co. Polyfect® was purchased from Qiagen Inc. Steady-Glo® Luciferase Assay reagent and CellTiter-Glo® Luminescent Cell Viability Assay Kit were purchased from Promega Co. All cell culture media was purchased from Invitrogen, Inc.

Measurements. ^1H NMR and ^{13}C NMR spectra were recorded on a Varian 300 MHz spectrometer interfaced to a UNIX computer using Mercury software. Chemical shifts were referenced to the solvent resonance signals. IR spectra were recorded on a Perkin-Elmer Spectrum BX FT-IR system, and data were analyzed using Spectrum v2.0

software. Tetrahydrofuran-based gel permeation chromatography (THF GPC) was conducted on a Waters Chromatography, Inc. (Milford, MA) model 1515, equipped with a Waters model 5414 differential refractometer, a Precision Detectors, Inc. (Bellingham, MA) model PD-2026 dual-angle (15˚ and 90˚) light scattering detector and a three-column set of Polymer Laboratories, Inc. (Amherst, MA) gel mixed-bed styrene-divinylbenzene columns (PLgel 5µm Mixed C, 500 Å, and 104 Å, 300 x 7.5 mm columns). The system was equilibrated at 35 ˚C in tetrahydrofuran (THF), which served as the polymer solvent and eluent (flow rate set to 1.00 mL/min). An injection volume of 200 µL was used. System calibration was performed using polystyrene standards. Data were analyzed using Precision Detectors, Inc. Discovery 32 software. N, N-Dimethylformamide-based gel permeation chromatography (DMF GPC) was conducted on a Waters system equipped with an isocratic pump model 1515, a differential refractometer model 2414 and a two-column set of Styragel HR 4 and HR 4E 5 µm DMF 7.8 x 300 mm columns. The system was equilibrated at 70 ˚C in pre-filtered N, N-dimethylformamide (DMF) containing 0.05 M LiBr, which served as polymer solvent and eluent (flow rate set to 1.00 mL/min). Polymer solutions were prepared at concentrations of *ca.* 3 mg/mL and an injection volume of 200 µL was used. Data collection and analysis was performed with Empower Pro software. The system was calibrated with poly(ethylene glycol) standards (Polymer Laboratories, Amherst, MA) ranging from 615 to 443,000 Da. Samples for transmission electron microscopy (TEM)

measurements were diluted with a 1 % phosphotungstic acid (PTA) stain (v/v, 1:1). Carbon grids were exposed to oxygen plasma treatment to increase the surface hydrophilicity. Micrographs were collected at 50,000 and 100,000 × magnifications. Hydrodynamic diameters (D_h) and size distributions were determined by dynamic light scattering (DLS). The DLS instrumentation consisted of a Brookhaven Instruments Limited (Worcestershire, U.K.) system, including a model BI-200SM goniometer, a model BI-9000AT digital correlator, a model EMI-9865 photomultiplier, and a model 95-2 argon ion laser (Lexel Corp.) operated at 514.5 nm. Measurements were made at 25 ± 1 ˚C. Scattered light was collected at a fixed angle of 90˚. A photomultiplier aperture of 100 μm was used, and the incident laser intensity was adjusted to obtain a photon counting of between 200 and 300 kcps. Only measurements in which the measured and calculated baselines of the intensity autocorrelation function agreed to within 0.1 % were used to calculate particle size. The calculations of the particle size distributions and distribution averages were performed with the ISDA software package (Brookhaven Instruments Company). All determinations were repeated 5 times.

PNA Synthesis. All PNAs and conjugates were synthesized on an Expedite 8900 PNA synthesizer on 2 μmol Fmoc-PAL-PEG-PS according to the standard automated Fmoc PNA synthesis procedure utilizing commercial monomers (Panagene Inc., Korea). Following the final step of automated synthesis the resin was washed with dry DMF (2 × 3 mL) and dry CH_2Cl_2 (2 × 3 mL), followed by drying under a stream of N_2. The resin

was then shaken in a vial with trifluoroacetic acid (300 μL) and *m*-cresol (100 μL) at room temperature for 2 h to release and deprotect the PNA. The solution was filtered from the resin, and added into ice-cold Et_2O (5 mL) and kept at 4 °C for 1 h. The resulting precipitate was collected by centrifugation and purified by reverse-phase HPLC on a Varian Microsorb-MV^{TM} C18 column (300 Å) with buffer A [0.1% TFA in H_2O] and buffer B [0.1% TFA in CH_3CN] on a Beckman System Gold instrument equipped with a UV-vis array detector. The fractions were collected and concentrated to dryness in a SpeedVac (Savant) and characterized by UV-vis and MALDI-TOF was carried out on a PerSpective Voyager mass spectrometer with α-cyano-4-hydroxycinnamic acid as the matrix and insulin as the external reference.

PNA. The PNA H-CCTCTTACCTCAGTTACA-NH_2 was synthesized and purified by the general procedure described above. MALDI: average $[M+H]^+$ expected: 4766.6, found: 4764.4.

HO_2C-PNA. Following automated PNA synthesis of H-CCTCTTACCTCAGTTACA-NH_2 and washing, but prior to cleavage and deprotection, the resin was removed from the column and shaken in piperidine (1 mL) and dry DMF (4 mL) for 30 min. The resin was then filtered and washed with dry DMF (2 × 3 mL), dry CH_2Cl_2 (2 × 3 mL), and dried under a stream of N_2. The resin was removed from the column and suspended in dry DMF (100 μL) to which succinic anhydride (20 μmol, 2.0 mg) was added, followed by diisopropylethylamine (20 μmol, 3.5 μL). The mixture was

shaken for 12 h before cleavage and deprotection. MS: average $[M+H]^+$ expected: 4866.7, found: 4867.8.

HO_2C-SS-PNA. Following automated PNA synthesis of H-CCTCTTACCTCAGTTACA-NH_2 and washing, but prior to cleavage and deprotection, the resin was removed from the column and shaken in piperidine (1 mL) and dry DMF (4 mL) for 30 min. The resin was then filtered and washed with dry DMF (2 × 3 mL), dry CH_2Cl_2 (2 × 3 mL), and dried under a stream of N_2. To a suspension of the resin in dry DMF (100 μL) was added 3,3'-dithiodipropionic acid (20 μmol, 4.2 mg) (Aldrich), followed by 4-dimethylaminopyridine (20 μmol, 2.4 mg) and *N*, *N'*-dicyclohexylcarbodiimide (20 μmol, 4.1 mg). The mixture was shaken for 12 h before filtration and final deprotection. MALDI: average $[M+H]^+$ expected: 4958.9, found: 4960.0.

HO_2C-SS-PNA-Lys(FITC). Following automated synthesis of H-CCTCTTACCTCAGTTACA-L-Lys(εMtt)-NH_2 using N-α-Fmoc-N-ε-4-methyltrityl-L-lysine (AnaSpec) but prior to Fmoc deprotection, the resin was removed from the column and treated multiple times with 2% trifluoroacetic acid in methylene chloride (5 mL) until the solution was colorless to selectively remove the Mtt group. The resin was then washed with dry DMF (2 × 3 mL) and dry CH_2Cl_2 (2 × 3 mL), and dried under a stream of N_2. To a suspension of the resin in dry DMF (100 μL) was added FITC (fluorescein isothiocyanate, isomer I, Aldrich) (20 μmol, 7.8 mg), followed by diisopropylethylamine

(20 μmol, 3.5 μL) and shaken for 12 h. The resin was then washed with dry DMF (2 × 3 mL) and dry CH_2Cl_2 (2 × 3 mL), followed by drying under a stream of N_2 prior to coupling with 3,3'-dithiodipropionic acid as described above.

General procedure for the conjugation of PNA to $PAEA_{128}$-*b*-PS_{40} and formation of micelles. PNA (0.68 μmol) was dissolved in dry DMSO (300 μL), to which 20 μL DMSO solution containing 4 equiv. of 1:1 (mol:mol) HBTU/HOBt was added to activate the carboxylic termini of the PNAs. After 30 min, 0, 9, 92 and 185 μL of the activated PNA solution was added to 4 vials, each containing 2 mg $PAEA_{128}$-*b*-PS_{40} 9 μL DIPEA (4 equiv. to the polymer NH_2 residues) in 386 μL DMSO and. The vials were then sealed and the solutions were allowed to stir for 48 h. Following the allocated reaction times, DMSO was added to each vial to give a final volume of 1 mL, and the mixtures were transferred to dialysis tubing (MWCO: 15 kDa) and dialyzed against 300 mM NaCl solution for 4 days, then nanopure water (18 MΩ·cm) for 2 days, to give the micelle precursor for the cSCK and cSCK-PNA conjugates. The final polymer concentration was 0.70 mg/mL. The number of PNA per polymer was calculated to be 0, 0.1, 1 and 2, based on UV-vis measurement of the PNA absorption at 260 nm. For the preparation of cSCK(Alexa Fluor 633)-SS-PNA$(FITC)_2$, Alexa Fluor 633 succinimidyl ester (Invitrogen) was added to the reaction mixture following the addition of HO_2C-SS-PNA(FITC).

General procedure for the crosslinking of cSCK and cSCK-PNA micelles. The diacid crosslinker (5.0 mg, 14 μmol) was activated by mixing with 2.2 equiv. of HOBt/HBTU (4 mg/12 mg, 1:1, mole:mole) in DMF (400 μL) and allowing to stir for 1 h. The activated crosslinker solution (0.67 μmol/19 μL, equiv. to 5% of polymer NH_2 groups) was then added slowly with stirring to 2.9 mL of the aqueous micelle solutions (~0.7 mg/mL), which had been adjusted to pH 8.0, using 1.0 M aqueous sodium carbonate, and cooled to 0 ˚C, using an ice bath. The reaction mixture was allowed to stir overnight, and was then transferred to dialysis tubing (8 kDa MWCO) and dialyzed against nanopure water (18 MΩ·cm) for 2 days. Clear solutions containing the cSCKs and cSCK-PNA conjugates with a final polymer concentration of 0.65 mg/mL were obtained.

Cell culture. cSCK-mediated PNA delivery was evaluated on pLuc705 HeLa cells. Cells were maintained in DMEM containing 10% FBS, streptomycin (100 μg/mL), penicillin (100 units/mL), G418 (100 μg/mL) and hygromycin B (100 μg/mL) at 37 ˚C in a humidified atmosphere with 5% CO_2.

Splice correction assay. pLuc705 HeLa cells were seeded in a 96-well microtiter plate at a density of 2×10^4 cells/well and cultured for 24 h in 100 μL DMEM containing 10% FBS. For delivery of covalent cSCK-PNA conjugates, pLuc705 cells were treated with 100 μL/well the cSCK-PNA solution in DMEM medium (10% FBS) for 24 h. For PNA/ODN heteroduplex (electrostatically associated) delivery, PNA/ODN duplexes were

formed prior to addition to the cell plates. Formation of PNA/ODN heteroduplexes was performed by gradual mixing of PNA (H-CCTCTTACCTCAGTTACA-NH_2) and complementary (underlined) ODN (5'-AATATGTAACTGAGGTA-3'). The PNA/ODN heteroduplex was then incubated with Lipofectamine 2000, Polyfect or cSCK in 20 μL of OPTI-MEM for 15 min, before addition to pLuc705 cell wells containing 80 μL of fresh culture medium. After 24 h incubation, 100 μL of Steady-Glo® Luciferase assay reagent were added. The contents were mixed and allowed to incubate at room temperature for 10 min to stabilize luminescence. Signals were recorded on a Luminoskan Ascent® luminometer (Thermo Scientific) with an integration time of 1 second per well.

Cytotoxicity assay. Cytotoxicities of the cSCK and cSCK-PNA conjugates were examined by CellTiter-Glo Luminescent Cell Viability Assay (Promega Co.). HeLa cells were seeded in a 96-well plate at a density of 2×10^4 cells/well and cultured for 24 h in 100 μL DMEM containing 10% FBS. Thereafter, the medium was replaced with 100 μL of fresh medium containing various concentrations of cSCKs, cSCK-PNA conjugates, Polyfect, Lipofectamine 2000 (positive controls), or no additive (negative control). After 24 h incubation at 37 ˚C, 100 μL of CellTiter-Glo reagent were added. The contents were mixed and the plate was allowed to incubate at room temperature for 10 min to stabilize the luminescence signals. Luminescence intensities were recorded on a Luminoskan Ascent® luminometer (Thermo Scientific) with an integration time of 1 second per well. The relative cell viability was calculated by the following equation

where $\text{luminescence}_{(\text{negative control})}$ is in the absence of particles and where $\text{luminescence}_{(\text{sample})}$ is in the presence of particles.

$$\text{Cell viability (\%)} = (\text{luminescence}_{(\text{sample})} / \text{luminescence}_{(\text{negative control})}) \times 100$$

RT-PCR. pLuc705 HeLa cells were seeded in a 24-well plate at a density of 5×10^4 cells/well and treated as described above for the splice correction assay. Total RNA was isolated using Trizol® (Invitrogen, Inc.) following the manufacturer's instructions. cDNA was synthesized with SuperScript™ II (Invitrogen Inc.), after TURBO® DNase (Ambion, Inc.) treatment. The cDNA was then used as a template for PCR, which was carried out using GoTaq® Flexi DNA Polymerase (Promega, Inc.). Primers for PCR were as follows: forward primer, 5′-TTGATATGTGGATTTCGAGTCGTC-3′; reverse primer, 5′-TGTCAATCAGAGTGCTTTTGGCG-3′. Forward primer was labeled by [γ-^{32}P]-ATP with T4 Polynucleotide Kinase. The PCR program was as follows: (95 ˚C, 2 min) × 1 cycle, (95 ˚C, 0.5 min; 55 ˚C, 0.5 min; 72 ˚C, 0.5 min) × 24 cycles, (72 ˚C, 5 min) × 1 cycle. The PCR products were analyzed on 8% native polyacrylamide gel with 1 × TBE buffer. Gel images were scanned by a BioRad Phosphorimager and analyzed by Quantity One software (Bio-Rad Co.).

Fluorescence confocal microscopy. HeLa cells (5×10^5) were plated in 35 mm MatTek glass bottom microwell dishes (MatTek Co.) 24 h prior to transfection. At the time of transfection, the medium in each dish was replaced with 2 mL of fresh medium. Then, cSCK(Alexa Fluor 633)-SS-PNA$(\text{FITC})_2$ (80 μL) was added. The dishes were

then returned to the incubator to incubate at 37 ˚C for 1 h or 24 h. Each dish was washed 3× with PBS buffer and viewed under bright field and fluorescence conditions using a Leica TCS SP2 inverted microscope, with excitation by an Ar laser (488 nm) and a HeNe laser (633 nm).

Results and Discussion

PNA Transfection Strategies. We investigated two strategies for introducing PNAs into cells that make use of the unique properties of the cSCKs (Fig. 6-1). The cSCKs were designed to resemble histone core particles in their nanoscopic size, positively-charged surfaces, and DNA packaging ability, while also possessing characteristics that would lead to their use as synthetic vectors for gene delivery. We have recently shown that cSCKs efficiently deliver negatively-charged plasmid and oligonucleotides into cells through an endocytotic mechanism, most likely macropinocytosis. (*19*) Therefore, in this current study, the first strategy was to deliver PNA through electrostatic complexation with the cSCK by hybridizing it to a negatively charged complementary ODN (Fig. 6-1a). The second strategy was to deliver the PNA through covalent attachment of the PNA to the cSCK (Fig. 6-1b). Because the cSCKs are large (about 10 nm in diameter) relative to the PNAs, a covalently attached PNA might be engulfed by the nanoparticle, thereby, being unable to enter the nucleus and/or bind to the splice correction site. In addition, it was recognized that, should the cSCKs be trapped in intracellular compartments, having an ability to disconnect the PNA from the

cSCK nanostructure would be important. We, therefore, decided to attach the PNA *via* a bioreductively cleavable disulfide linkage. This linkage is expected to be stable in serum, but upon exposure to the cytosol be reduced, thereby, liberating the PNA.

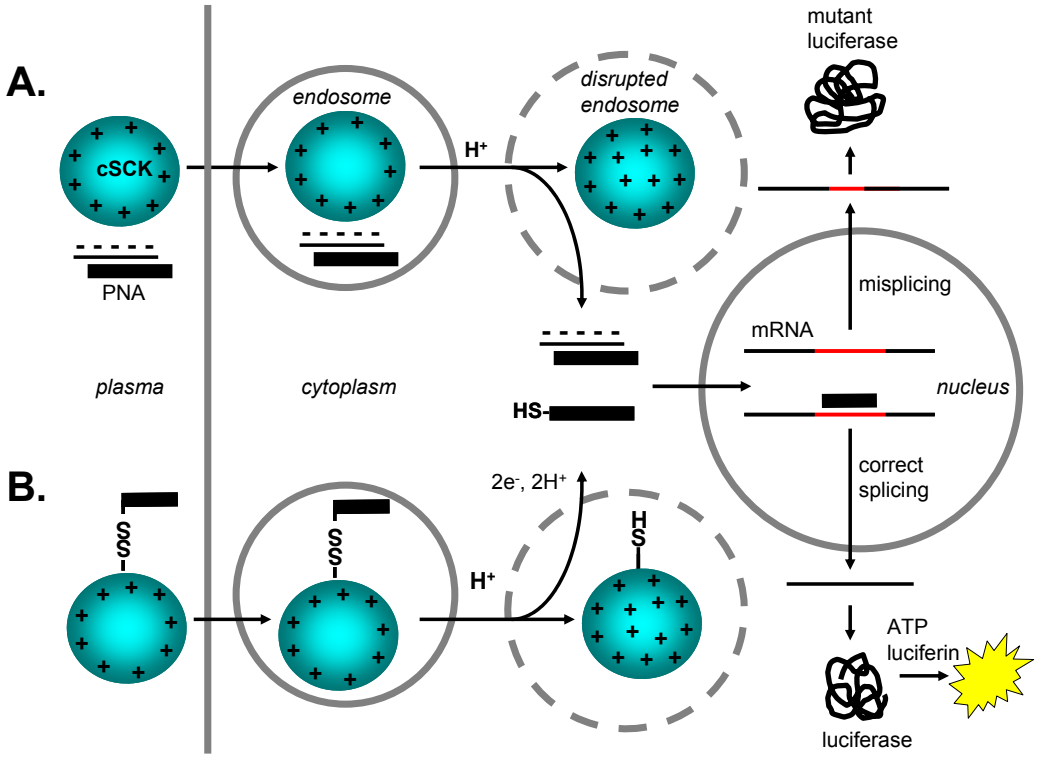

Figure 6-1. Strategies for the development of electrostatic and covalent-based nanoparticle agents for transfection of PNA. A) Electrostatic system, B) Bioreductively cleavable covalent system. At pH 7 most of the amines of the cSCK are protonated resulting in a cationic shell that facilitates both electrostatic binding of PNA•ODN duplexes and macropinocytosis. The remaining basic groups act as a proton sponge that acquire additional protons and counterions thereby causing disruption of the endosome. In system A, this disruption causes release of the PNA•ODN into the cytoplasm from where it can translocate into the nucleus. Binding of the PNA to the mis-splicing site in the pLuc705 luciferase gene corrects the splicing which results in active luciferase which can be assayed by the production of light in the presence of luciferin. In the case of the covalently linked system B, disruption of the endosome exposes the cSCK to reducing agents which cleave the disulfide bond and cause the release of the splice-correcting PNA.

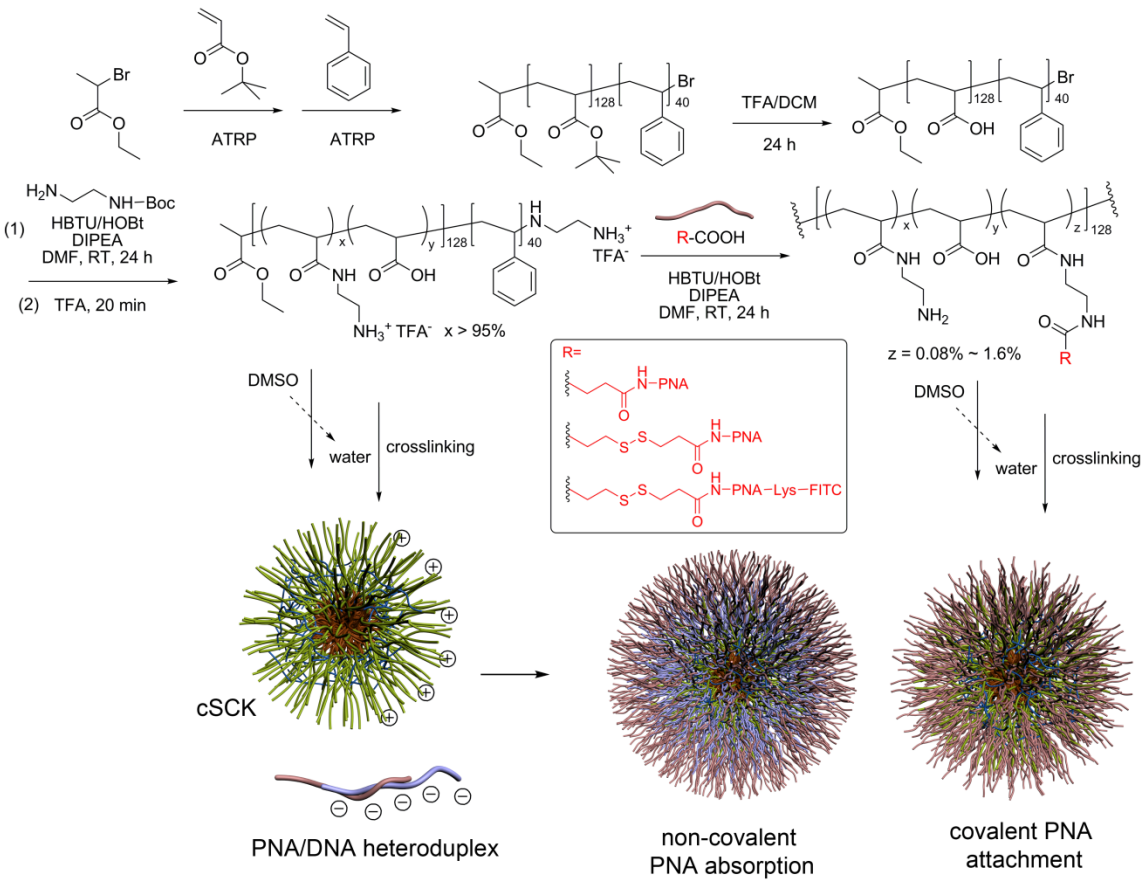

Figure 6-2. Synthesis of the electrostatic and covalent-based nanoparticle transfection agents. The starting material consisted of a block copolymer having a hydrophobic styrene block and a hydrophilic primary amine-bearing block ($PAEA_{128}$-*b*-PS_{40}). Micellization of this block copolymer by dialysis of its DMSO solution against water followed by crosslinking with an activated diester affords the cSCKs. Subsequent electrostatic association with PNA•ODN gives the cSCK carrying PNA via non-covalent PNA absorption. To make the covalently linked cSCK-SS-PNA nanoparticles, the block copolymer was coupled to a carboxy-terminated disulfide-linked PNA and then micellized and crosslinked.

Design and synthesis of the cSCK and constructs. The particular cSCK was chosen for its ability to efficiently transfect negatively charged plasmid DNA and 2'-O-methyl phosphorothioate oligoribonucleotides.(*19*) The cSCK was synthesized by

micellization and crosslinking of a block copolymer consisting of a 40-mer polystyrene block and a 128-mer poly N-(2-aminoethyl)acrylamide block (Fig. 6-2). The block copolymer was prepared by sequential atom transfer radical polymerization of protected monomers followed by three steps of post-polymerization modifications. The lengths of the blocks were estimated from GPC and ^{1}H NMR spectroscopy after each step of polymerization. Micellization was carried out by rapid dilution of a DMSO solution of the block copolymer into water at pH 6. The shell is then crosslinked by the addition of an activated diester. The cSCKs were characterized by DLS, TEM and ζ potential measurements. They were found to be of a globular morphology having a number-average diameter of approximately 10 nm (TEM) and with a ζ potential value of 21.3 mV. From TEM measurement of the particle core size, each cSCK is estimated to be comprised of *ca*. 60 chains, or *ca*. 7700 amines.

The cSCKs bearing a covalently linked PNA were prepared by linking of a carboxy terminal PNA with the block copolymer, facilitated by HBTU/HOBt, prior to micellization. The PNAs were coupled so as to give 0.1, 1 or 2 PNAs/polymer chain and purified by extensive dialysis against 300 mM NaCl solution, and then against nanopure water. The amount of PNA per chain was calculated from the estimated molar absorption coefficients for the PNA. The polymer-PNA conjugates were micellized by the same procedure as for the cSCK and similarly characterized by DLS, TEM and ζ potential measurement. They were found to be indistinguishable in size and surface charge from

the non-PNA-conjugated cSCKs. Three types of construct were prepared. One with a non-bioreductively cleavable linker, cSCK-PNA, one with a bioreductively cleavable disulfide bearing linker, cSCK-SS-PNA, and one with a Alexa Fluor 633 label on the cSCK linked to a FITC labeled PNA *via* a disulfide linker, cSCK(Alexa Fluor 633)-SS-PNA$(FITC)_2$.

PNA Transfection Efficiency Assays. To rapidly and quantitatively assay for the effectiveness of our two PNA transfection strategies, we adopted the luciferase splice correction assay developed by Kole and coworkers (*21*) and later used to evaluate PNAs.(*8*) This assay relies on a luciferase gene (pLuc705) that results in a longer, mis-spliced mRNA that encodes a defective luciferase (Fig. 6-1). In the presence of a PNA complementary to the aberrant splice site, correct splicing is restored, resulting in a shorter mRNA and an active luciferase. The extent to which splicing is corrected can then be monitored easily in a high throughput fashion, by measuring the light produced by the luciferase enzyme in the presence of luciferin. The light output is, thus, a function of the transfection efficiency and cytotoxicity. The extent of splice correction can also be directly and quantitatively assayed by RT-PCR. To evaluate the cytotoxicity of the agents, we relied on cell viability measurements based on quantification of the amount of ATP produced by metabolically active cells.

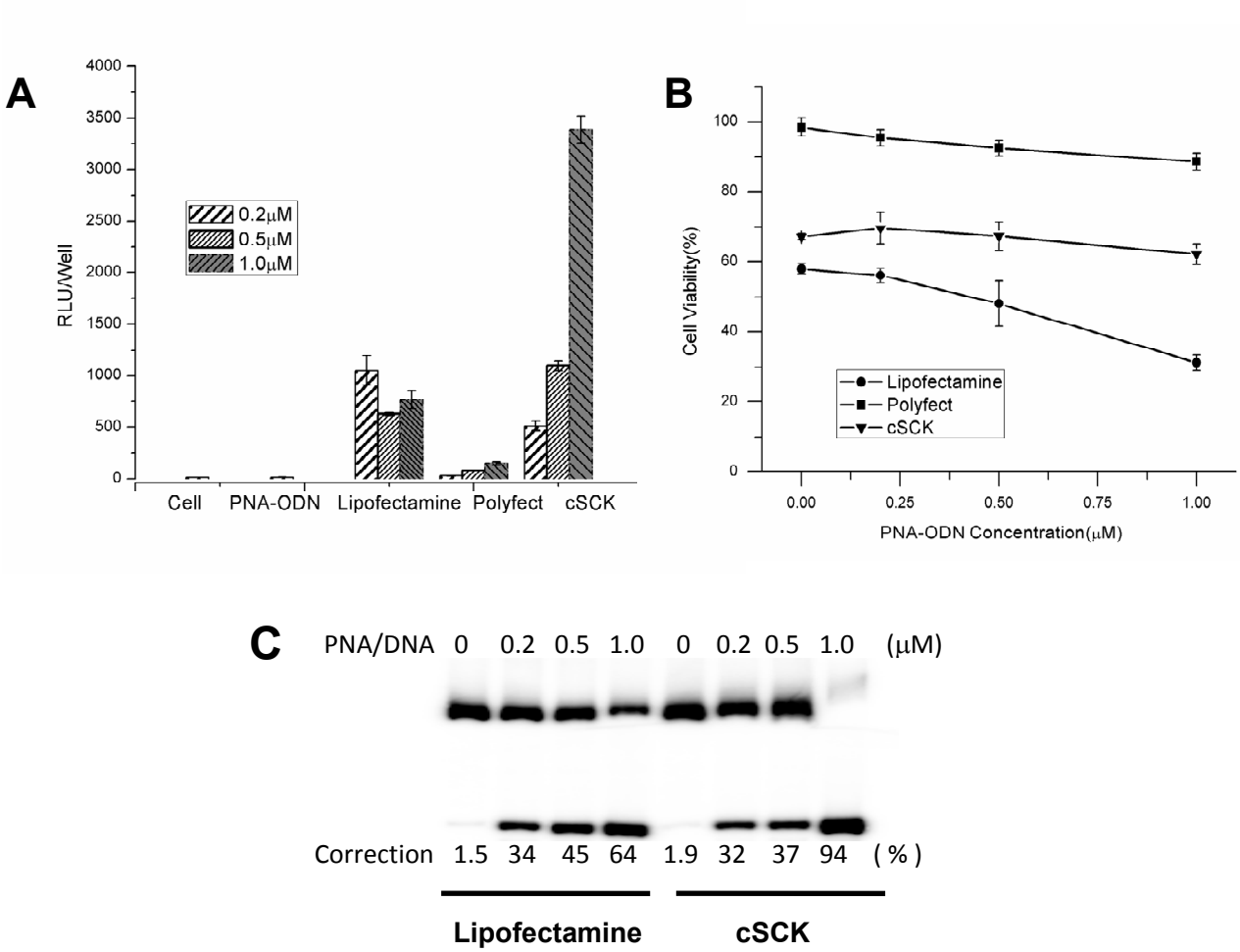

Figure 6-3. Bioactivity and cytotoxicity of electrostatically-mediated PNA•ODN delivery by cSCKs and conventional agents. Splice-correcting PNA that was hybridized to an equimolar amount of partially complementary ODN and then was mixed with 10 μg/mL of Lipofectamine 2000, 20 μg/mL Polyfect, or 20 μg/mL cSCK to give 0.2, 0.5, 1 μM final concentration of PNA. A) pLuc705 HeLa cells were incubated with transfection agent for 24 h, and then assayed for PNA bioactivity *via* luciferase activity. B) Cell viability was assayed by an ATP assay and shown as a percentage of the viability of the control cells. C) Percentage splice correction by an RT-PCR assay for the different PNA•ODN concentrations. The upper band corresponds to a 268 bp fragment from mis-splicing, while the lower band corresponds to a 142 bp fragment from correct splicing.

Transfection of PNA•ODN hybrids by cSCKs. Cationic transfection agents have been developed that can efficiently deliver negatively-charged nucleic acids into cells in culture, but cannot deliver PNAs because of their lack of charge. A simple solution to this problem is to hybridize the PNA to a partially complementary oligodeoxynucleotide (ODN) prior to transfection with a cationic agent, and in this particular case, the cationic lipid Lipofectamine.(*6*) Many factors have been found to affect the bioactivity of pLuc705 PNA•ODN hybrids, such as the length, sequence, and complementarity of the ODN, the PNA/ODN ratio, and the ratio of the PNA•ODN to the cationic transfection agents, Lipofectamine and PEI, and their cytotoxicity.(*8*) We selected the PNA•ODN hybrid found to have the highest bioactivity in that study and compared its bioactivity in the presence of cSCK to Lipofectamine 2000, and Polyfect, a cationic dendrimer (*22*) (Fig. 6-3A). At a low concentration of PNA•ODN 0.2 μM, the bioactivity was two times higher with Lipofectamine 2000 than with cSCK, both of which were better than Polyfect. Increasing the amount of PNA•ODN to 1.0 μM decreased slightly the bioactivity with Lipofectamine 2000, perhaps due to an increase in cytotoxicity, as indicated by a drop in cell viability from 58% to 30% (Fig. 6-3B). In contrast, increasing the PNA•ODN concentration 5-fold from 0.2 μM to 1.0 μM, increased the bioactivity about 7-fold when cSCK was used, without increasing the cytotoxicity. The bioactivity for the 1 μM PNA•ODN in the presence of the cSCK was about 5-fold greater than observed for Lipofectamine 2000. Polyfect was not found to be

effective for PNA•ODN delivery at any concentration even though its cytotoxicity is lower than Lipofectamine 2000 and cSCK.

The correlation between bioactivity in the luciferase assay and splice correction was investigated by RT-PCR analysis of the luciferase mRNA (Fig. 6-3c). Whereas increasing the PNA•ODN concentration from 0.2 μM to 1.0 μM in the presence of 10 μg/mL of Lipofectamine 2000 resulted in a slight decrease in bioactivity, the amount of splicing increased 2-fold from 34 % to 64 %. This result is consistent with the greater cytotoxicity at the higher PNA•ODN concentrations, which would reduce the number of viable cells and hence the light output (bioactivity). In contrast, the increase in bioactivity with increasing PNA•ODN concentration in the presence of 20 μg/mL of cSCK correlated better with the amount of splice correction, consistent with a minimal change in cytotoxicity. Changing the concentration of PNA•ODN 2-fold from 0.5 μM to 1.0 μM increased the bioactivity about 3-fold, while the amount of splice correction increased 2.6-fold. The non-linear increase in splice correction with PNA•ODN concentration may reflect changes in the cell penetrating properties of the cSCK when loaded with increasing amounts of PNA•ODN. It may also be due to a reduced binding affinity of the cSCK for the PNA•ODN at higher loadings, due to a reduction in the number of excess positive charges that would facilitate release of the PNA•ODN in the cell.

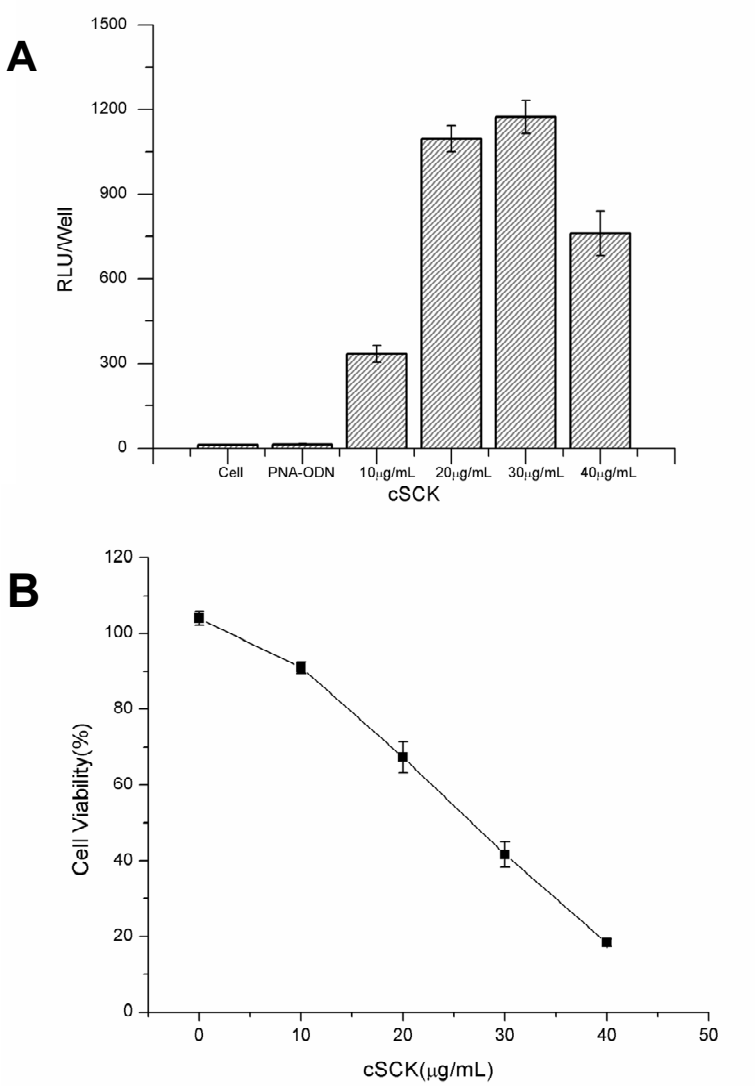

Figure 6-4. Relative cellular luciferase antisense activity and cytotoxicity in HeLa pLuc705 cells of cSCK-PNA•ODN complexes. Cells were incubated with 0.5 μM PNA/ODN hybrids complexed to the indicated amount of cSCK. A) PNA bioactivity as measured by luciferase activity B) cell viability.

The optimal bioactivity for transfection with the cSCK results from a delicate balance between transfection efficiency and cytotoxicity (Fig. 6-4). The bioactivity of 0.5 μM PNA•ODN increased from 10 to 1200 RLU as the concentration of the cSCK

was increased from 0 to 30 μg/mL, then dropped on going to 40 μg/mL (Fig. 6-4A). The cytotoxicity increased over these concentrations, with the cell viability dropping almost linearly from 90% at 10 μg/mL to about 20% at 40 μg/mL of cSCK (Fig. 6-4B). The large increase in bioactivity on going from 10 μg/mL to 20 μg/mL may be indicative of the capacity of the cSCK to bind to 0.5 μM PNA•ODN, or may be due to a change in size or charge that facilitated cell entry. The leveling off of the bioactivity at 30 μg/mL might then be due to an otherwise further increase in transfection by the cytotoxic effect, which then dominates at 40 μg/mL. The optimal transfection conditions in terms of bioactivity and cell viability would, therefore, appear to be between 10 and 20 μg/mL with 0.5 μM PNA•ODN.

Synthesis of the covalently linked cSCKs. The second transfection system that we explored involved covalent attachment of the PNA to the cSCK *via* a bioreductively cleavable linker. We chose the disulfide linkage because it has been found to be relatively stable in serum, but easily cleaved under the reducing conditions found inside cells and has been used to deliver PNAs conjoined to other delivery agents.(*23, 24*) PNAs were covalently linked to the block copolymer prior to micelle formation and crosslinking in a 1:1 and 2:1 ratio. The amount of PNA bound could be assayed by the UV absorptivity at 260 nm (Fig. 6-5A). Treatment of the cSCK-SS-PNA with DTT followed by dialysis removed 77% of the PNA, as judged by the decrease in absorbance at 260 nm (Fig. 6-5B). TEM of cSCKs and cSCKs conjugated with increasing amounts

of PNAs showed no noticeable differences in size, ruling out any size effects on the efficiency of cell uptake and subsequent bioactivity (Fig. 6-5C & D).

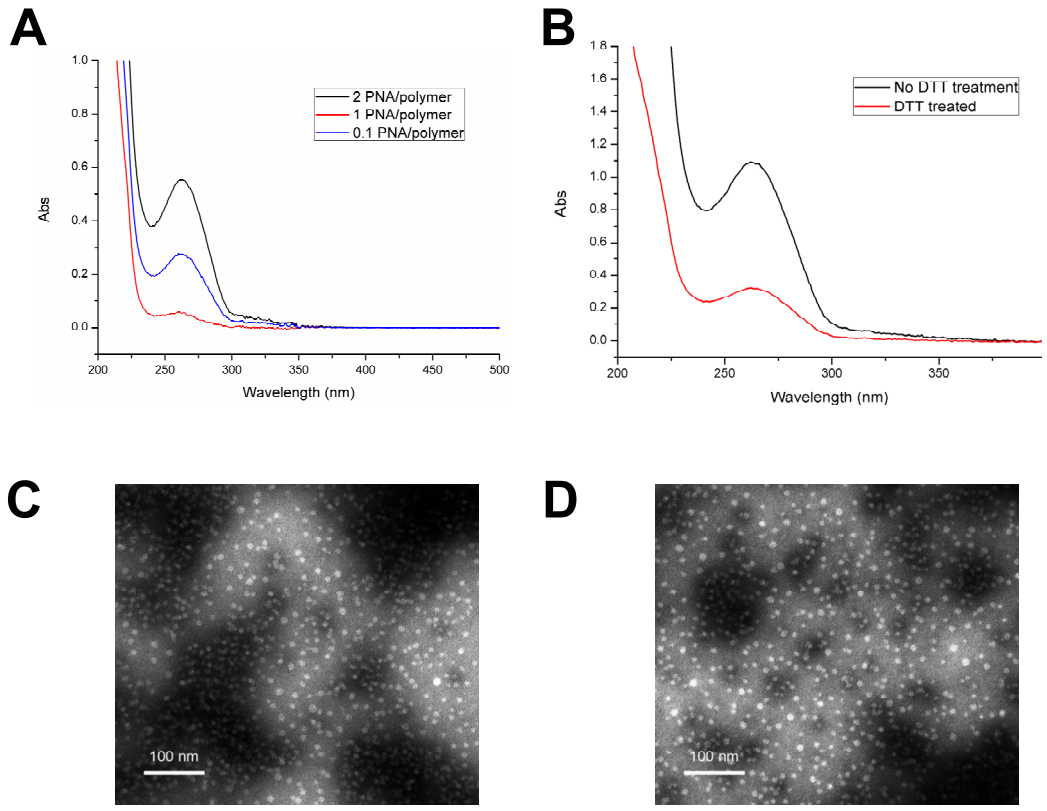

Figure 6-5. A) UV characterization of the cSCK-PNA conjugates. B) UV assay before and after reductive cleavage of the disulfide with DTT and extensive dialysis. TEM images of cSCK-SS-PNAs at C) 2 PNA/polymer chain and D) 0.1 PNA/polymer chain.

Transfection of PNAs covalently linked to cSCKs. We determined the bioactivity of the bioreductively cleavable cSCK-SS-PNA and cSCK-SS-PNA_2 with one and two PNAs/chain, respectively, in comparison to the non-cleavable cSCK-PNA by the splice correction assay. Both cSCKs with 1 and 2 PNAs/chain showed comparable bioactivity at 0.2 and 0.5 μM PNA concentration (Fig. 6-6A). The cSCK with one

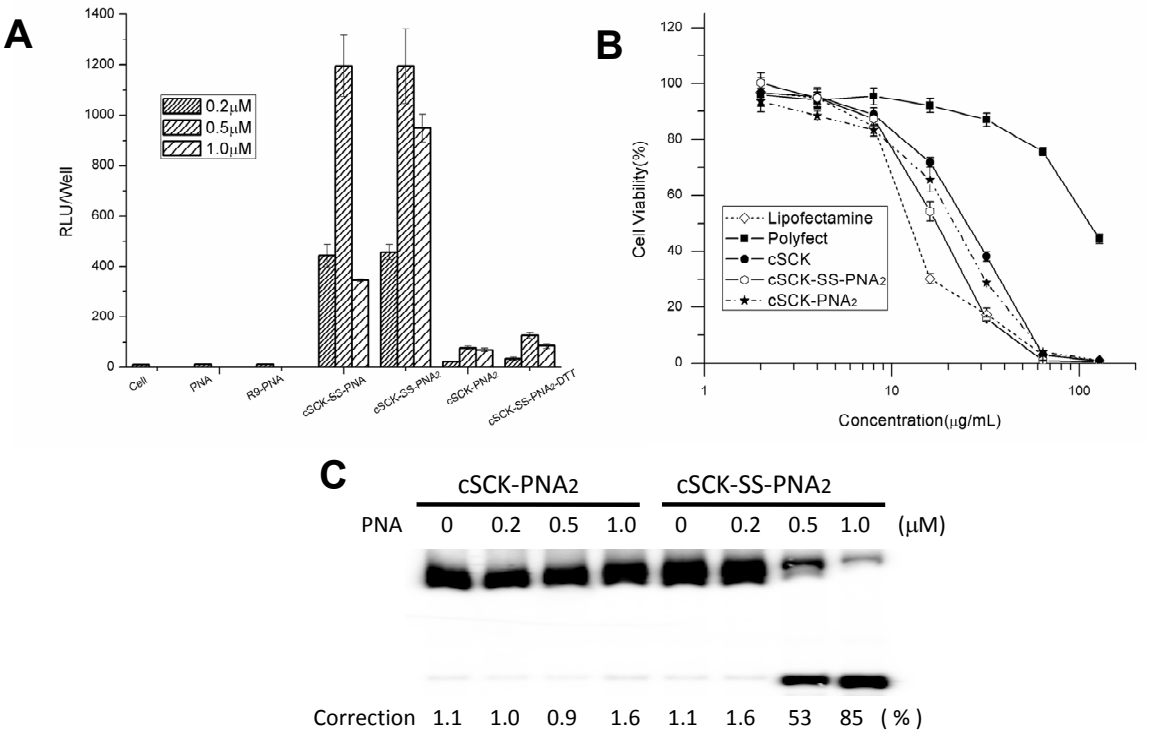

Figure 6-6. Splice correcting ability and cell viability of covalently linked cSCKs. A) Splice correction efficiency of the bioreductively cleavable cSCK-SS-PNA and cSCK-SS-PNA_2 containing 1 and 2 PNAs/chain respectively and the non-cleavable cSCK-PNA as a function of total PNA concentration. For a PNA concentration of 0.5 μM, the cSCK-SS-PNA_2 concentration was 12 μg/mL. B) Cell viability as a function of concentration of the delivery agent in μg/mL. C) Splice correction efficiency for cSCK-PNA and cSCK-SS-PNA_2.

PNA/chain showed significantly less bioactivity, however, at 1 μM PNA concentration compared to the one with two PNAs/chain. The 3-fold lower bioactivity of cSCK-SS-PNA than cSCK-SS-PNA_2 at 1 μM PNA can be explained in part by the higher cytotoxicity of the 2-fold higher concentration of the cSCK-SS-PNA (48 μg/mL) needed to deliver 1 μM PNA (Fig. 6-6B). It is not clear, however, why the bioactivity is the same for 0.5 μM PNA concentration, when the 24 μg/mL concentration of cSCK-SS-

PNA is much more toxic than the 12 μg/mL concentration needed for cSCK-SS-PNA_2. Splicing correction with cSCK-SS-PNA_2 is more efficient at 1 μM PNA than at 0.5 μM PNA (85% *vs*. 53%) (Fig. 6-6C) but comes at the expense of higher cytotoxicity (40% viability *vs*. 80% viability, respectively) (Fig. 6-6B).

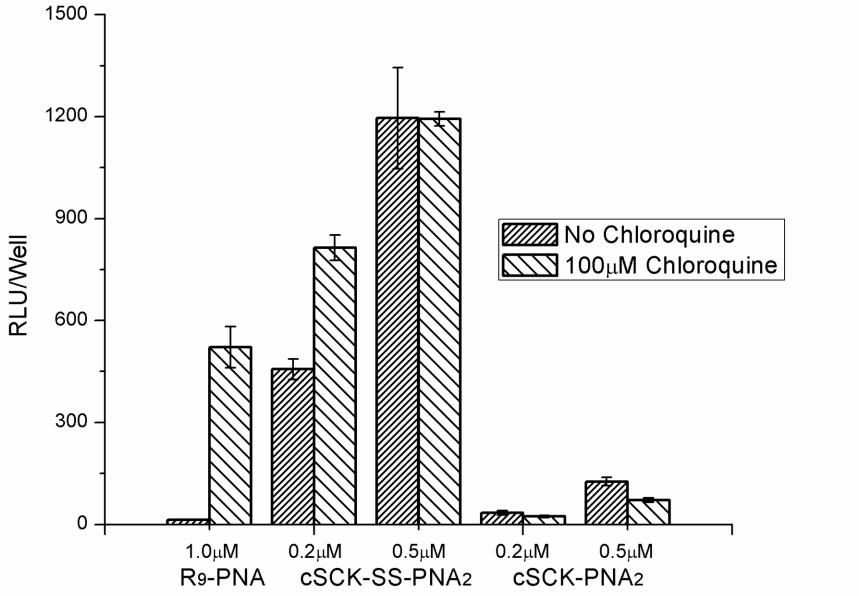

Figure 6-7. Effect of endosomal disrupting agents on PNA bioactivity as measured by luciferase activity. Cells were treated with 1 μM Arg_9-PNA, with 0.2 or 0.5 μM PNA from cSCK-SS-PNA_2, or with cSCK-PNA in the presence or absence of 100 μM chloroquinone.

Effect of endosome disrupting agents on bioactivity. It has been found that the antisense activity of PNA conjugated with cell penetrating peptides such as the TAT peptide or Arg_9 is significantly augmented by chloroquine, calcium ions, or by photochemical internalization (PCI) using photosensitizers, all of which are known to promote endosome disruption.(*25-27*) Since it was likely that the cSCKs were also

entering cells by an endocytotic mechanism, we were interested to see whether or not these agents would also enhance the bioactivity of the cSCK-PNA conjugates. The pLuc HeLa cells were, therefore, treated with cSCK-SS-PNA conjugates in the presence or absence of 100 μM chloroquine in comparison to PNA-Arg_9 (Fig. 6-7). As expected, chloroquine greatly enhanced the bioactivity of PNA-Arg_9 by two orders of magnitude. On the other hand, the cSCK-SS-PNAs were orders of magnitude more active than PNA-Arg_9 and chloroquine had little (2-fold) or no effect on the activity of cSCK-SS-PNA_2 at 0.2 and 0.5 μM PNA, respectively. In contrast, the non-cleavable cSCK-PNA showed much less activity that was also not enhanced by chloroquine. One interpretation of these results is that the cSCK not only facilitates endocytosis, but also endosomal escape of the PNA and/or the PNA-cSCK conjugate, without the need for chloroquine. The lower activity of the non-cleavable cSCK-PNA either suggests that the cSCK-PNA is not able to escape, or that the cSCK-PNA is not able to enter the nucleus and/or bind to the RNA due to inaccessibility of the PNA in the shell.

Tracking cSCK mediated PNA delivery and release inside cells. To track the intracellular path of the cSCK-SS-PNA_2 and its bioreductive cleavage products, we prepared a dual fluorescently labeled particle. The cSCK was labeled with Alexa Fluor 633 and the PNA was labeled at the ε-amino group of a carboxy terminal lysine with fluorescein isothiocyanate (FITC). The pLuc705 HeLa cells were incubated with the dual labeled cSCK(Alexa Fluor)-SS-PNA$(FITC)_2$ and examined by confocal microscopy

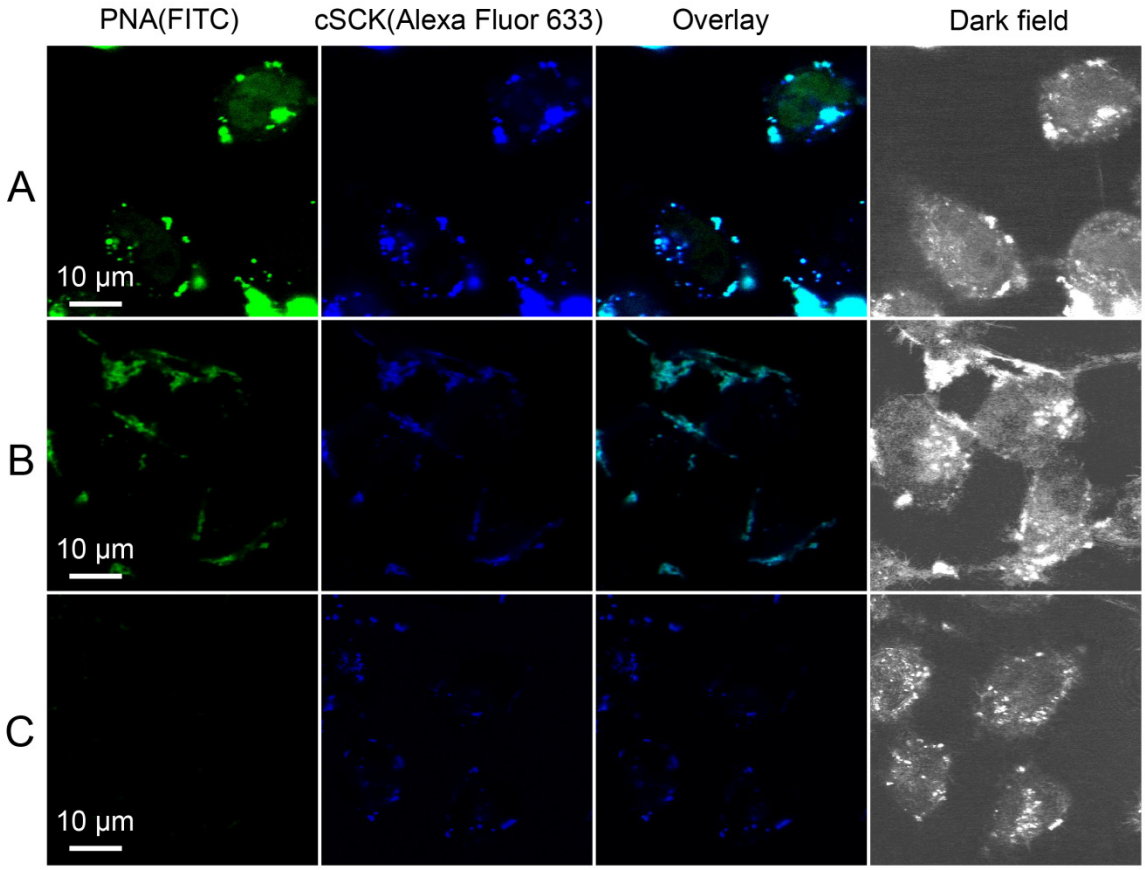

Figure 6-8. Cell localization of cSCK-SS-PNA and products. pLuc705 HeLa cells were incubated with a dual fluorescently labeled cSCK(Alexa Fluor 633)-SS-PNA(FITC)$_2$, having Alexa Fluor 633 (excitation 633 nm, emission 650 nm) on the cSCK and FITC (excitation 488 nm, emission 510 nm) on the PNA. Row A: 24 h incubation. Row B: 1 h incubation. Row C: 1 h incubation with DTT-pretreated nanoparticles.

after 1 h and 24 h (Fig. 6-8). After 1 h, cSCK and PNA fluorescence were co-localized and concentrated near the membrane surface (Fig. 6-8b). After 24 h, cSCK fluorescence was exclusively concentrated in endosomal and/or lysosomal-like vesicles, whereas PNA fluorescence was observed in the nucleus as well as being partially co-localized with the cSCK fluorescence in the vesicles (Fig. 6-8a). Transfection following reductive cleavage

with DTT and dialysis shows only the cSCK fluorescence localized in vesicles, and little PNA fluorescence (Fig. 6-8c). We interpret these data to support a model (Fig. 6-1B) in which a cSCK-SS-PNA binds to the membrane surface and is then slowly endocytosed. Endosomal acidification then causes cSCK-mediated destabilization of the endosome and exposes the cSCK-SS-PNA to cytoplasmic reducing environment, causing release of the PNA, which then binds to the RNA mis-splicing site in the nucleus. The destabilization is not sufficient, however, to enable release of the cSCK, which remains trapped in the endosomes, or of sufficient duration to allow all of the PNA to be bioreductively cleaved and escape from the endosome. The inability of the cSCKs to efficiently escape the endosome would explain the lower activity of the non-cleavable cSCK-PNA. Given that the precleaved cSCK also remains trapped in the endosomal compartments, it is likely that transfection of PNA•ODN by cSCK also proceeds by a similar mechanism in which either the PNA•ODN or the PNA alone escapes from the endosome (Fig. 6-1A).

The ability of the cSCK to promote endosomal escape of the PNA could be ascribed to a "proton sponge" effect,(*28*) in which the remaining basic amino groups on the cSCK react with protons produced during endosomal acidification. As a result of this buffering reaction, the cSCK further enhances the influx of protons, chloride counterions, and water leading to endosomal destabilization and permeabilization by the increased osmotic pressure within the endosome. This process either causes the cSCK-SS-PNA_2 to be released into, or exposed to, the cytoplasm whereupon the disulfide linkage is cleaved

allowing translocation of PNA to the nucleus. The proton sponge effect has also been recently used to enhance cytosolic delivery of core-shell nanoparticles bearing otherwise impermeable molecules (*29*) and quantum dots.(*30, 31*)

Conclusions

We have demonstrated that cationic shell crosslinked knedel-like nanoparticles are highly efficient agents for the delivery of bioactive PNAs into HeLa cells by both electrostatic complexation with PNA•ODN hybrids, or by conjugation of the PNA *via* a bioreductively cleavable linker. The cSCK at 20 μg/mL results in three times more bioactivity and two-fold less toxicity than Lipofectamine 2000 at 10 μg/mL when delivering 1 μM PNA•ODN into HeLa cells, and results in a much higher splicing correction efficiency (94% *vs* 64%). The bioreductively cleavable cSCK-SS-PNA_2 conjugates are similarly effective for HeLa cells at 1 μM PNA, showing only slightly higher cytotoxicity and slightly lower splicing efficiency (85%), but are orders of magnitude better than Arg_9-mediated delivery. The cSCK-SS-PNA system may be very useful for *in vivo* applications, where it would be important to minimize dissociation of the PNA from the cSCK prior to reaching the target cell. Initial mechanistic studies indicate that the cSCK is not only able to facilitate endocytosis, but also endosome disruption, thereby facilitating release of the PNA into the cytoplasm from where it can translocate into the nucleus, while the cSCK remains trapped in the endosomal/lysosomal

compartments. This type of delivery mechanism may also be quite attractive for *in vivo* purposes if the cSCK can be later exocytosed and excreted, thereby preventing it from accumulating within the cytoplasm of cells. If not, acid- or bio-degradable nanoparticles under development could be used. For in vivo experiments, we will incorporate DOTA into the polymer side chains to bind ^{64}Cu for PET imaging of cSCK biodistribution and pharmacokinetics. Based on prior experience with SCKs, (*32*) we also expect that PEG chains will also have to be attached to minimize detection by the RES system and enhance the bioavailability of the cSCKs. The bioactivity of the PNAs could then be assessed through the use of the EGFP-654 transgenic mouse that utilizes EGFP as a reporter for splicing correction .(*33*) In this way we will be able to determine the extent to which the bioactivity correlates with the bioavailability of the cSCK for different tissues.

Acknowledgments

This work is supported by the National Heart Lung and Blood Institute of the National Institutes of Health as a Program of Excellence in Nanotechnology (NHLBI-PEN HL080729) and by grants to the Washington University NIH Mass Spectrometry Resource (Grant No. P41 RR000954) and Washington University NMR facility (Grant No. RR1571501). We thank Bereket Oquare for the 18-mer PNA, and Zhenghui Wang for obtaining the MALDI data on the PNAs. We also thank G. Michael Veith of the

Washington University Department of Biology Microscopy Facility for providing technical support with TEM and fluorescence confocal microscopy, Cindy Fogal of Dr. Kranz's group for help with the luminometer, and Dr. R. Kole (University of North Carolina, Chapel Hill, NC) for the pLuc705 HeLa cell line.

References and Notes

(1) Nielsen, P. E. (2004) *PNA Technology*, *Mol. Biotechnol. 26*, 233-48.

(2) Zhilina, Z. V., Ziemba, A. J., and Ebbinghaus, S. W. (2005) Peptide nucleic acid conjugates: synthesis, properties and applications. *Curr. Top. Med. Chem. 5*, 1119-31.

(3) Porcheddu, A., and Giacomelli, G. (2005) Peptide nucleic acids (PNAs), a chemical overview. *Curr. Med. Chem. 12*, 2561-99.

(4) Lundin, K. E., Good, L., Stromberg, R., Graslund, A., and Smith, C. I. (2006) Biological activity and biotechnological aspects of peptide nucleic acid. *Adv. Genet. 56*, 1-51.

(5) Hu, J., and Corey, D. R. (2007) Inhibiting gene expression with peptide nucleic acid (PNA)-peptide conjugates that target chromosomal DNA. *Biochemistry 46*, 7581-9.

(6) Braasch, D. A., and Corey, D. R. (2001) Synthesis, analysis, purification, and intracellular delivery of peptide nucleic acids. *Methods 23*, 97-107.

(7) Braasch, D. A., and Corey, D. R. (2002) Lipid-mediated introduction of peptide nucleic acids into cells. *Methods Mol. Biol. 208*, 211-23.

(8) Rasmussen, F. W., Bendifallah, N., Zachar, V., Shiraishi, T., Fink, T., Ebbesen, P., Nielsen, P. E., and Koppelhus, U. (2006) Evaluation of transfection protocols for unmodified and modified peptide nucleic acid (PNA) oligomers. *Oligonucleotides 16*, 43-57.

(9) Abes, S., Moulton, H., Turner, J., Clair, P., Richard, J. P., Iversen, P., Gait, M. J., and Lebleu, B. (2007) Peptide-based delivery of nucleic acids: design, mechanism of uptake and applications to splice-correcting oligonucleotides. *Biochem. Soc. Trans. 35*, 53-5.

(10) Koppelhus, U., Shiraishi, T., Zachar, V., Pankratova, S., and Nielsen, P. E. (2008) Improved cellular activity of antisense peptide nucleic acids by conjugation to a cationic peptide-lipid (CatLip) domain. *Bioconjug. Chem.*

(11) Reineke, T. M., and Grinstaff, M. W. (2005) Designer materials for nucleic acid delivery. *MRS Bull. 30*, 635-638.

(12) Toub, N., Malvy, C., Fattal, E., and Couvreur, P. (2006) Innovative nanotechnologies for the delivery of oligonucleotides and siRNA. *Biomed. Pharmacother. 60*, 607-20.

(13) Sokolova, V., and Epple, M. (2008) Inorganic nanoparticles as carriers of nucleic acids into cells. *Angew. Chem. Intl. Ed. 47*, 1382-1395.

(14) Zhang, K., Fang, H., Chen, Z., Taylor, J.-S. A., and Wooley, K. L. (2008) Shape effects of nanoparticles conjugated with cell-penetrating peptides (HIV Tat PTD) on CHO cell uptake. *Bioconjugate Chem. 19*, 1880-1887.

(15) Juliano, R., Alam, M. R., Dixit, V., and Kang, H. (2008) Mechanisms and strategies for effective delivery of antisense and siRNA oligonucleotides. *Nucl. Acids Res. 36*, 4158-4171.

(16) Becker, M. L., Remsen, E. E., Pan, D., and Wooley, K. L. (2004) Peptide-derivatized shell-cross-linked nanoparticles. 1. Synthesis and characterization. *Bioconjug. Chem. 15*, 699-709.

(17) Becker, M. L., Bailey, L. O., and Wooley, K. L. (2004) Peptide-derivatized shell-cross-linked nanoparticles. 2. Biocompatibility evaluation. *Bioconjug. Chem. 15*, 710-7.

(18) O'Reilly, R. K., Hawker, C. J., and Wooley, K. L. (2006) Cross-linked block copolymer micelles: functional nanostructures of great potential and versatility. *Chem. Soc. Rev. 35*, 1068-83.

(19) Zhang, K., Fang, H., Wang, Z., Taylor, J. S., and Wooley, K. L. (2009) Cationic shell-crosslinked knedel-like nanoparticles for highly efficient gene and oligonucleotide transfection of mammalian cells. *Biomaterials 30*, 968-77.

(20) Ma, Q., and Wooley, K. L. (2000) The preparation of t-butyl acrylate, methyl acrylate, and styrene block copolymers by atom transfer radical polymerization:

precursors to amphiphilic and hydrophilic block copolymers and conversion to complex nanostructured materials. *J. Polym. Sci., Part A: Polym. Chem. 38*, 4805-4820.

(21) Kang, S. H., Cho, M. J., and Kole, R. (1998) Up-regulation of luciferase gene expression with antisense oligonucleotides: implications and applications in functional assay development. *Biochemistry 37*, 6235-9.

(22) Tang, M. X., Redemann, C. T., and Szoka, F. C., Jr. (1996) In vitro gene delivery by degraded polyamidoamine dendrimers. *Bioconjug. Chem. 7*, 703-14.

(23) Koppelhus, U., Awasthi, S. K., Zachar, V., Holst, H. U., Ebbesen, P., and Nielsen, P. E. (2002) Cell-dependent differential cellular uptake of PNA, peptides, and PNA-peptide conjugates. *Antisense Nucleic Acid Drug Dev. 12*, 51-63.

(24) Reshetnyak, Y. K., Andreev, O. A., Lehnert, U., and Engelman, D. M. (2006) Translocation of molecules into cells by pH-dependent insertion of a transmembrane helix. *Proc. Natl. Acad. Sci. U.S.A. 103*, 6460-5.

(25) Hallbrink, M., Oehlke, J., Papsdorf, G., and Bienert, M. (2004) Uptake of cell-penetrating peptides is dependent on peptide-to-cell ratio rather than on peptide concentration. *Biochim. Biophys. Acta 1667*, 222-8.

(26) Abes, S., Williams, D., Prevot, P., Thierry, A., Gait, M. J., and Lebleu, B. (2006) Endosome trapping limits the efficiency of splicing correction by PNA-oligolysine conjugates. *J. Controlled Release 110*, 595-604.

(27) Shiraishi, T., and Nielsen, P. E. (2006) Enhanced delivery of cell-penetrating peptide-peptide nucleic acid conjugates by endosomal disruption. *Nat. Protoc. 1*, 633-6.

(28) Boussif, O., Lezoualc'h, F., Zanta, M. A., Mergny, M. D., Scherman, D., Demeneix, B., and Behr, J. P. (1995) A versatile vector for gene and oligonucleotide transfer into cells in culture and in vivo: polyethylenimine. *Proc. Natl. Acad. Sci. U.S.A. 92*, 7297-301.

(29) Hu, Y., Litwin, T., Nagaraja, A. R., Kwong, B., Katz, J., Watson, N., and Irvine, D. J. (2007) Cytosolic delivery of membrane-impermeable molecules in dendritic cells using pH-responsive core-shell nanoparticles. *Nano Lett. 7*, 3056-3064.

(30) Duan, H., and Nie, S. (2007) Cell-penetrating quantum dots based on multivalent and endosome-disrupting surface coatings. *J. Am. Chem. Soc. 129*, 3333-3338.

(31) Yezhelyev, M. V., Qi, L., O'Regan, R. M., Nie, S., and Gao, X. (2008) Proton-sponge coated quantum dots for siRNA delivery and intracellular imaging. *J. Am. Chem. Soc. 130*, 9006-12.

(32) Sun, G., Hagooly, A., Xu, J., Nystrom, A. M., Li, Z., Rossin, R., Moore, D. A., Wooley, K. L., and Welch, M. J. (2008) Facile, efficient approach to accomplish tunable chemistries and variable biodistributions for shell cross-linked nanoparticles. *Biomacromolecules 9*, 1997-2006.

(33) Sazani, P., Gemignani, F., Kang, S. H., Maier, M. A., Manoharan, M., Persmark, M., Bortner, D., and Kole, R. (2002) Systemically delivered antisense oligomers upregulate gene expression in mouse tissues. *Nat. Biotechnol. 20*, 1228-33.

Chapter 7

Composite soft-matter nanoscale objects: nanocylinder-templated assembly of nanospheres

[Portions of this work have been published previously as Ke Zhang, Huafeng Fang, Zhou Li, Jun Ma, Sophia V. Hohlbauch, John Stephen A. Taylor and Karen L. Wooley *Soft Matter* **2009**, 5(9), 3585-3589.]

Abstract

We extend the surface layer-by-layer self-assembly strategy to the preparation of block copolymer-based composite nanoconstructs utilizing nanoscale building blocks. These composite materials are well-defined, hierarchically-organized nanoscale objects of a cylindrical form and core-shell morphology, having an outer coating of cationic shell-crosslinked knedel-like nanospheres (cSCK). In addition to standard characterization techniques, a fluorescent resonance energy transfer (FRET) experiment is designed and used to study the coating of anionic cylinders by cationic spheres. Expedited HeLa cell uptake is found for the composite nanostructures compared with the non-coated cylinders, indicating that this simple assembly strategy is a facile method to allow the secondary structure to inherit properties from its individual building blocks.

Introduction

New frontiers in nanomaterial research are evolving towards the development of nanoparticles (NPs) that are of greater complexity in structure and function (*1*). This increase in complexity may refer not only to the nanocolloids themselves, which often combine one or two materials, such as NPs made from polymer blends (*2-3*), or inorganic NPs stabilized with functional organic ligands (*4-5*), but also to the super-structures of their assemblies (*6-11*). Self-assembly of nanostructures has proven to be an efficient and rapid method to create higher order complexities and functions. For example, the organization of nanocrystals in multi-dimensional superlattices shows remarkable collective properties from their individual isolated counterparts (*12*). This strategy is also commonly used in Nature in creating three-dimensional, complex biological structures such as multi-subunit proteins or viruses, which have genes made from either DNA or RNA, and a self-assembled protein coat to protect these genes. However, although the assembly of nanostructures on macroscopically-flat surfaces has been studied extensively (*13-14*), which has resulted in many key developments in optical materials, electronic devices, sensing devices and biological applications, the templated assembly of nanostructures on a curved, three-dimensional nanoscopic substrate is only recently emerging as a technique to prepare intelligent nanoscale constructs (*15*). A few interesting examples include the use of carbon nanotubes to template the self assembly of metal nanospheres and nanorods (*16-18*), metal oxide nanoparticles (*19*) and polymerized

lipid assemblies (*20*); the assembly of oligonucleotide-functionalized gold nanoparticles on living fungi templates (*21*); multilayer assembly of TiO_2 nanoparticles on electrospun polymer nanofibers (*22*); selective permeable nano-micro colloidosomes from colloidal nanoparticles assemblies (*23*), and silver nanoparticle assemblies along silver nanowires (*24*). However, a component still largely missing from the current systems are completely soft-matter-based, hierarchically-organized nanoscale objects, which are potentially useful in a broad range of biomedical applications, such as drug/gene delivery, due to their tunability in chemistry which in turn can provide many appealing properties such as rapid biodegradation (*25*).

In self-assembly, specific non-covalent forces are essential in organizing macromolecular or nanoscopic entities into spontaneously forming multi-dimensional, hierarchical and complex structures. Among the many kinds of such non-covalent interactions, such as hydrogen bonding, van der Waals interactions, wettability at interfaces, and magnetic force, electrostatic attractions provide versatile, effective and inexpensive approaches to the formation of higher-order structures. For example, functional thin films are conveniently prepared by alternate adsorption of oppositely-charged species from aqueous solutions, a process that is commonly termed layer-by-layer (LbL) adsorption, resulting in unique thin films containing a number of different functional organic/inorganic materials, including NPs (*26-27*). Recently, this LbL strategy has also been applied to the formation of versatile hybrid NPs with a gold core

and multiple shell layers, which render a number of desired properties to the NPs, such as bio-stealthiness and triggerable release of drug (*28*). In this chapter, we expand on this concept of functional organization and report the assembly of cationic shell-crosslinked knedel-like nanospheres (cSCK) on anionic shell-crosslinked nanocylinder templates to afford hierarchically-organized nanoscale objects of cylindrical form and core-shell morphology having an outer coating of spheres. The cSCK is known to undergo rapid cell internalization and lead to transfection if carrying genes (*29-30*). In this chapter, the cSCK cell entry characteristics are shown to be transferred to the nanocylinders upon assembly. The final assembled products were imaged by Transmission Electronic Microscopy (TEM) and Atomic Force Microscopy (AFM). Zeta potential analysis and a fluorescent resonance energy transfer (FRET) experiment were designed and used to monitor and quantify the involvement of charged groups of both the nanocylinders and the cSCKs during the assembly process. In addition, cell uptake of the complexes was studied as a demonstration of the modified biological properties that result for the nanocylinders upon coverage by the cSCKs.

Experimental Section

Block copolymers and nanostructures were prepared according to literature reported procedures (*30-32*). All other reagents and buffers were purchased from Sigma Aldrich and Invitrogen, Inc. cSCK-mediated cylinder cell uptake was evaluated on

Chinese Hamster Ovary (CHO-K1) cells. Cell were incubated in Ham's F-12K containing 10% fetal bovine serum (FBS) and 1% antibiotics (penicillin–streptomycin, 10,000 U/mL) at 37 °C in a humidified atmosphere containing 5% CO_2 prior to assay.

TEM images were obtained on a Hitachi H600. Samples for TEM were diluted with a 1% phosphotungstic acid (PTA) stain (v/v, 1:1), and air-dried on a plasma-treated carbon-coated copper grid. AFM images were obtained on a Asylum Research MFP-3D BIO mounted onto a Nikon Eclipse TE2000-U. All images were acquired in AC mode in pure water using 100 μm long Olympus cantilevers, model TR400PSA. Samples containing the cationic spheres and sphere/cylinder complexes were prepared by incubating them onto freshly cleaved mica for 10 minutes. The anionic nanocylinders were incubated onto AP-mica for 10 minutes before imaging. Fluorescence spectroscopy measurements were performed using a Varian Cary Eclipse fluorescence spectrophotometer. LSCM images were obtained on a Leica TCS SP2 inverted microscope. CHO cells (5×10^5) were incubated at 37 °C with sphere/cylinder mixtures of various concentrations in the presence of 10% FBS in 35 mm MatTek glass bottom microwell dishes (MatTek Co.) for 4 h. Each plate was washed 3 times with phosphate buffered saline and viewed under dark field and fluorescent conditions. The labeling of the paritcles with fluorescent tags was achieved following literature reported protocols (*30, 32*).

Results and Discussion

The preparation of the NPs has been detailed in previous studies (*30, 32*). Briefly, amphiphilic block copolymers were micellized and shell-crosslinked in water to give cationic, spherical (diameter: 9 ± 2 nm, Fig. 7-1A) or anionic, cylindrical (cross-section diameter: 20 ± 2 nm, 100-500 nm in lengths, Fig. 7-1B) NPs. The differences in surface charge and particle shape result from the different polymers used to create these assemblies (Scheme 1). The cSCKs were assembled from polyamidoethylamine$_{128}$-*b*-polystyrene$_{40}$ (PAEA$_{128}$-*b*-PS$_{40}$), while the nanocylinders were assembled from poly(acrylic acid)$_{96}$-*b*-polystyrene$_{49}$ (PAA$_{96}$-*b*-PS$_{49}$). A third polymer, PAA$_{128}$-*b*-PS$_{40}$, was also used to afford anionic spherical particles of similar size (12 ± 3 nm, Fig. 7-1C) to the cSCKs, but to be used as a control sample for investigation of the importance of electrostatic interactions for the sphere-cylinder assembly processes.

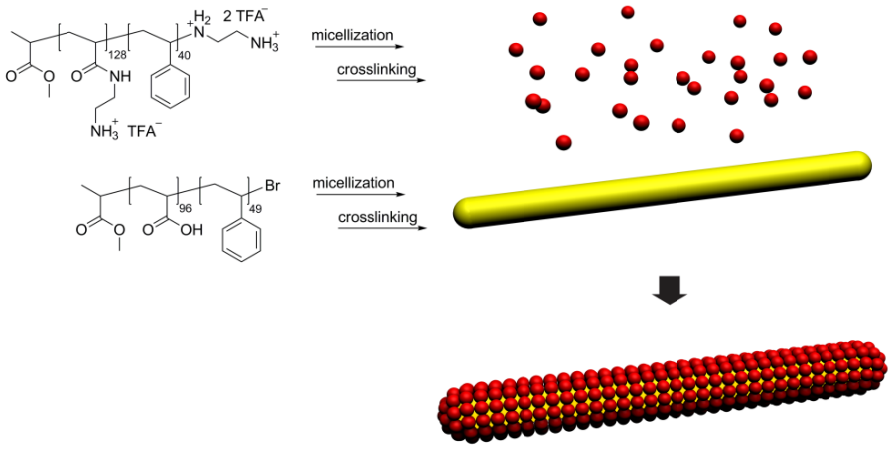

Scheme 7-1. Formation of shell-crosslinked nanoparticles of spherical and cylindrical shapes, and the templated self-assembly of the spheres on the surface of a cylinder.

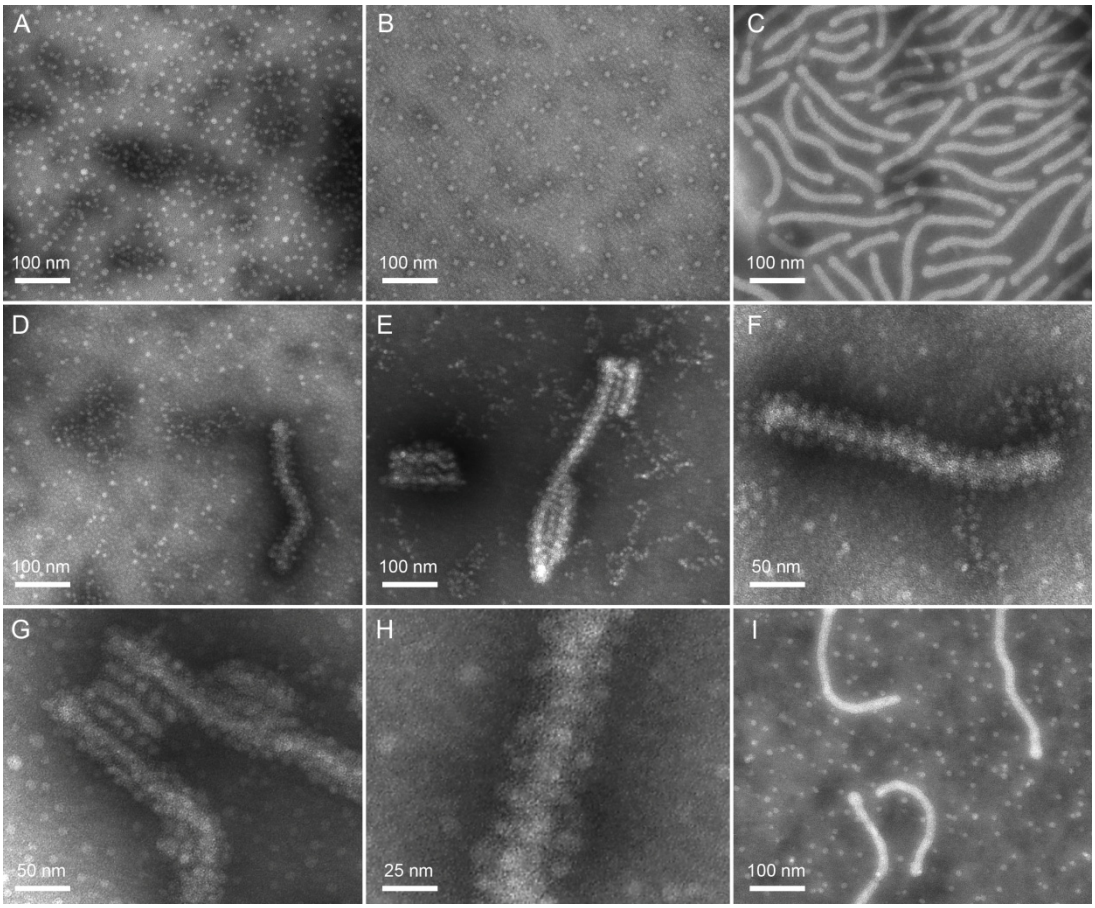

Figure 7-1. TEM images of the polymer-based cationic spheres (A), anionic spheres (B) and anionic nanocylinders (C). Upon mixing, the cationic spheres assembled on the nanoscopic curved surfaces of the nanocylinders and form a close-packed dense layer, for which the entire assembled morphology is observed by TEM imaging (D-H). In contrast, a mixture of anionic spheres and cylinders does not form assembled structures (I), rather, discrete cylinders and spheres are observed by TEM, confirming electrostatic interactions to be the driving force for assembly.

Our initial interest was to test whether the cSCKs having surface amine groups would exhibit high affinity for the nanocylinders with surface carboxylic acids, and as such, could form nanoscopic complexes upon mixing (Scheme 1). For this experiment, spheres were gradually mixed with cylinders at different sphere:cylinder, amine:carboxylate ratios (N/C ratios), and were imaged by TEM (Fig. 7-1D-H). A dense,

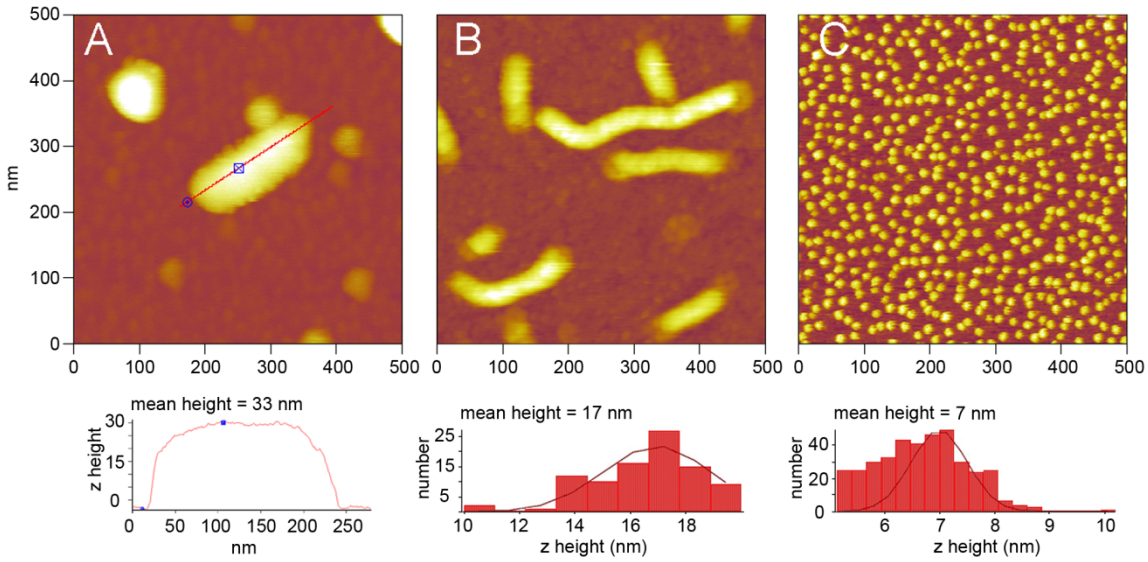

Figure 7-2. AC-mode AFM images collected under solution: (A) a sphere/cylinder complex, with the section analysis shown below, (B) cylinders alone (without added spheres), with a histogram of the height distribution, and (C) spheres alone, with a histogram of the height distribution.

close-packed layer of cSCKs over the surface of the nanocylinders, completely covering the cylinders, was observed. Sometimes, especially at lower N/C ratios (2-6), multiple cylinders were observed as aggregates with the spheres in between them, binding to both cylinders (Fig. 7-1E and G). This effect could be minimized by using larger excesses of spheres (N/C of 10 or higher) while keeping the concentration of the cylinders constant. In contrast, control mixtures involving the use of anionic nanospheres and nanocylinders, each having carboxylates in their shells and possessing anionic surface charges, showed no templated-assembly behavior (Fig. 7-1I), thus, confirming electrostatic interactions to be the driving force for assembly. The average height of the nanocomplexes, measured by solution-state AFM, was 33 nm (Fig. 7-2A), roughly coinciding with the sum of the

height of a cylinder (17 nm, Fig. 7-2B) plus the combined height of two spheres (7 nm each, Fig. 7-2C). Although AFM could not distinguish the entire internal morphology, individual spheres could be recognized upon the surface of the overall complex, and the total height was in agreement with the TEM diameter.

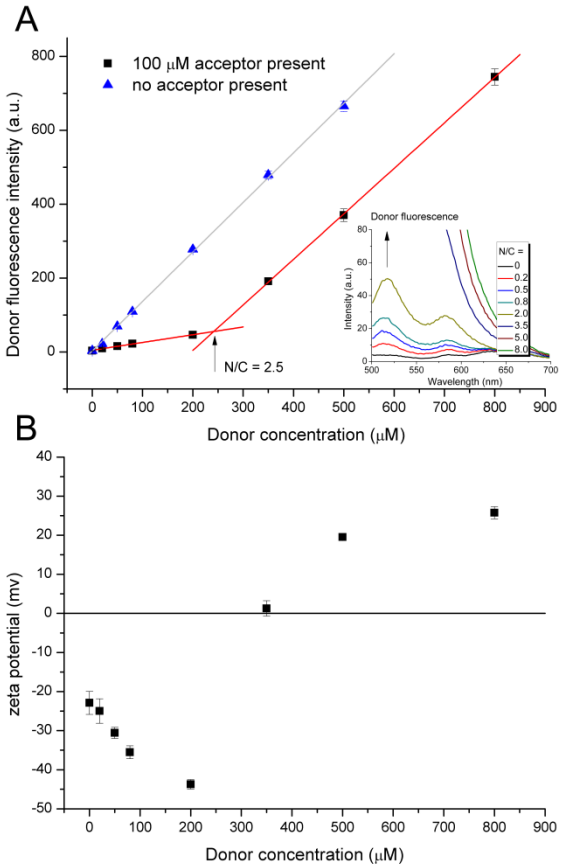

Figure 7-3. (A) Fluorescence intensities of fluorescein-tagged cSCKs at different concentrations in the presence (■) and absence (▲) of 100 μM of rhodamine-labeled nanocylinders. The inset shows the fluorescence spectra of the complexes at different N/C ratios (cSCK:nanocylinder stoichiometries). (B) Zeta potential values for the mixtures from (A). The charge-inversion region (200-350 μM) of the zeta potential data of (B) coincides with the concentration at which the slope change occurs for the donor fluorescence data of (A), considered to be the end-point at which the anionic nanocylinders became coated by cationic nanospheres.

To better understand the cSCK/nanocylinder assembly, it is of interest to investigate the stoichiometry of the NPs and the utilization of the charged species of each kind of NP. In related work that involves the co-assembly of cSCK with negatively-charged DNA, the stoichiometry can be measured easily as cSCK amine:DNA phosphate molar ratios (N/P ratios) by a gel retardation assay. Upon binding with cSCKs, some DNA becomes immobilized while free DNA remains mobile during gel electrophoresis. By varying the cSCK:DNA stoichiometry, the N/P value varies, and an "end-point" of complete DNA binding can be determined. However, such an assay is not suitable for the cSCK/nanocylinder complexes, because the cylindrical nanostructures are immobile in the gel. To circumvent this problem, we instead designed a FRET experiment to determine the end-point. The nanocylinders were labeled with an acceptor fluorescent tag (rhodamine) and the cSCKs were labeled with a donor (fluorescein). Then, the two NP solutions were mixed at different cSCK amine:cylinder carboxylate ratios (N/C ratios). Upon assembly, donor fluorescence is attenuated by transferring a portion of the fluorescence energy to the acceptor due to spatial proximity. As a result, donor (cSCK) fluorescence increases with regard to its concentration at a lower rate before the nanocylinder surface is consumed, and at a higher rate thereafter. Each stage appears to have a linear relationship. By plotting the donor fluorescence against various donor concentrations, in the presence of a fixed amount of acceptor, the end-point, that is, when the surface of the nanocylinders becomes completely occupied, can be identified (Fig. 7-

3A). For the cSCK/nanocylinder complexes, the end-point N/C value was calculated by extrapolation to be 2.5. At N/C ratios between 2.0 and 3.5, precipitation of the nanocomplexes prevented acquiring data in this range. This end-point N/C value is of importance not only because it provides stoichiometric information regarding the numbers of each kind of NPs associated with the assembly, but also because it is a function of the two particles' binding affinity and the availability of amine and carboxylate groups on the NP surfaces for binding, thus providing structural information. For example, previous studies measured the end-point N/P ratio for the cSCK/DNA complexes to be 2.0 (*30*), likely because many amines buried beneath the cSCK surface are unable to bind to the phosphates along the DNA backbone. Following this logic, the cSCK/cylinder complexes should have an N/C value lower than 2.0, because the cylinders also have such steric effects, leading to incomplete consumption of the carboxylates. The unexpectedly increased N/C value of 2.5 indicates that, unlike in cSCK/DNA complexes, the utilization of amines in cSCK/cylinder complexes is much reduced, likely because of the rigidity of the nanocylinder, relative to the flexibility of DNA, and also because of close-packing of the cSCKs along the cylinders.

The end-point as determined by FRET coincides with the charge inversion region from negative to positive values in zeta potential analysis (Fig. 7-3B). As the N/C ratio increased, increasingly negative character was observed initially, possibly due the

formation of multi-cylinder aggregates. Further increasing the N/C ratio led to an inversion of charge. Finally, at a large excess of spheres the zeta potential value became equal to that of the cSCK. Although zeta potential analysis conveniently identified a range N/C ratios in which the end-point is located, it does not provide an accurate determination due to both the non-linear relationship between zeta potential and cSCK concentration, and to the unstable nature of the complexes near the end-point.

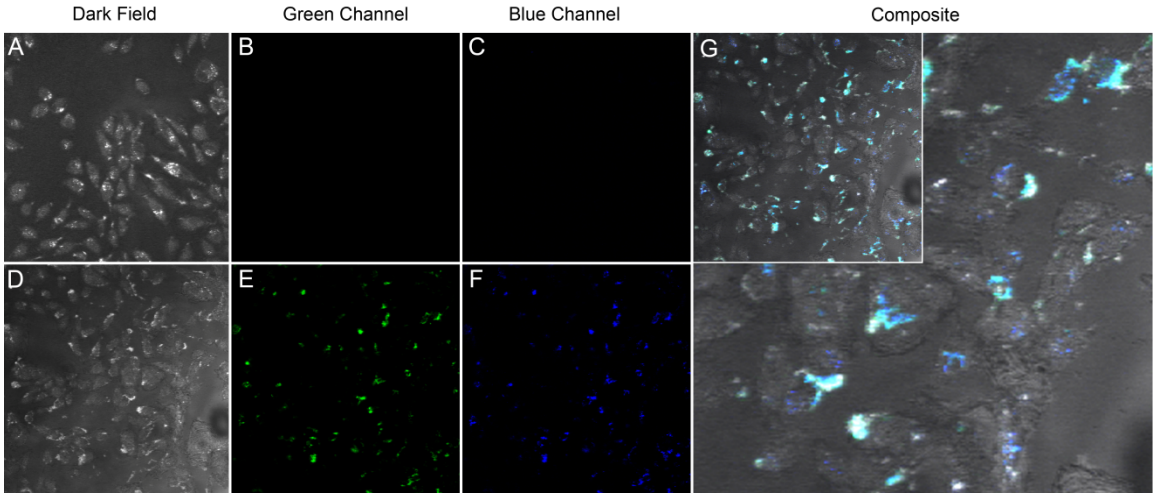

Figure 7-4. Dark field and confocal fluoresence images of dual-labeled cSCK/nanocylinder complexes (A-C) and fluorescein-labeled nanocylinders (D-F). After incubation with CHO cells at 37 °C for 4 h, the cylinders showed no signal in the green channel (cylinder) (B) or the blue channel (cSCK) (C), while the cSCK/cylinder complexes show signals in both channels (E, F). A composite image (G) shows the details of internalized complexes, with an expanded view.

It has been demonstrated that the nanoparticle size, shape and surface chemistry play critical roles in their cellular internalization pathways (*33*). The negatively-charged cylinders used in this study have been shown previously to be unable to undergo cell

internalization within eight hours, due to their relatively large sizes and negative surface charge. Upon conjugation with the protein transduction domain (PTD) peptide of the HIV Tat protein, the cylinders were able to be taken up by CHO cells (*32*). It has been postulated that the positively-charged peptide sequence associates with the plasma membrane in a non-specific manner, similar to polyethyleneimine, which is known to interact with negatively-charged cell surfaces *via* heparan sulfates (*34*). Also being highly positively charged, the cationic spheres were expected to serve similar functions in helping to transport the cylinder into the cell.

To test our hypothesis, the spheres were labeled with Alexa Fluor (AF) 633, which then assembled onto fluorescein-labeled cylinders to give solution-stable nanocomplexes at an N/C ratio of 3.7, allowing for the tracking of each individual component by laser scanning confocal microscopy (LSCM). The complex structures were then incubated with CHO cells for 4 h at a series of concentrations. Control samples, using only the cylinders without the cSCK coating, were also prepared. Indeed, compared to the control samples, which shows no signal in either the fluorescein (cylinders) or the AF 633 (spheres) channel, the complex nanoassemblies exhibited fluorescence in both channels, suggesting that the nanocylinders had inherited the properties from the cSCKs, *i.e.* the ability to translocate across the plasma membrane,

despite the overall larger size of the complexes than either the cylinders or spheres alone (Fig. 7-4).

Conclusions

In summary, we have described a facile method to prepare templated nanoscale objects of cylindrical form having an outer coating of spheres *via* the self assembly of shell-crosslinked polymer nanospheres on oppositely-charged nanocylinders. TEM and AFM visualized a closely-packed layer of nanospheres on the surface of nanocylinders. Independently, zeta potential analysis and a FRET experiment determined the stoichiometry for the saturation point of the cylinders' surfaces for binding by the spheres, while the FRET experiment also identified a cSCK amine-to-nanocylinder carboxylate (N/C) ratio of 2.5 at this point. By labeling the respective particles with fluorescein and AF 633, the cationic sphere-coated cylinders were tracked by LSCM and were observed to undergo cell internalization, while the non-coated cylinders were not able to be taken up by CHO cells. It was demonstrated, therefore, that the characteristics of the original cylindrical nanoscale template could be modified by a simple surface assembly process, using nanoscale objects as each of the building blocks. It is expected that, by enabling each parent building block with different properties, such as nucleic acid delivery and receptor-targeting ability, a multi-functional complex NP could be

accessed by this method in a facile, modular fashion. This procedure resembles the layer-by-layer assembly technique that has become common for polymer components. We believe this general method for preparing electrostatic assemblies of oppositely-charged nanostructures is of broad interest as a means to assemble complex nanoscale objects that combine function from the individual components. Such a technique may be useful for the construction of complex materials that can serve in a variety of applications, such as drug delivery, environment and energy, catalysis, and bio-sensing. Furthermore, the nanocylinder template could be replaced with a selective degradable material, which upon degradation may release the surface-bound cSCKs, leading to a triggered disassembly. If the cSCKs are inter-crosslinked, then a soft, hollow nanocage material is also possible.

Acknowledgments

Financial support from the National Heart Lung and Blood Institute of the National Institutes of Health as a Program of Excellence in Nanotechnology (U01 HL080729) is gratefully acknowledged.

References and Notes

(1) Kotov, N. A., and Stellacci, F. (2008) Frontiers in nanoparticle research: Toward greater complexity of structure and function of nanomaterials. *Adv. Mater. 20*, 4221-4222.

(2) Cui, H., Chen, Z., Zhong, S., Wooley, K. L., and Pochan, D. J. (2007) Block copolymer assembly *via* kinetic control. *Science 317*, 647-650.

(3) Gadt, T., Ieong, N. S., Cambridge, G., Winnik, M. A., and Manners, I. (2009) Complex and hierarchical micelle architectures from diblock copolymers using living, crystallization-driven polymerizations. *Nat. Mater. 8*, 144-150.

(4) Biju, V., Itoh, T., Anas, A., Sujith, A., and Ishikawa, M. (2008) Semiconductor quantum dots and metal nanoparticles: syntheses, optical properties, and biological applications. *Anal. Bioanal.Chem. 391*, 2469-2495.

(5) Zhao, W., Brook, M. A., and Li, Y. (2008) Design of gold nanoparticle-based colorimetric biosensing assays. *ChemBioChem 9*, 2363-2371.

(6) Hammond, P. T. (2004) Form and function in multilayer assembly: New applications at the nanoscale. *Adv. Mater. 16*, 1271-1293.

(7) Rana, R. K., Murthy, V. S., Yu, J., and Wong, M. S. (2005) Nanoparticle self-assembly of hierarchically ordered microcapsule structures. *Adv. Mater. 17*, 1145-+.

(8) Caruso, F., Caruso, R. A., and Mohwald, H. (1998) Nanoengineering of inorganic and hybrid hollow spheres by colloidal templating. *Science 282*, 1111-1114.

(9) Krishnan, R. S., Mackay, M. E., Duxbury, P. M., Pastor, A., Hawker, C. J., Van Horn, B., Asokan, S., and Wong, M. S. (2007) Self-assembled multilayers of nanocomponents. *Nano Lett. 7*, 484-489.

(10) Akhrass, S. A., Gal, F., Damiron, D., Alcouffe, P., Hawker, C. J., Cousin, F., Carrot, G., and Drockenmuller, E. (2009) Design of crosslinked hybrid multilayer thin films from azido-functionalized polystyrenes and platinum nanoparticles. *Soft Matter 5*, 586-592.

(11) Mirkin, C. A., Letsinger, R. L., Mucic, R. C., and Storhoff, J. J. (1996) A DNA-based method for rationally assembling nanoparticles into macroscopic materials. *Nature 382*, 607-609.

(12) Urban, J. J., Talapin, D. V., Shevchenko, E. V., and Murray, C. B. (2006) Self-assembly of PbTe quantum dots into nanocrystal superlattices and glassy films. *J. Am. Chem. Soc. 128*, 3248-3255.

(13) Boker, A., He, J., Emrick, T., and Russell, T. P. (2007) Self-assembly of nanoparticles at interfaces. *Soft Matter 3*, 1231-1248.

(14) Kinge, S., Crego-Calama, M., and Reinhoudt, D. N. (2008) Self-assembling nanoparticles at surfaces and interfaces. *ChemPhysChem 9*, 20-42.

(15) Rycenga, M., Camargo, P. H. C., and Xia, Y. (2009) Template-assisted self-assembly: a versatile approach to complex micro- and nanostructures. *Soft Matter 5*, 1129-1136.

(16) Correa-Duarte, M. A., and Liz-Marzan, L. M. (2006) Carbon nanotubes as templates for one-dimensional nanoparticle assemblies. *J. Mater. Chem. 16*, 22-25.

(17) Correa-Duarte, M. A., Perez-Juste, J., Sanchez-Iglesias, A., Giersig, M., and Liz-Marzan, L. M. (2005) Aligning an nanorods by using carbon nanotubes as templates. *Angew. Chem. Int. Ed. 44*, 4375-4378.

(18) Han, X. G., Li, Y. L., and Deng, Z. X. (2007) DNA-wrapped single-walled carbon nanotubes as rigid templates for assembling linear gold nanoparticle arrays. *Adv. Mater. 19*, 1518-+.

(19) Ajayan, P. M., Stephan, O., Redlich, P., and Colliex, C. (1995) Carbon nanotubes as removable templates for metal-oxide nanocomposites and nanostructures. *Nature 375*, 564-567.

(20) Thauvin, C., Rickling, S., Schultz, P., Celia, H., Meunier, S., and Mioskowski, C. (2008) Carbon nanotubes as templates for polymerized lipid assemblies. *Nature Nanotechnol. 3*, 743-748.

(21) Li, Z., Chung, S.-W., Nam, J.-M., Ginger, D. S., and Mirkin, C. A. (2003) Living templates for the hierarchical assembly of gold nanoparticles. *Angew. Chem. Int. Ed. 42*, 2306-2309.

(22) Lee, J. A., Krogman, K. C., Ma, M., Hill, R. M., Hammond, P. T., and Rutledge, G. C. (2008) Highly reactie multilayer-assembled TiO_2 coating on electrospun polymer nanofibers. *Adv. Mater. 20*, 1-5.

(23) Dinsmore, A. D., Hsu, M. F., Nikolaides, M. G., Marquez, M., Bausch, A. R., and Weitz, D. A. (2002) Colloidosomes: Selectively permeable capsules composed of colloidal particles. *Science 298*, 1006-1009.

(24) Tran, M. L., Centeno, S. P., Hutchison, J. A., Engelkamp, H., Liang, D., Van Tendeloo, G., Sels, B. F., Hofkens, J., and Uji-i, H. (2008) Control of surface plasmon localization via self-assembly of silver nanoparticles along silver nanowires. *J. Am. Chem. Soc. 130*, 17240-17241.

(25) Bae, Y. H., Huh, K. M., Kim, Y., and Park, K.-H. (2000) Biodegradable amphiphilic multiblock copolymers and their implications for biomedical applications. *J. Controlled Release 64*, 3-13.

(26) Kotov, N. A., Dekany, I., and Fendler, J. H. (1995) Layer-by-layer self-assembly of polyelectrolyte-semiconductor nanoparticle composite films. *J. Phys. Chem. 99*, 13065-13069.

(27) Srivastava, S., and Kotov, N. A. (2008) Composite Layer-by-layer (LBL) assembly with inorganic nanoparticles and nanowires. *Acc. Chem. Res. 41*, 1831-1841.

(28) Schneider, G. F., Subr, V., Ulbrich, K., and Decher, G. (2009) Multifunctional cytotoxic stealth nanoparticles. A model approach with potential for cancer therapy. *Nano Lett. 9*, 636-642.

(29) Fang, H., Zhang, K., Shen, G., Wooley, K. L., and Taylor, J.-S. A. (2009) Cationic shell-cross-linked knedel-like (cSCK) nanoparticles for highly efficient PNA delivery. *Mol. Pharm. 6*, 615-626.

(30) Zhang, K., Fang, H., Wang, Z., Taylor, J.-S. A., and Wooley, K. L. (2009) Cationic shell-crosslinked knedel-like nanoparticles for highly efficient gene and oligonucleotide transfection of mammalian cells. *Biomaterials 30*, 968-977.

(31) Ma, Q., and Wooley, K. L. (2000) The preparation of tbutyl acrylate, methyl acrylate, and styrene block copolymers by atom transfer radical polymerization: precursors to amphiphilic and hydrophilic block copolymers and conversion to complex nanostructured materials. *J. Polym. Sci., Part A: Polym. Chem. 38*, 4805-4820.

(32) Zhang, K., Fang, H., Chen, Z., Taylor, J.-S. A., and Wooley, K. L. (2008) Shape effects of nanoparticles conjugated with cell-penetrating peptides (HIV Tat PTD) on CHO cell uptake. *Bioconjugate Chem. 19*, 1880-1887.

(33) Gratton, S. E. A., Ropp, P. A., Pohlhaus, P. D., Luft, J. C., Madden, V. J., Napier, M. E., and DeSimone, J. M. (2008) The effect of particle design on cellular internalization pathways. *Proc. Nat. Acad. Sci. U.S.A. 105*, 11613-11618.

(34) Zou, S.-M., Erbacher, P., Remy, J.-S., and Behr, J.-P. (2000) Systemic linear polyethylenimine (L-PEI)-mediated gene delivery in the mouse. *J. Gene Med. 2*, 128-134.

Chapter 8

Conclusions

This dissertation has focused on developing block copolymer-based nanostructures as intracellular delivery vehicles, with the ultimate purpose of using them as integrated systems for diagnosis and therapy. Because of the many kinds of "passengers" (ions, small molecules, DNA, *etc*.) and "destinations" (cell lines, tissues, *etc*.), the "vehicles" must be designed to incorporate specific characteristics accordingly. The first part (Chapters 2 and 3) of the dissertation discusses the use of spherical and cylindrical SCKs with poly(acrylic acid) shells as the base upon which functionalization was performed. Depending on the chemical moiety that was attached to the surface of the nanoparticles, PTD or folate, a different trend in cell internalization with regard to the particle size/shape was observed. The spherical PTD-SCK was internalized by HeLa cells more rapidly compared with its cylindrical counterpart, while the spherical folate-SCK showed less KB cell uptake than the cylindrical folate-SCK. This information may be useful in drug delivery applications. For example, assuming the cores of the SCKs are loaded with a therapeutic, to be delivered to cancerous tissues *via* recepted-mediated endocytosis, a cylindrical morphology may be more beneficialto maximize selectivity and efficiency of delivery. On the other hand, if the therapeutic was to be delivered intracellularly in a systemic fashion, a smaller, spherical PTD-functionalized SCK may be a better suited delivery vehicle.

Chapters 4 - 6 form the second part of the dissertation. In this part, the "passengers" are more specified: genetic materials capable of altering gene expression or

being expressed inside a living cell. Such genetic materials may include DNA, RNA or a synthetic mimic, PNA. Because DNAs carry the same negative charge as the poly(acrylic acid) shells of the SCKs, simple mixing does not allow the formation of complexes between the SCK and the DNA. In Chapter 4, a cationic SCK, or cSCK, was described, which was made to bear primary amines that upon protonation render the particles a positively charged character. These cSCKs not only serve as an object around which DNA could wrap, which allows for the DNA to be protected from enzymatic degradation, the primary amines were also capable of disrupting the endosomes through a proton-sponge effect, thereby releasing the DNA into the cytoplasm. The efficiency of DNA delivery was then conveniently quantified by its bioactivity, through a luciferase splice correction assay (oligo) or an EGFP expression assay (plasmid). Chapter 5 builds upon the ideas developed in Chapter 4, and further explores the structure-activity relationships between various modified cSCKs and their transfection/cytotoxicity. It was realized that the chemical composition of the cSCK's shell affected its ability to bind to DNA, to disrupt the endosome, and ultimately, to deliver DNA. By optimizing the particle buffering capacity and DNA binding affinity through fine-tuning of primary/tertiary amine ratio, a more refined "vehicle" was developed, which exhibited much higher transfection efficiency and lower cytotoxicity compared to the original cSCK and other commonly available transfection agents. Even better performances are expected when the particles are conjugated with appropriate ligands for receptor-mediated endocytosis such as the tripeptide RGD for integrin receptors, and moieties for enhancing endosomal release.

Having backbones made of peptide bonds, the PNAs lack the negative charge associated with DNAs. As such, these special "passengers" required unique approaches to be loaded onto the cSCKs. Two strategies were employed in Chapter 6 to achieve this purpose: either through electrostatic complexation with a PNA•ODN hybrid, or through a bioreductively-cleavable disulfide linkage to a PNA. These delivery systems are much better than the standard lipofectamine/ODN-mediated method and superior to the Arg_9-mediated method for PNA delivery in HeLa cells, showing lower toxicity and higher bioactivity. The cSCK were also found to facilitate both endocytosis and endosomal release of the PNAs, while themselves remaining trapped in the endosomes. Such cSCK-PNA systems may be very useful for *in vivo* applications, where it would be important to minimize dissociation of the PNA from the cSCK prior to reaching the target cell.

The last part of this dissertation, Chapter 7, challenges a more daunting task: can something as large as a cylindrical nanoparticle be carried by the cSCKs into the cells? The cylindrical SCKs, as found in Chapter 2, did not undergo rapid cell uptake after 24 hours of incubation with HeLa cells, even when conjugated with PTD. In Chapter 7, a strategy involving the use of a cSCK coating was exploited. Instead of conjugating PTD moieties to nanoparticles to assist cell uptake, cSCKs were used as a coating, which formed a closely packed layer on the surface of the cylinders. These nanocomplexes resemble the morphology of a virus, which are essentially DNA/RNA packed inside a protein coat. The cSCKs are very efficient in cell entry, as reported in Chapters 3-6, due to its positively charged shell. This simple strategy allowed the cylinders to inherit the cell entry capabilities of the cSCKs, which assisted the cylinders to populate the cellular interior in less than 2 hours. Although it was not demonstrated in this chapter, it may be

speculated that *other* characteristics of the spheres, if installed, may also be transferred to the final assembled structure. For example, if targeting spheres, reporting spheres and endosome-disrupting spheres are all assembled onto one common cylinder, which may be loaded with drugs itself, a truly hierarchical, complex, multifunctional nanostructure can be synthesized in a facile, modular fashion, obviating the need for multi-step, complicated chemical synthesis. The connecting region between the cationic and anionic particles may also be crosslinked reversibly or irreversibly, if needed, to prevent premature dissociation of the functional spheres from the cylinders when ionic strength/pH of the solution changes. If crosslinked irreversibly, the cylinder may also be chemically etched to afford a cage-like, hollow material that may have potential application in nanomedicine.

It is hoped that this dissertation has conveyed the notion that nanomedicine is a highly promising field that could benefit the lives of generations to come. Many unusual and unique properties from being small in size are beginning to be recognized and utilized. At an early stage, nanomedicine already demonstrates broad applications and profound impact. The National Nanotechnology Initiative expects new commercial applications in the pharmaceutical industry that may include advanced drug delivery systems, new therapies, and *in vivo* imaging. Neuro-electronic interfaces and other nanoelectronics-based sensors are another active area of research. Further down the line, the speculative field of molecular nanotechnology believes that cell repair machines could revolutionize medicine and the medical field. Before any of these goals can be fully realized, however, much still remains to be explored, including understanding the issues related to toxicity and environmental impact of nanoscale materials.